FACULTY OF ELECTRICAL
ENGINEERING
UNIVERSITY OF WEST BOHEMIA

DOCTORAL THESIS

Nuclear District Cooling System: Evaluation and Optimization

Author: Hussein Abdulkareem Saleh Abushamah, M.Sc.

Supervisor: Prof. Ing. Radek Škoda, Ph.D.

Pilsen, 2023

Declaration

I declare that I have elaborated the dissertation thesis individually and have used sources which I cite and list in the bibliography.

Pilsen, date

……
signature

Acknowledgments

I would like to express my thanks and appreciation to my respected supervisor, Prof. Radek Škoda, for his valuable support throughout this significant scientific journey. I am also thankful to the personnel of the Department of Electrical Power Engineering, including Dr. Jana Jiřičková, Ms. Jana Lepičová, and my colleagues, including David Mašata, who assisted me with administrative procedures and provided help whenever I needed it. Furthermore, I extend my thanks to the personnel of the International Office at the Faculty of Electrical Engineering, specifically Ing. Jana Čečilová and Dr. Jan Michalík, for their prompt, gracious, and supportive responses when required.

بسم الله الرحمن الرحيم وله الحمد والشكر أولا وأخيرا

تحية خاصة لأبي الغالي وأمي الحنونة، أطال الله في عمرهما وحفظهما كمأوى لنا. أشكر زوجتي الحبيبة على تحملها مصاعب الفراق والصبر، وتحمل المسؤولية في رعاية أطفالنا، أحباء القلب، الذين كل ما نقوم به هو لمساعدتهم ودعمهم في بناء مستقبل زاهر.

Abstract

The air conditioning sector is one of the major contributors to electricity consumption and carbon emissions in many regions over the world. For example, in hot climate regions such as the Gulf Cooperation Council (GCC), about half of the annual generated electricity is for air-conditioning, leading to significant carbon emissions. The widely adopted scenario is burning the fuel to produce heat, converting the heat to electricity, transporting the electricity through HV/MV/LV grids to supply electric-driven cooling systems. Proceeding in this manner puts pressure on power grids, raises investments for expanding the electrical infrastructure, drives up carbon emissions, and leads to more energy losses due to unwanted energy conversions and transmissions. This study presents a carbon-free thermally driven district cooling system to overcome these issues of the electric-driven cooling scenario. The proposed system here employs a nuclear heat-only reactor called Teplator as a carbon-free primary heat source driving absorption chillers. This idea is techno-economically evaluated from two different perspectives, namely, the energy policy viewpoint and the investor's point of view. First, from an energy policy viewpoint, adopting the proposed system is compared to the electric scenario based on levelized values for cooling demand, costs, and energy consumption without dealing with details of a specific case-based design or operation. From an investor's viewpoint, a detailed method is developed to optimize the proposed system's design and operation, including the heat transmission system and a centralized cooling plant, for supplying an hourly-based demand model. A competition-based optimization process is performed by including several alternative units, such as thermal energy storage, gas boilers, and compression chillers, which simultaneously also checks the electric-driven option. The developed models are coded in MATLAB and simulated. The results confirm the proposed system's superiority in cost, electricity, and carbon emission saving compared with fossil fuel-based electrically driven district cooling systems. However, the performed sensitivity analyses show that this superiority could be limited as the electricity price decreases and heat transmission pipeline length increases.

Keywords

District Cooling, Nuclear Heat-Only Small Modular Reactors, Teplator, Electricity and Carbon Emission Saving, Power Grid, Optimization.

Contents

List of figures

List of tables

Abbriviations

GCC	The Gulf Cooperation Council	*PNEf*	Piping Network Efficiency factor
CHD	Cooling and Heating Demand	*PPC*	Power Plant Capacity
DCS	District Cooling System	*HPC*	Heating Plant Capacity
ACS	Air Conditioning Systems	*THPCC*	Total Heating Plant Capital Cost
DC	District Cooling.	*LHPCC*	Levelized Heating Plant Capital Cost
DCHS	District Cooling and Heating System.	*TPPCC*	Total Power Plant Capital Cost
SMR	Small Modular Reactor	*LPPCC*	Levelized Power Plant Capital Cost
MWth	Thermal Mega Watt	*THDCSCC*	Total Heat-Driven Cooling System Capital Cost
MWe	Electrical Mega Watt	*TEDCSCC*	Total Electric-Driven Cooling System Capital Cost
LWR	Light Water Reactor	*LHDCSCC*	Levelized Heat-Driven Cooling System Capital Cost
COP	Coefficient Of Performance	*LEDCSCC*	Levelized Electric-Driven Cooling System Capital Cost
T&D	Transmission and Distribution	*DMP*	Decision Making Period
O&M	Operation and Maintenance	COP_{EDC}	Average Coefficient Of Performance of Electric-Driven Chillers
CDDC	Cooling Demand Duration Curve	COP_{HDC}	Average Coefficient Of Performance of Heat-Driven Chillers
HDDC	Heating Demand Duration Curve	*RVP*	Returned Value Percent
LDC	Load Duration Curve	*TPEE*	Total Produced Electrical Energy
PCD	Peak Cooling Demand	*TPTE*	Total Produced Thermal Energy
ACD	Average Cooling Demand	*VOMC*	Variable Operation and Maintenance Cost
PCP	Peak Cooling Period	*AFOMC*	Annual Fixed Operation and Maintenance Cost
ACP	Average Cooling Period	*TPPOMC*	Total Power Plant Operation and Maintenance Cost
PHD	Peak Heating Demand	*THPOMC*	Total Heating Plant Operation and Maintenance Cost
AHD	Average Heating Demand	*TCOE*	Total amount of CO_2 emissions
PHP	Peak Heating Period	*TSCC*	Total Social Carbon Cost
AHP	Average Heating Period	*LCPTD*	Levelized Cost of Power Transmission and Distribution

TCED	Total Cooling Energy Demand	*PTDCR*	Power Transmission and Distribution Cost Reduction
THED	Total Heating Energy Demand	*HCP*	Heating Capacity Price
ETDLf	Electricity Transmission & Distribution Loss factor	*ISHC*	Income of Serving Heating Capacity

Symbols

$\boldsymbol{A_{hex}}$	Heat transfer area of heat exchanger ($\boldsymbol{m^2}$).	$\boldsymbol{P}$	Pumping power (MWe).
$\boldsymbol{c}$	Flow velocity (m/s).	Q_{hs}^{i}	Hourly charged/discharged thermal power by heat storage (MWt).
$\boldsymbol{CG_{ac}^{i}}$	Hourly cooling power of absorption chillers (MWc).	Q^{HTL}	Heat transmission losses (MWt).
$\boldsymbol{CG_{cc}^{i}}$	Hourly cooling power of compression chillers (MWc).	Q_{bht}^{i}	Hourly transported heat (MWt).
$\boldsymbol{CG_{cs}^{i}}$	Hourly charged/discharged cooling power by cold storage (MWc).	Q_{gb}^{i}	Hourly heat generation by gas boiler (MWt).
$\boldsymbol{COP_{ac}}$, $\boldsymbol{COP_{cc}}$	Average coefficient of performance of absorption, and compression chillers.	Q_{nhp}^{i}	Hourly heat generation by nuclear plants (MWt).
$\boldsymbol{C_p}$	Specific heat capacity of water (W.s/kg.K).	Re	Reynolds number.
$\boldsymbol{Cp_{hex}}$	Thermal power capacity of heat exchanger (MWt).	RR_{ac}	Ramp rate of absorption chilling (% of capacity).
$\boldsymbol{Cp_{hs}}$	Thermal energy capacity of heat storage (MWth).	R_{hs}^{ch}, R_{hs}^{dch}	Charging/discharging power rate of heat storage (% of capacity).
$\boldsymbol{Cp_{ac}}$	Cooling capacity of absorption chillers (MWc).	RC_{css}	Reconstruction cost of cooling supply station ($).
$\boldsymbol{Cp_{cc}}$	Cooling capacity of compression chillers (MWc).	RC_{hss}	Reconstruction cost of heat supply station ($).
$\boldsymbol{Cp_{cs}}$	Cooling energy capacity of cold storage (MWch).	RC_{bht}	Reconstruction cost of bulk heat transmission system ($).
$\boldsymbol{Cp_{gb}}$	Thermal capacity of gas boiler (MWt).	RR_{cc}	Ramp rate of compression chilling (% of capacity).
$\boldsymbol{Cp_{nhp}}$	Thermal capacity of one nuclear plant (MWt).	RR_{cs}^{ch}, RR_{cs}^{dch}	Charging/discharging power rate of the cold storage (% of capacity).
$\boldsymbol{Cp_{pump}}$	Electrical capacity of pumping station (MWe).	RR_{gb}	Ramp rate of gas boiler (% of capacity).
$\boldsymbol{D, D_{out}}$	Inner diameter and outer diameter of heat transmission pipe (m).	RR_{nhp}^{up} RR_{nhp}^{down}	Increasing and decreasing ramp rates of nuclear units (% of capacity).
$\boldsymbol{EC_{ac}}$	Absorption chiller's auxiliary electrical power consumption per supplied cooling power (MWe/MWc) (%).	s	Pipe insulation thickness (mm)
$\boldsymbol{EC_{cc}}$	Compression chiller's auxiliary electrical power consumption per supplied cooling power (MWe/MWc) (%).	SE_{hs}^{i}	Heat storage's stored thermal energy at the hour (i), (MWth).

$\boldsymbol{EC_{gb}}$	Gas boiler's auxiliary electrical power consumption per supplied thermal power (MWe/MWt) (%).	SE_{cs}^{i}	Hourly cooling energy stored in cold storage (MWch).
$\boldsymbol{EC_{nhp}}$	Nuclear heat plant's auxiliary electrical power consumption per supplied thermal power (MWe/MWt) (%).	SFC_{gb}	Specific fuel cost of gas boiler ($/MWth).
$\boldsymbol{f}$	Friction factor.	SFC_{nhp}	Specific fuel cost of nuclear plants ($/MWth).
$\boldsymbol{hi}$	Thermal conductivity of pipe insulation (W/m.K).	Sg	Specific gravity of water.
$\boldsymbol{IC_{bht}}$	Initial capital cost of heat transmission system ($).	SOM_{hs}^{f} SOM_{cs}^{f}	Specific fixed O&M cost of heat, cold storage ($/MWth/yr).
$\boldsymbol{IC_{css}}$	Initial capital cost of cooling supply station ($).	SOM_{ac}^{f}	Specific fixed O&M cost of absorption chiller ($/MWc/yr)
$\boldsymbol{IC_{hss}}$	Initial capital cost of the heat supply station ($).	SOM_{ac}^{v}	Specific variable O&M cost of absorption chiller ($/MWch)
$\boldsymbol{IC_{hex}^{hss}}$, $\boldsymbol{IC_{hex}^{css}}$	Initial capital cost of heat exchangers at the endpoints of the pipe (on heating station side and cooling station side) ($).	SOM_{cc}^{f}	Specific fixed O&M cost of compression chiller ($/MWc/yr)
$\boldsymbol{IC_{hs}}$	Initial capital cost of heat storage ($).	SOM_{cc}^{v}	Specific variable O&M cost of compression chiller ($/MWch)
$\boldsymbol{IC_{nhp}}$	Initial capital cost of the nuclear heat plants ($).	SOM_{gb}^{f}	Specific fixed O&M cost of gas boiler ($/MWt/yr).
$\boldsymbol{IC_{pipe}}$	Initial capital cost of pipes including insulation ($).	SOM_{gb}^{v}	Specific variable O&M cost of gas boiler ($/MWth).
$\boldsymbol{IC_{pump}}$	Initial capital cost of pressure-boosting pump ($).	SOM_{nhp}^{f}	Specific fixed O&M cost of nuclear plants ($/MWt/yr).
$\boldsymbol{IR}$	Annual interest rate (%).	SOM_{nhp}^{v}	Specific variable O&M cost of nuclear plants ($/MWth).
$\boldsymbol{L}$	The one-way pipeline length (m).	U	Heat transfer coefficient of heat exchanger (W/m^2.K).
$\boldsymbol{LMTD}$	The logarithmic mean temperature difference (K).	V_{cs}^{s}	Cold storage volume (m^3)
$\boldsymbol{\dot{m}_{bht}^{i}}$	Hourly mass flow rate of water in transmission pipe (kg/s).	V_{ins}	Insulation volume (m^3)
$\boldsymbol{N}$	Number of hours in a year.	Wt_{pipe}	Weight of pipe (kg)
$\boldsymbol{N_{nhp}}$	Number of nuclear heat plants.	ΔT_A	Temperature difference between the inlet hot water and outlet cold water of heat exchanger (K).
$\boldsymbol{OF}$	Objective function ($).	ΔT_B	Ttemperature difference between the outlet hot water and the inlet cold water of heat exchanger (K).

$\boldsymbol{OM_{hss}^{af}}$	Annual fixed operation and maintenance (O&M) cost of heat supply station ($/yr).	ΔT_{cs}	Cold storage supply/return difference temperature (K).
$\boldsymbol{OM_{hss}^{av}}$	Annual variable O&M cost of heat supply station ($/yr).	ΔT_{bht}	Difference between heat transmission supply and return temperatures (K).
$\boldsymbol{OMC_{hss}}$	Present value of total O&M cost of the heat supply station ($).	ΔP	Pressure drop along the pipeline (kPa).
$\boldsymbol{OMC_{bht}}$	Present value of total O&M cost of the heat transmission system ($).	η_{ps}	Pump efficiency.
$\boldsymbol{OMC_{css}}$	Present value of total O&M cost of the cooling supply station ($).	η_{cs}	Efficiency of cold storage.
		ε	Roughness of the pipe (mm).
		ν	Kinematic viscosity of water (m^2/s).
		ρ	Density of water (kg/m^3)

1 Introduction

Using ACS is expected to rise rapidly during the next three decades, placing extensive pressure on power grids and rising pollution emissions in various states [1]. Half of the total energy consumption in Europe in 2015 was for cooling and heating purposes, of which 66% was produced from fossil fuels [2]. In the United States in 2019, about 38% of consumed energy was for building sector heating and air conditioners, where air conditioning is responsible for about 6% of the total produced electricity [3]. In China, energy consumption in the buildings, for H&C purposes, is forecasted to rise 35% compared with total energy demand in 2020, while space cooling and heating constitute a substantial share of this energy growth [4]. Fig. 1 and Fig. 2 indicate that in the case of carrying on with conventional electric-driven cooling, the global power generation capacity required to meet the cooling will move from 850 to 3,350 GW, electricity consumption will grow from 2000 TWh to 6200 TWh, and the resulted carbon emissions will double between 2016-2050 [1].

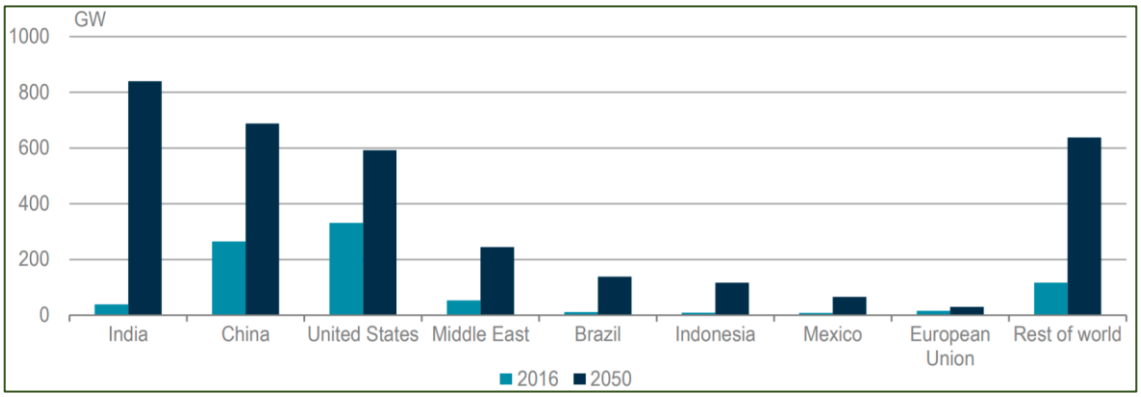

Figure 1: Required electrical power generation capacity for conventional cooling technologies by country/region [1].

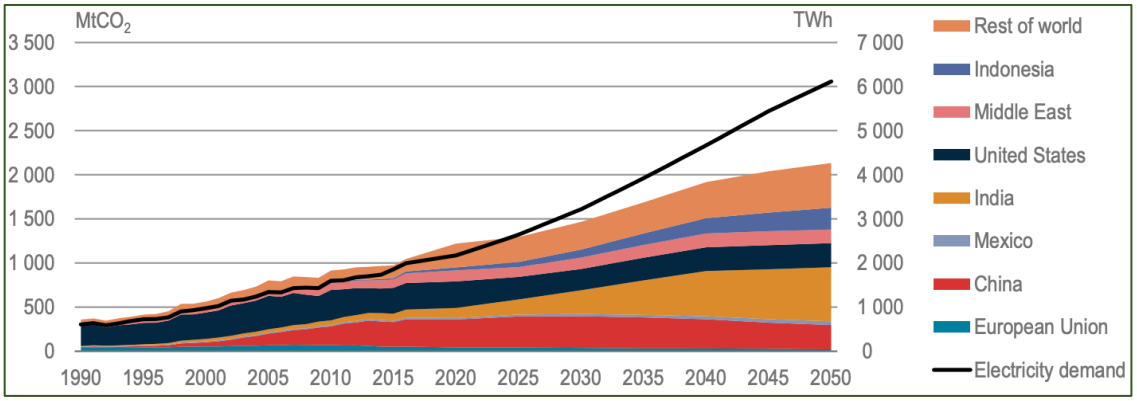

Figure 2: Electricity demand and resulting CO2 emissions from space cooling [1].

1.1 Cooling challenges in hot climate regions

The significant electricity consumption and resulting carbon emissions are the main challenges of the cooling sector in hot countries. For example, the Gulf Cooperation Council (GCC) includes six states, namely Saudi Arabia, Kuwait, Bahrain, Oman, Qatar, and the United Arab Emirates, located near the tropics and categorized by one of the hottest climates in the world. ACS in the GCC accounts for about 50 percent of consumed electricity annually and constitutes 70 percent of peak electricity consumption. Between 2010 and 2030, it is estimated that cooling demand in this region will triple [5]. In the KSA, about 70% of household electricity is for air conditioning systems. In Oman, cooling demand is responsible for about 60% of the residential energy consumption, and cooling load is responsible for 36% of the total electricity consumption in the UAE [6][7][8]. About 60 percent of the electrical power generation expansion is needed to meet the air cooling sector's energy growth; at the same time, the load factor tends to be around 55–60% due to a sizable unused generation capacity during winter [9][10]. In this context, Fig. 3 shows the average hourly cooling demand per month in Qatar [11], and Fig. 4 shows a typical energy consumption profile of a house on different days of a year. During the summer, electricity consumption for cooling is about 90% of the total demand, while in winter, the cooling demand is almost zero [12]. The cooling demand during summer is so high. At the same time, there is no demand in winter, and this causes a low capacity factor for the power plants due to a significant unused generation capacity during winters [13].

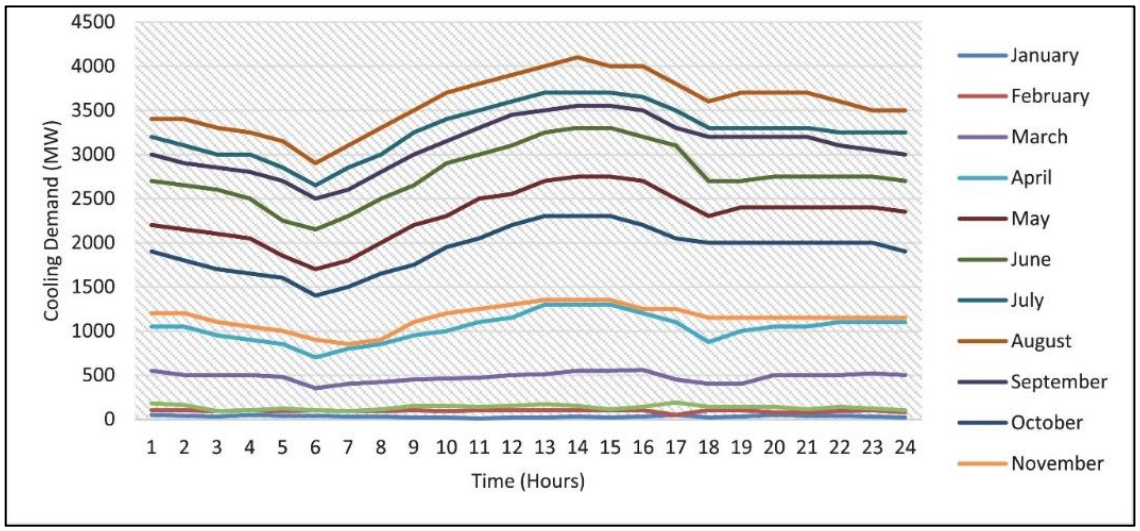

Figure 3: Average monthly cooling demand per hour in the State of Qatar [11].

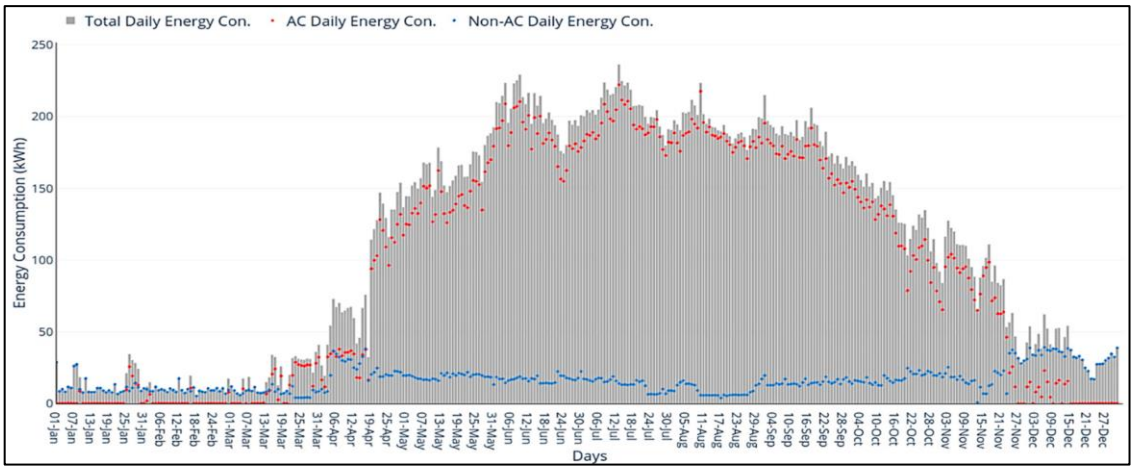

Figure 4: Daily energy consumption in a typical house in Qatar [12].

Fig. 5 illustrates how Qatar's electricity consumption growth results in carbon emission growth. At the same time, there is an ongoing surge in cooling demand in this typical region (GCC), as illustrated in Fig. 6. Consequently, decarbonizing the air conditioning sector is crucial to limit its growing significant carbon emissions and the idea of extending large scale carbon-free heat-driven cooling systems could effectively reduce electricity consumption and emissions, especially in the hot weather countries.

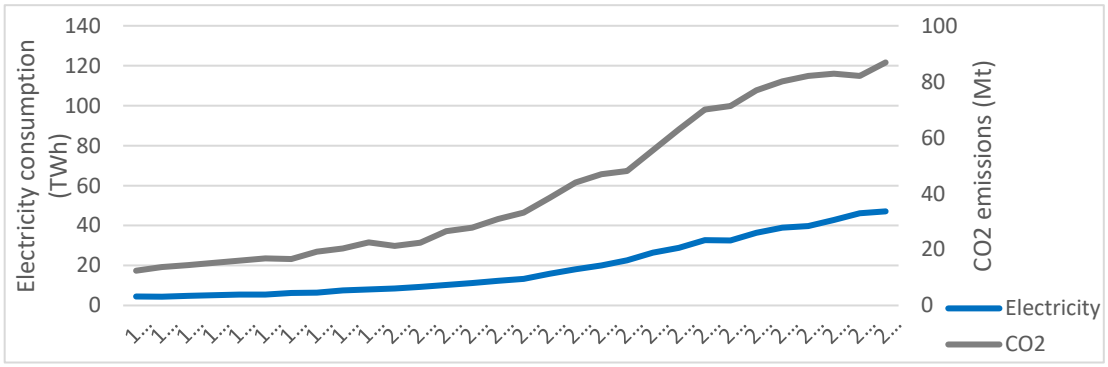

Figure 5: The growth of Qatar's electricity consumption and total CO2 emissions [14].

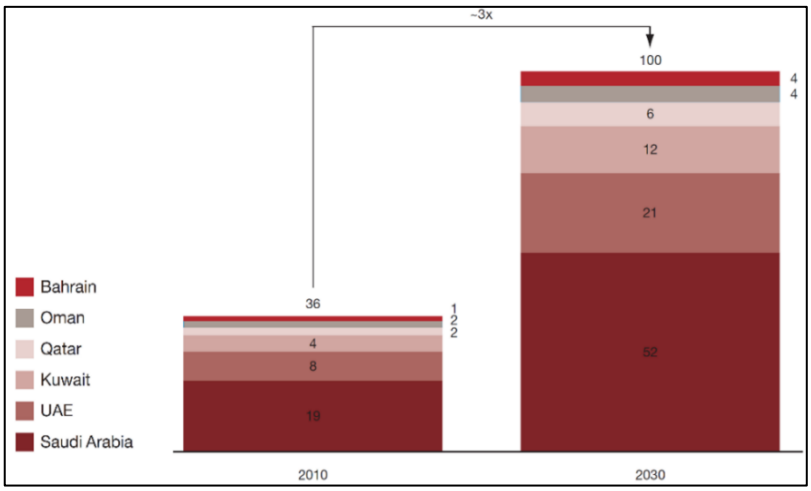

Figure 6: GCC peak cooling demand in millions of refrigerator ton (RT), 1 RT = 0.0035 MW [15].

1.2 District cooling systems

District cooling system (DCS) is a system in which cooling energy is produced in the form of chilled water by centralized chiller plants and circulated throughout the residential, commercial, industrial, etc., buildings and consumers through a piping distribution network, to be used for space cooling and dehumidification. The four main parts of this system are the central chiller plant, the heat rejection system, the distribution piping network, and the end user, as illustrated in Fig. 7 [16]. The development of DCSs has a long history from 1889 when the first known DCS began operation in 1889 in Denver's Colorado Automatic Refrigerator Company. In the US, DCSs covered approximately 20 cities and towns until 1996. In Europe, the first DCS was built in Paris in 1960, and then this system began extending to several European countries like Germany, Italy, Sweden, etc. Because of DCSs' high efficiency and lower carbon emissions, there is a growing interest in DCSs in Japan, where more than 154 DCSs were installed between 1970-2005. Considering population growth, urbanization, global warming, and economic growth, cooling demand continues to grow, and the share of district cooling systems is expected to rise sharply.

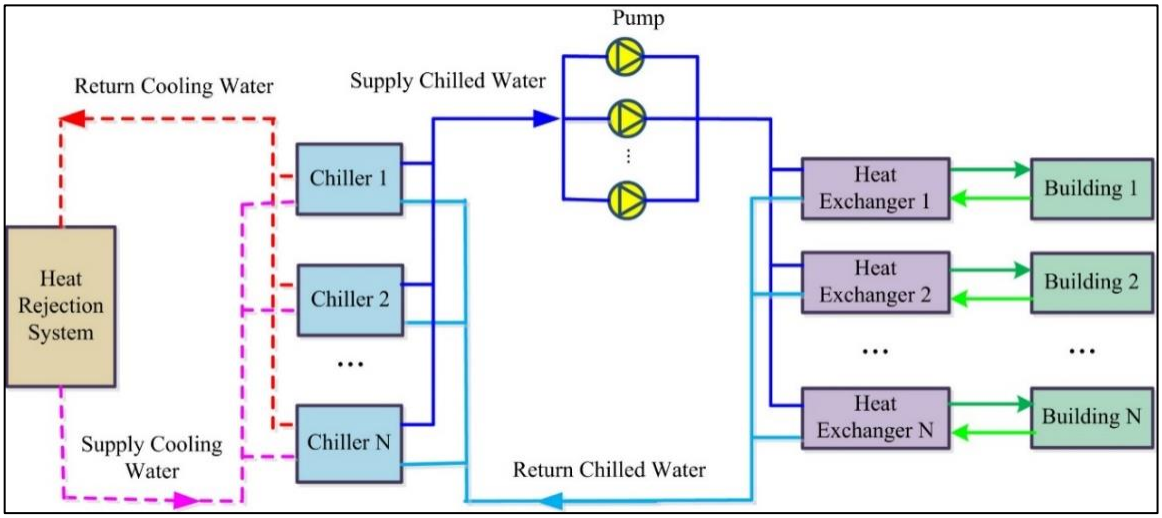

Figure 7: Schematic diagram of a typical district cooling system [16].

To supply the rapid rise of cooling demand in regions of high cooling demand density, the expansion of large power concentrated district cooling systems is the economical option. In contrast, the conventional small power disperses or individual air conditioners are optimal for areas of low cooling density demand, as shown in Fig. 8 [17]. For example, the economic shares of DCSs and individual air conditioners by 2030 for the GCC were estimated and illustrated in Fig. 9. This figure shows that DCSs could provide 30% of the total forecasted cooling needs by 2030 [17], reflecting the economic potential high penetration of DCSs in

hot climate and densely populated cities. GCC currently owns about 32% of the global installed DC capacity [5], [15], where one of the largest DC plants in the world is located in The Pearl-Qatar with a cooling capacity of 450 MW [18].

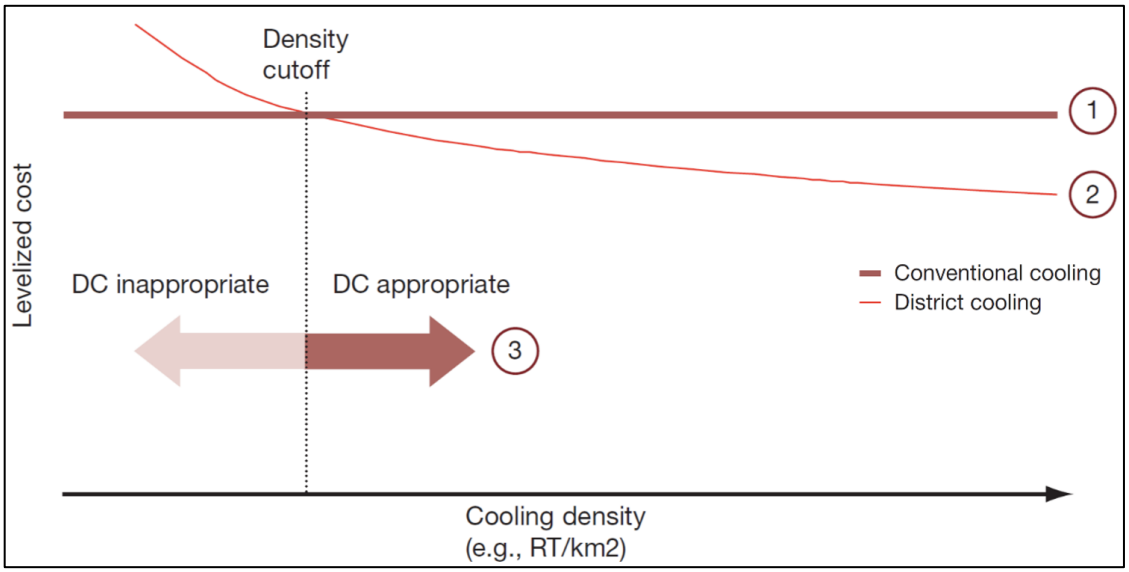

Figure 8: Levelized cost of cooling technologies vs. cooling density [17].

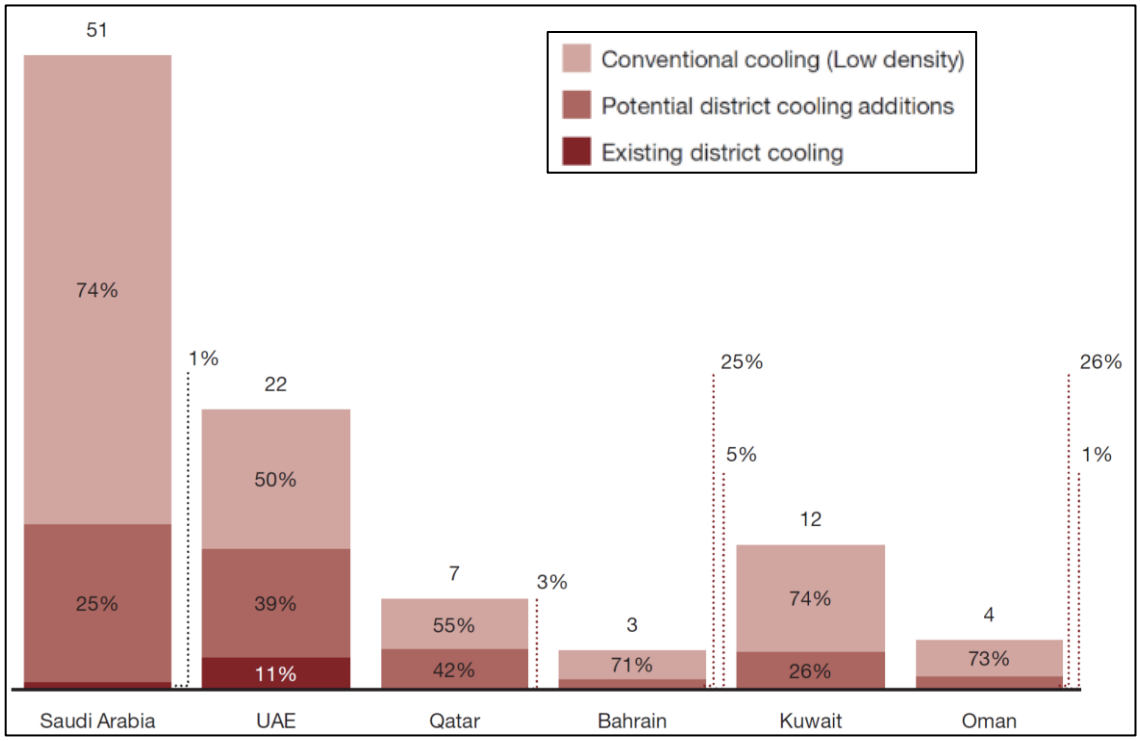

Figure 9: Forecasted cooling requirements in the GCC, 2030 (in millions of RT) [17].

The district cooling plants could be of either electric-driven or thermally-driven technologies. Although DCSs employing electric-driven compression cycle technology represent a higher efficiency solution than the individual air conditioning approach, the heat-

driven absorption cycle technology can significantly eliminate the cooling sector's electricity consumption and the associated emissions. The specifications of different heat-driven chillers are illustrated in Table 1 [19]. H_2O-NH_3 absorption chillers are mainly used in industrial cooling applications, while H_2O/Silica-Gel adsorption chillers have low market penetration and low Coefficient of Performance (COP). Employing the LiBr-H_2O chillers in the cooling systems is more common thanks to the refrigerant (H_2O) that is available everywhere, not expensive, not toxic, and due to its high latent heat of evaporation, a significant amount of cooling can be produced [20]. Two typical cycles of this technology, single-effect and double-effect, are illustrated in Figures 10 and 11, respectively. The double-effect LiBr-H2O absorption chiller has a higher COP than the single-effect one but requires a higher inlet temperature of 130-200 ˚C. Therefore, the single-effect absorption chilling technology could be an appropriate option for the system proposed in this study, as low-temperature heat sources like Teplator could drive it.

Table 1: Specifications of thermally driven chillers [19]**.**

	Thermal				
Technology	Absorption				Adsorption
Type	LiBr/H_2O			H_2O/NH_3	H_2O/Silicagel
	single-effect	double-effect	single-effect/double-lift		
Heat source	warm water, district heat, steam	steam, direct fired	district heat	steam, district heat, solar thermal heat, steam	low heat source is sufficient
Inlet Temperature	75 - 110°C	135 - 200°C	80 - 100°C	100 - 180°C	55 - 90°C
Capacity	(15) 35 kW - 12 MW	200 kW - 6 MW	600 kW - 6 MW	100 kW - 10 MW	50 - 500 kW
COP	0.6 – 0.8	0.9 – 1.3	0.4 – 0.75	0.25 – 0.5	0.5 – 0.7
Price / kW_{th}	1,200 - 200 €	-	> 400 €	1,250 - 400 €	1,500 - 350 €
Space	(1.8) 15 - 96 m^3	17 - 56	25 - 168 m^3	> 50 m^3	12 - 70 m^3
Weight	(0.6) 5 - 41 t	10 - 30 t	15 - 60 t	> 11 t	5 - 25 t
Application	Air-conditioning	Air-conditioning & industrial	Air-conditioning & district cooling	Retailing, industry	Air-conditioning
Market penetration	high	high	small	small	small
# Suppliers	> 8	> 5	Entropie (Patent)	> 2	2

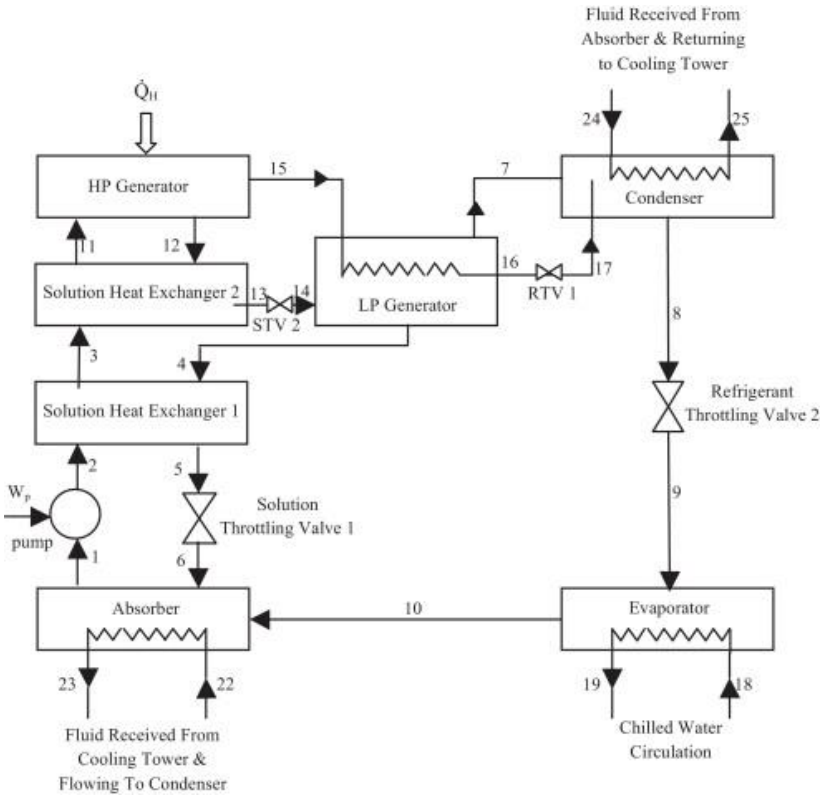

Figure 10: Schematic diagram of a water-cooled single-effect absorption chiller [20]**.**

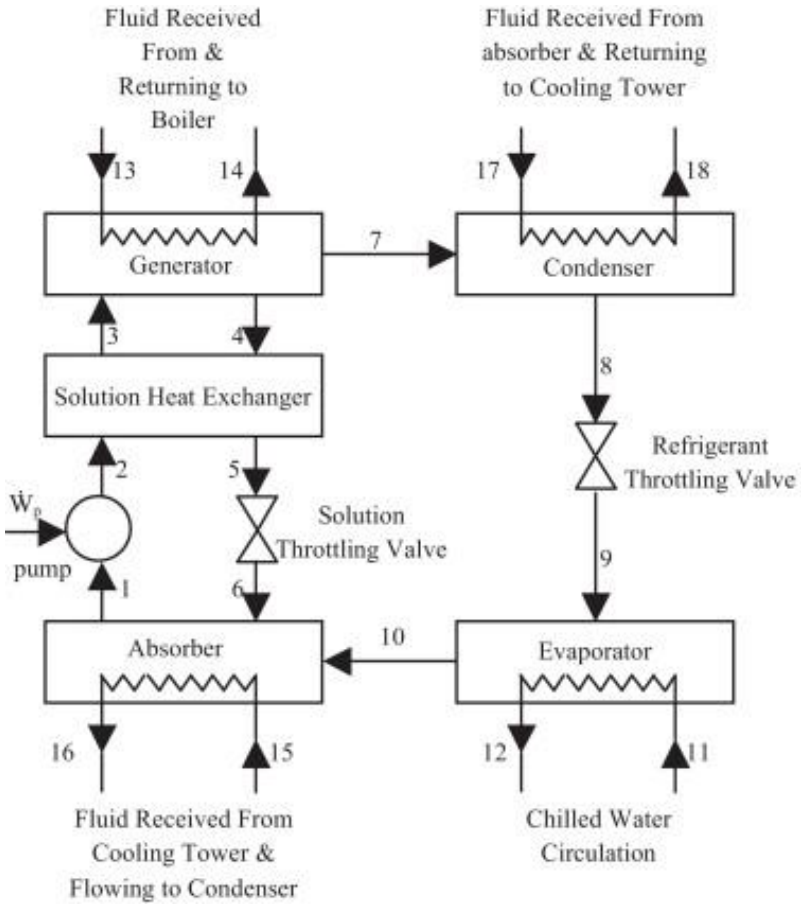

Figure 11: Schematic diagram of a water-cooled single-effect absorption chiller [20]**.**

1.3 Teplator

SMR technology carries important advantages such as enhanced safety, uncomplicated and standardized modular design, less capital cost, and shorter construction times. SMRs can be small enough to be transported and be clustered in a single site to provide a large-capacity power plant [21]. The Teplator [22] is a Small Modular Reactor (SMR) designed for clean district heating energy production with an output power range of 50-200 MWt and output temperature from 98 ˚C up to 200 ˚C as customers require. The estimated capital cost for building the first Teplator DEMO is 30 million euros [23]. The possibility to reuse the irradiated spent nuclear fuel from commercial light water reactors is one of the unique features of Teplator. Hence, no new nuclear wastes are produced. Moreover, online refueling is an optional feature that maximizes availability[22]. From the safety viewpoint, "Teplator operating conditions (e.g., fuel/coolant temperature, pressure, linear heat rate) are much lower than those for which the used FAs were certified and used in LWRs. The safety features establish a defense in depth against radiological hazards. The Teplator leverages the inherent safety characteristics of the basic LWR reactor design and supplements them with passive and active safety features that improve safety". A schematic view of the reactor is illustrated in Fig. 12, and the heat production cycle is presented in Fig. 13 [22][23]. A basic feasibility study of the Teplator concept for district heating applications in Europe is shown lately in [24], and in this paper, the Teplator is evaluated for district cooling purposes.

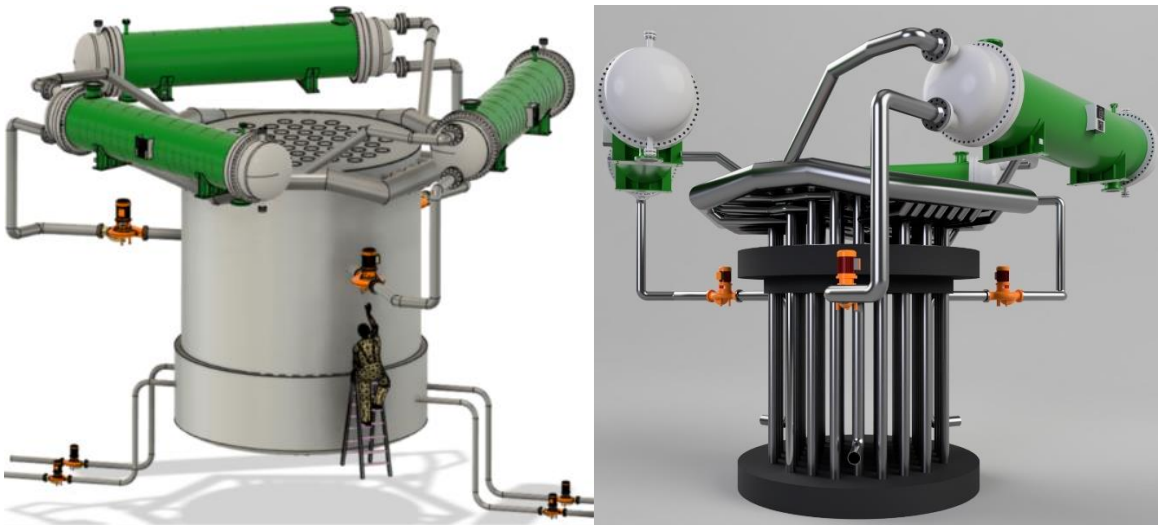

Figure 12: Teplator [22]**.**

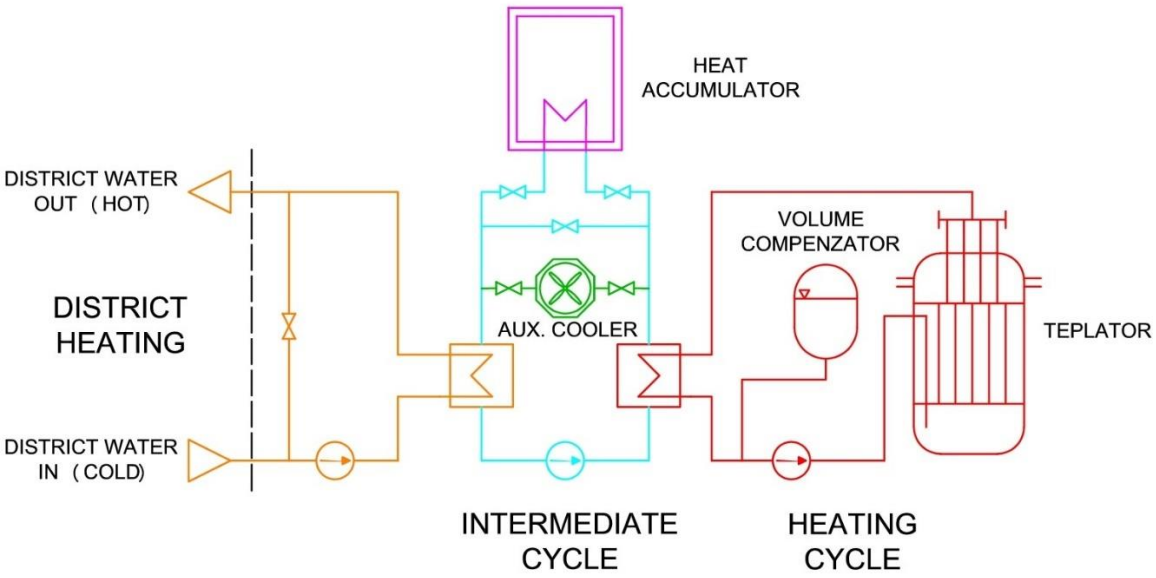

Figure 13: Heat production cycle in the Teplator [22].

1.4 State of the art

Addressing greenhouse gas emissions is critical in tackling global warming and mitigating climate change. Consequently, it is crucial to develop low-carbon energy systems that can fulfill the energy requirements of various sectors. Globally, air conditioning in buildings accounts for nearly 20% of the building's electricity consumption. This percentage increases dramatically in hotter regions such as the Gulf countries and Central Asia, where it rises to 73% and 80%, respectively, and leads to enormous pressure on electricity grids and substantial carbon emissions. At the same time, factors such as economic growth, population increase, global warming, and urbanization are causing an unprecedented surge in global cooling energy demand. This demand is forecasted to almost triple by 2050, reaching 6,200 TWh [25][26][27]. Therefore, carbon-neutral thermally driven district cooling systems provide a viable solution to the cooling sector's main challenges: high electricity consumption and carbon emissions [28]. In this context, Inayat et al. [29] conducted a comprehensive review of various studies that explored the application of carbon-neutral energy sources in district cooling systems. These include solar thermal energy, geothermal energy, biomass, industrial waste heat, and recovered heat from power plants. In addition, the potential of natural cooling energy sources like seas, rivers, and lakes for cooling applications has also been investigated [16]. Fangtian et al. identified two major challenges large-scale solar-driven district cooling and heating systems face: the time discrepancy between supply and demand and the spatial mismatch due to the wide area required for solar collectors. Thermal energy storage could mitigate the issue of time

discrepancy. A large temperature difference between supply/return hot water could lead to cost-effective long-distance heat transmission. Therefore, solar collectors can be installed in an appropriate area far from the demand. However, the design method they developed did not incorporate the optimization of the heat transmission pipeline [30].

Hsu et al. proposed an optimization method for designing and evaluating waste heat-driven DCSs. Their model considers the total capital and operation cost as the objective function, with the capacities of the absorption chiller and cold storage tank as objective variables. However, their optimization method is limited to local DCSs as it does not include the heat transmission infrastructures. Mohsen et al. [31] techno-economically investigated a thermally driven DCS using natural gas as a heat source. Their study demonstrated its capability to significantly reduce electricity consumption in a typical hot climate region in Iran. They developed an optimizing method for determining the capacity of chillers and the chilled water distribution network. When it comes to the use of nuclear power, nuclear facilities are typically situated far from urban areas, necessitating long-distance heat transportation when utilizing nuclear heat for district heating and cooling applications. This heat may be recovered from conventional nuclear power plants or generated by heat-only small modular reactor technologies [28].

Given that a nuclear heat-driven DCS is proposed here, the heat transmission system is an essential part that should be meticulously modeled. Safa [32] conducted a case study-based techno-economic evaluation concerning the recovery and long-distance transportation of large-scale heat from a nuclear power plant for district heating purposes. The study demonstrated the feasibility of heat transmission over long distances (greater than 100 km). The potential economic benefits and the elimination of carbon emissions through upgrading nuclear power plants to a co-generation mode have been evaluated for several European nuclear power plants [33]. A detailed techno-economic model was developed to examine the feasibility of heat transportation for district heating. It was shown that the most critical factors influencing the economics of long-distance heat transmission are the heat transmission temperature, heat production or recovery cost, the price of electricity, the amount of transported thermal power, and the transmission distance [34]. In another study, the design of a heat transportation system that connects a co-generation-operated nuclear power plant to a district heating network was optimized. The objective variables to be optimized include pipe diameter, insulation thickness, supply/return temperature, and the number of pumping stations [35].

According to this review, nuclear heat-driven district cooling systems could provide several benefits, such as saving electricity and reducing carbon emissions. However, several limitations and challenges should be taken into consideration. Defining the site for nuclear facilities involves various administrative, social, environmental, and techno-economic factors, sometimes leading to installations far from urban areas [36]. Therefore, it is crucial to carefully investigate the techno-economic limitations of long-distance heat transmission, including costs, pumping requirements, heat losses, temperature drops, etc. [34]. Moreover, certain technical challenges and constraints can limit the load-following capability of nuclear power plants [37]. District cooling systems may not be the most competitive solution in areas with low population density due to the significant rise in capital costs for the distribution piping network [38]. One of the main drawbacks of thermally driven refrigeration technologies is their low coefficient of performance (COP). Numerous ideas and technologies have been developed to overcome this limitation to enhance the COP of absorption-based chillers. For instance, water/lithium bromide double-effect absorption chillers offer a doubled COP (typically 1.7) compared to single-effect types (typically 0.7), but they require operation with a higher temperature heat source [39]. However, this enhancement of COP presents trade-offs that must be carefully considered, such as the impact of increased heat transmission losses and associated costs resulting from raising the temperature of the driving fluid.

1.5 The proposed system and the objectives

The novel idea proposed in this thesis is employing heat-only small modular reactor technology for district cooling applications. This study evaluates this idea from two perspectives, energy policy, and investor's viewpoints, in addition to studying the power grid under high penetration of the proposed system. First, to investigate the techno-economic aspects of the proposed system from an energy policy viewpoint, two approaches are modeled and compared. The electric-driven district cooling approach, which is currently the most adopted scenario in the world, against the proposed carbon-neutral thermally driven DCS as illustrated in Fig. 14 and Fig. 15. The evaluation focuses on the energy supply side, regardless of the distribution piping network, which is identical for both approaches. The proposed system's economic and environmental aspects, including the reduction of the electrical power generation expansion, elimination of CO2 emissions, and the levelized costs of the supplied cooling demand, are evaluated compared with the electric-driven scenarios.

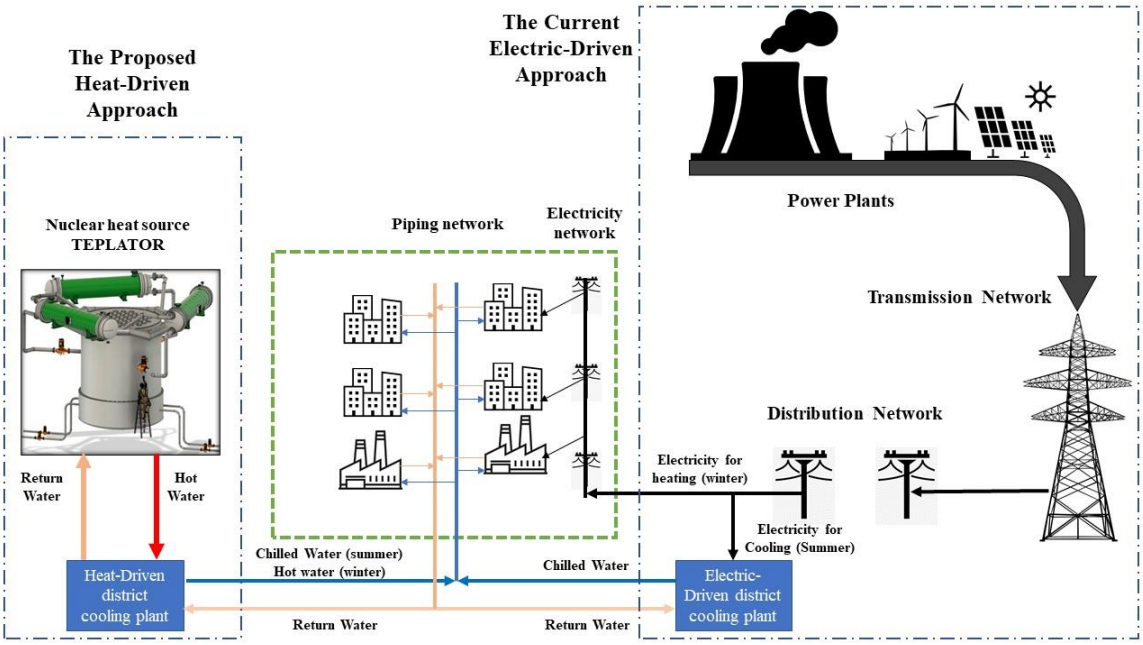

Figure 14: Current and the proposed strategy for serving cooling and heating demand.

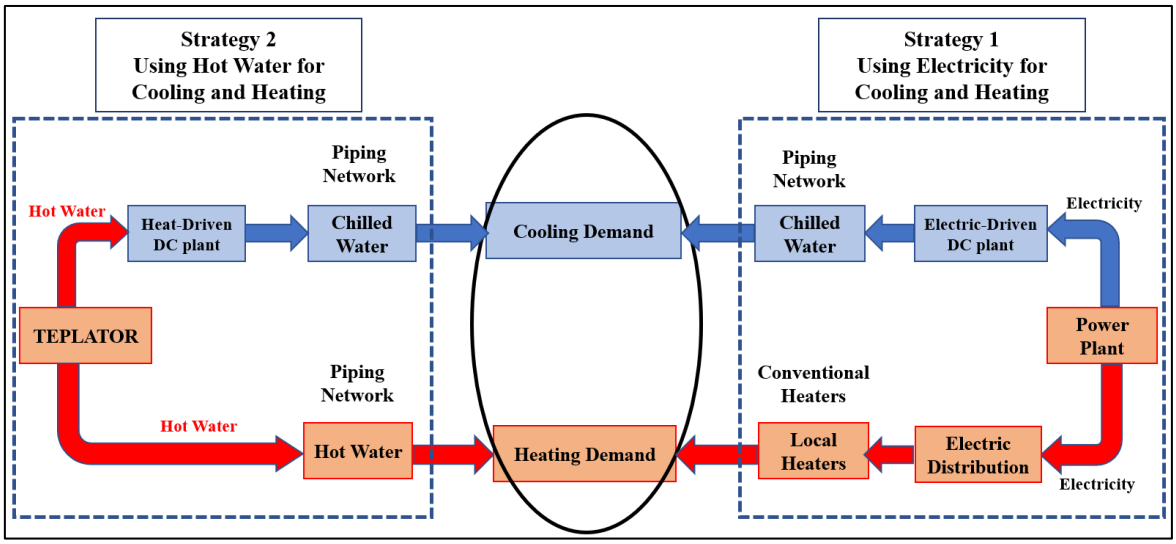

Figure 15: The approaches for serving the cooling and heating demand.

The second purpose is to study the effects of high penetration of thermally driven district cooling systems on the power grid (generation and transmission of electricity). A conceptual drawing of this purpose is shown in Fig. 16. A typical power system is simulated using a load flow method, assuming several cases of different shares of thermally driven DCSs in different locations. The critical indices investigated here are the power flow in the transmission grid, saving power generation capacity, and the marginal cost of electricity generation.

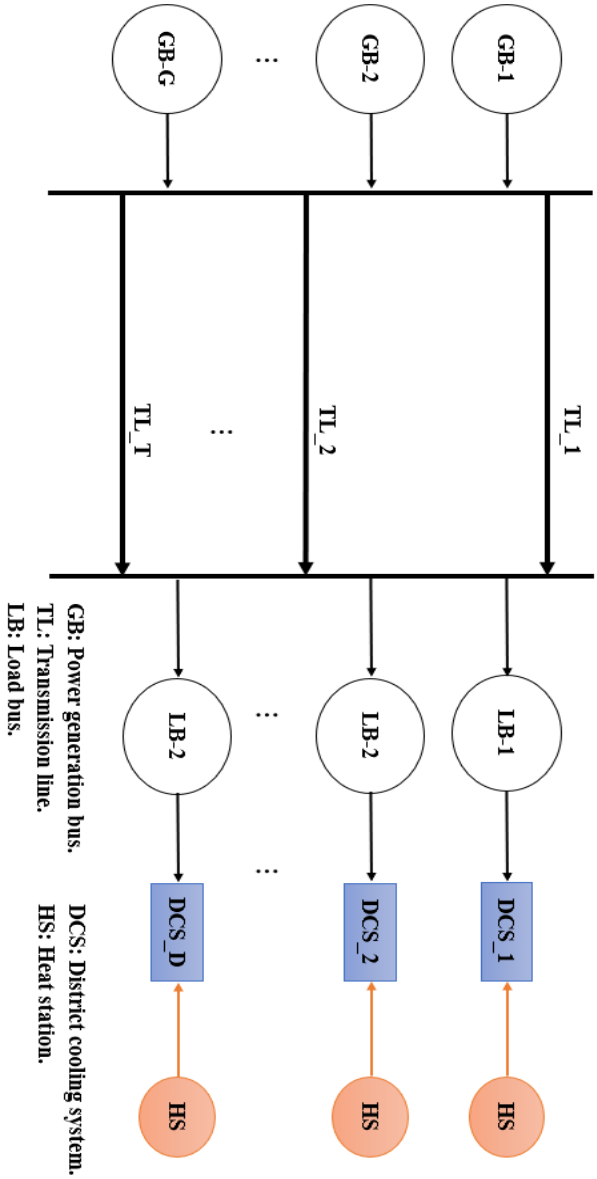

Figure 16: Schematic diagram of power system and DCSs expansion.

The third objective of this dissertation is to develop a design and operation optimization method for the proposed system and investigate its economic feasibility from an investor's perspective. Therefore, a more detailed model for the proposed heat-driven DCS is developed as illustrated in Fig. 17. The alternative/supportive units, such as thermal storage, gas boilers, and compression cycle chillers, are included to provide a competitive optimization environment between the heat sources (nuclear heat source vs. gas boiler and heat storage), and between cold supply units (absorption chillers vs compression chillers vs cold storage). The purpose is to optimize the design and operation of such a system, where the techno-economic aspects are formulated and an appropriate algorithm is developed.

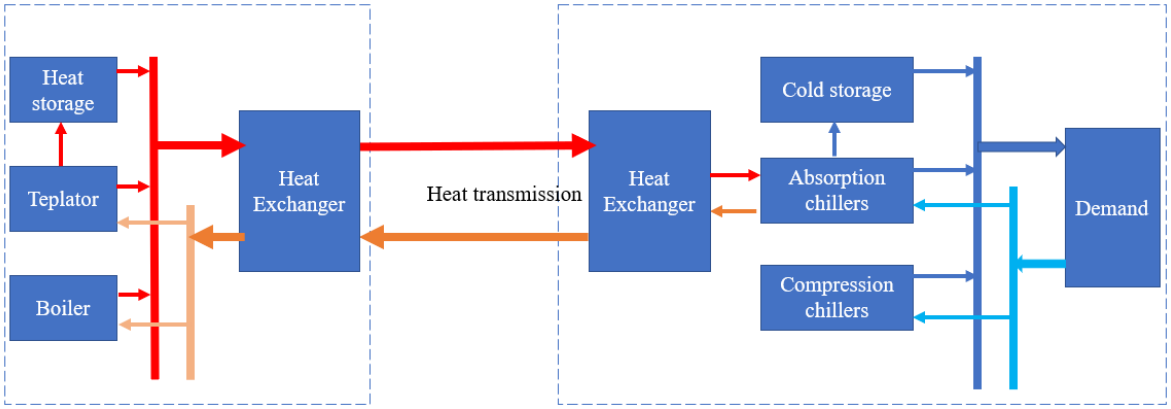

Figure 17: The conceptual illustration of the proposed system.

2 Models and formulations

This dissertation has three main objectives. The first one is evaluating the proposed nuclear heat-driven district cooling approach from an energy policy perspective. The second target is an assessment of the electrical power grid under high penetration of thermally driven DCSs. The third purpose is to optimize the proposed system's design and operation and evaluate its feasibility from the investor's viewpoint. Therefore, the models and formulations are structured in three main subsections.

2.1 Evaluation of the proposed system from energy policy perspective

To clarify the problem, Fig. 18 illustrates the currently most adopted cooling approach, i.e., electric-driven district cooling (Strategy 1), and the proposed system, Strategy 2, where the general steps of energy generation, transmission, conversion, and final distribution are indicated. The heat-driven DC approach needs heat plants to produce heat (hot water), BHT pipelines, and absorption cycle cooling plants. The same infrastructure could also cover the heating needs during winter. In contrast, the electric-driven DC leads to the installation of power plants to generate electricity to supply the electric-driven (compression cycle) cooling plants through the electricity transmission and distribution network. In this case, the heating demand is provided using local heaters at the consumer site.

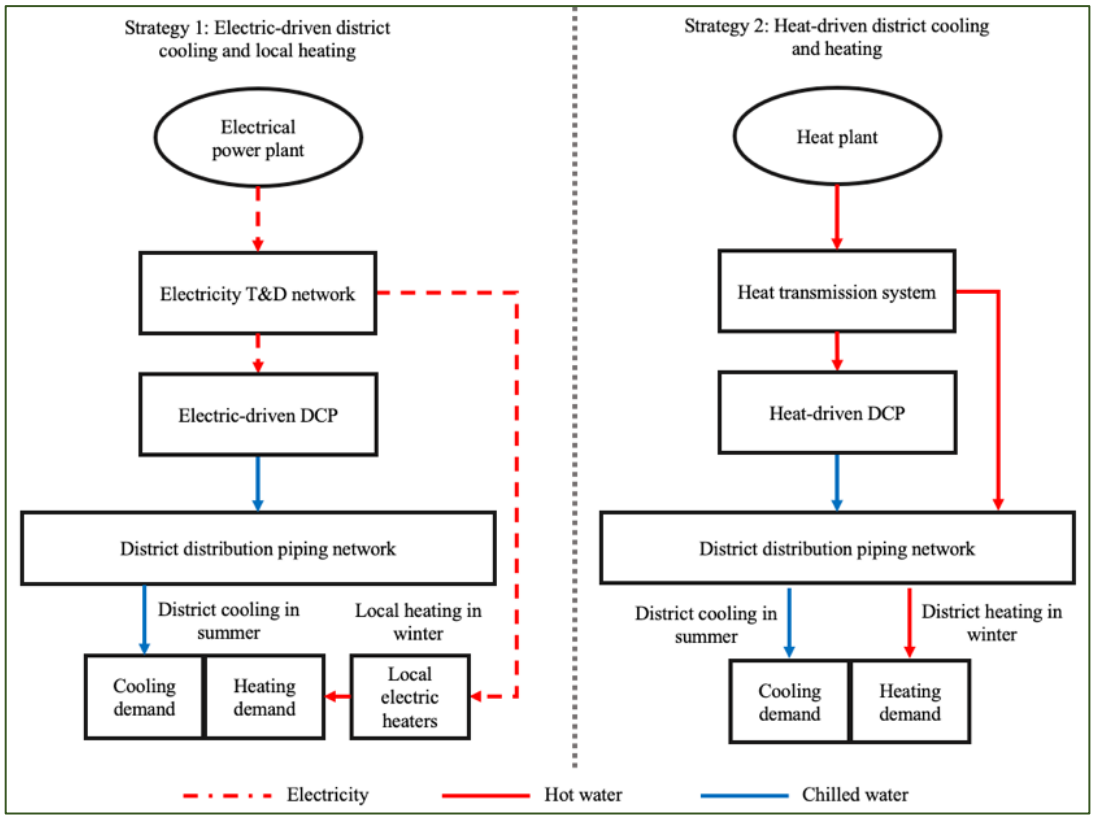

Figure 18: Electric-driven and heat-driven cooling/heating approaches.

The developed economic method to compare these two strategies is based on the present value of the costs addressed in Table 2, formulated based on per unit (specific) costs, i.e., without dealing with a specific and detailed case study. According to the capacities, the construction and fixed O&M costs, and according to the calculated generated energy, the fuel, variable O&M, and carbon emissions costs are achieved. The calculation flowchart evaluating these strategies is shown in Fig. 19, and the associated formula number is addressed within parentheses in each block. The formulations are given in detail in the following subsections.

Table 2: The decision-making factors.

Heat-driven approach	Electric-driven approach
Construction cost of heat-plant	Construction cost of electrical power plant
Construction cost of heat-driven DCP	Construction cost of electrically driven DCP
O&M cost of heat-plant and DCP	O&M Cost of the power plant and DCP
Heat-plant fuel cost	Power plant fuel cost
Bulk heat transmission cost	Electricity T&D cost
Carbon emission cost	Carbon emission cost

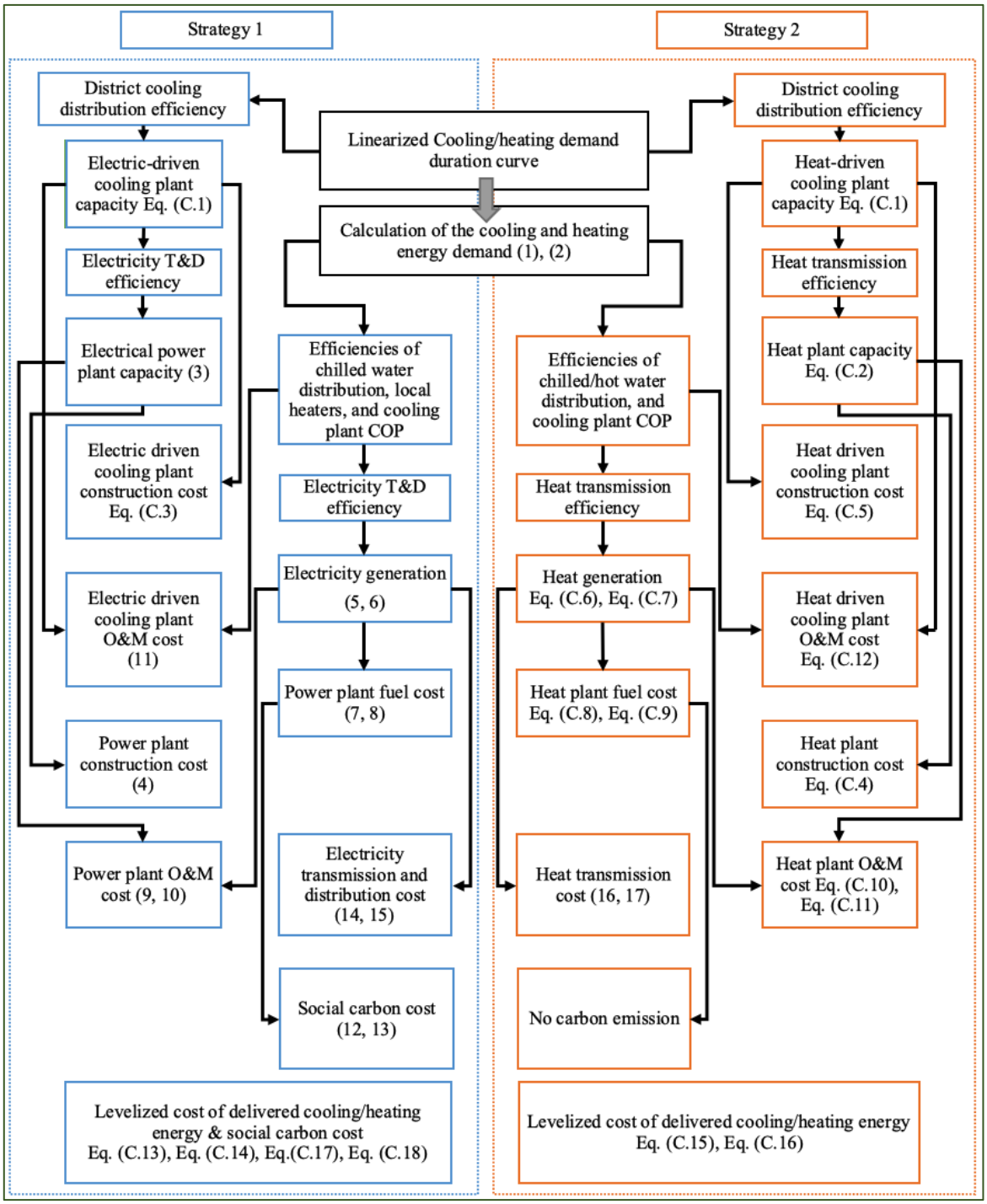

Figure 19: Calculation flowchart.

2.1.1 Formulation of cooling and heating demand duration curve

The complete customer energy profiles are usually used for analyzing the operating conditions and the dynamics of systems. The concept of load duration curve is mainly used for planning purposes, indicating the "relationship between time and demand" and for showing the "percent of the time, the demand is greater or equal to a certain level" [40]. Here, the linearized load duration curve of cooling and heating demand (LCHDC) is modeled in peak and average levels, as shown in Fig. 20.

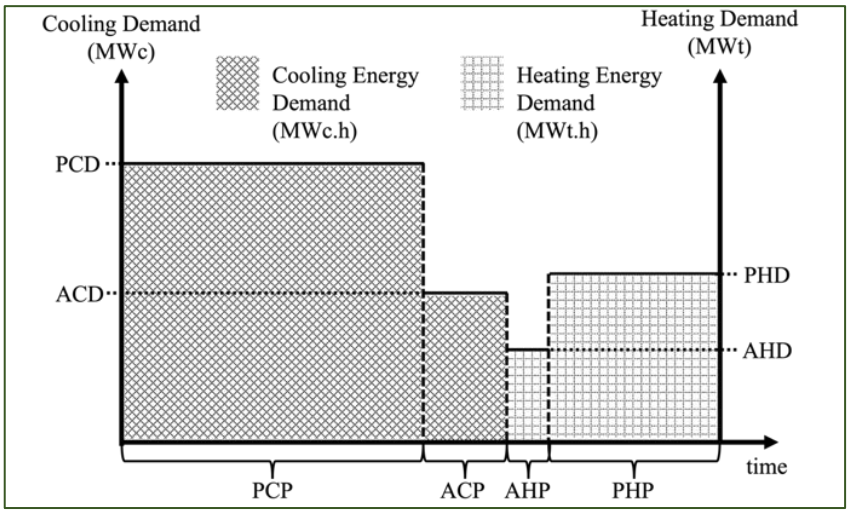

Figure 20: Cooling and heating demand duration curve.

Total cooling energy demand (*TCED*) in (MW_c.h) and total heating energy demand (*THED*) in (MW_t.h) are formulated in (1a) and (2a), where (*PCD*) and (*ACD*) are in (MW_c) and (*PHD*) and (*AHD*) are in (MWt).

$$TCED = PCD \times PCP + ACD \times ACP \quad (1a)$$

$$THED = PHD \times PHP + AHD \times AHP \quad (2a)$$

2.1.2 Formulation of power plant capacities and capital Costs

Strategy 1 represents the electric-driven district cooling approach, where electrical power plants supply the electric-driven district cooling plant through the electricity T&D network. In this case, the required power plant capacity (*PPC*) is formulated in (3a), where (*CDC*) is the estimated total cooling demand capacity. ($Ef_{T\&D}^{El}$) is electricity T&D efficiency and (Ef_D^{cw}) is the efficiency of chilled water distribution. The present value of construction costs of the power plant (CC_{PP}^{pv}) is formulated in (4a), where the specific construction cost of the power plant is (CC_{PP}^{S}). The reconstruction cost along the DMP required at the end of each lifetime (lt) on year (r) is included in the formulations, and (RCP_{PP}) represents the reconstruction cost of the power plant determined as a percentage of the initial construction cost. The capacity of the cooling plant is given in (5a), and the present value of its construction costs is given in (6a).

$$PPC = \frac{CDC}{Ef_D^{cw} \times Ef_{T\&D}^{El} \times COP_{EDC}} \quad (3a)$$

$$CC_{PP}^{pv} = PPC \times CC_{PP}^{S} \times \left[1 + \sum_{r}^{DMP} RCP_{PP} \times (1+i)^{-r}\right], \quad r = \begin{cases} x \times lt_{PP}, & r < DMP \\ x = 1, 2, \dots, \frac{DMP}{lt_{PP}} \end{cases} \quad (4a)$$

$$CPC = \frac{CDC}{Ef_D^{cw}} \quad (5a)$$

$$CC_{ECP}^{pv} = CPC \times CC_{ECP}^{S} \times \left[1 + \sum_{r}^{DMP} RCP_{ECP} \times (1+i)^{-r}\right], \quad r = \begin{cases} x \times lt_{ECP}, & r < DMP \\ x = 1, 2, \dots, \dfrac{DMP}{lt_{ECP}} \end{cases} \tag{6a}$$

In the case of Strategy 2, the heat plants supply hot water through BHT pipelines to drive the heat-driven district cooling plant. The heat-driven cooling plant capacity is the same as the electric-driven, formulated in (5a). A similar method is used for calculating the capacity of the heat plant given in (7a) and the present value of construction costs of the heat plant and heat-driven cooling plant given in (8a) and (9a), respectively.

$$HPC = \frac{CPC}{Ef_{T}^{BH} \times COP_{HDC}} \tag{7a}$$

$$CC_{HP}^{pv} = HPC \times CC_{HP}^{S} \times \left[1 + \sum_{r}^{DMP} RCP_{HP} \times (1+i)^{-r}\right], \quad r = \begin{cases} x \times lt_{HP}, & r < DMP \\ x = 1, 2, \dots, \dfrac{DMP}{lt_{HP}} \end{cases} \tag{8a}$$

$$CC_{HCP}^{pv} = CPC \times CC_{HCP}^{S} \times \left[1 + \sum_{r}^{DMP} RCP_{HCP} \times (1+i)^{-r}\right], \quad r = \begin{cases} x \times lt_{HCP}, & r < DMP \\ x = 1, 2, \dots, \dfrac{DMP}{lt_{HCP}} \end{cases} \tag{9a}$$

2.1.3 Formulation of the produced energy and fuel cost

In the case of Strategy 1, electricity drives the electric-driven cooling plant for district cooling and is locally consumed by heaters for heating applications. Therefore, the total generation of electricity required for cooling (TGEC) and heating (TGEH) are formulated in (10a) and (11a), respectively, where (Ef_{LH}) is the efficiency of local electric heating. The present value of costs of fuel consumed by the power plant for supplying the cooling is given in (12a), and for heating is formulated in (13a).

$$TGEC = \frac{TCED}{COP_{EDC} \times Ef_{D}^{cw} \times Ef_{T\&D}^{El}} \tag{10a}$$

$$TGEH = \frac{THED}{Ef_{LH} \times Ef_{T\&D}^{El}} \tag{11a}$$

$$FC_{PP}^{pv,C} = \sum_{r=1}^{DMP} \frac{TGEC \times HRPP \times FP}{DMP} \times (1+i)^{-r}) \tag{12a}$$

$$FC_{PP}^{pv,H} = \sum_{r=1}^{DMP} \frac{TGEH \times HRPP \times FP}{DMP} \times (1+i)^{-r} \tag{13a}$$

In the case of Strategy 2, heat (hot water) is used to drive the heat-driven cooling plant for district cooling and supply the heating demand during winter. The electricity needed for

a heat-driven cooling plant is about 5% of the total produced thermal energy [41]; therefore, it has been neglected. Thus, the total generation of heat required for cooling (TGHC) and heating (TGHH) are formulated in (14a) and (15a), respectively. The present value of the costs of fuel consumed by the heat plant for supplying the cooling and heating is given in (16a) and (17a), respectively.

$$TGHC = \frac{TCED}{COP_{HDC} \times Ef_D^{cw} \times Ef_T^{BH}} \quad (14a)$$

$$TGHH = \frac{THED}{Ef_D^{hw} \times Ef_T^{BH}} \quad (15a)$$

$$FC_{HP}^{pv,C} = \sum_{r=1}^{DMP} \frac{TGHC \times HRHP \times FP}{DMP} \times (1+i)^{-r} \quad (16a)$$

$$FC_{HP}^{pv,H} = \sum_{r=1}^{DMP} \frac{TGHH \times HRHP \times FP}{DMP} \times (1+i)^{-r} \quad (17a)$$

2.1.4 Formulation of operation and maintenance costs

The fixed O&M cost represents the annual independence of generation costs such as staff salaries, recurring maintenance costs, insurance, and administration fees. For Strategy 1, the present value of the O&M cost of the electrical power plant (for cooling and heating durations) and electric-driven cooling plant (for the cooling duration), represented by ($OMC_{PP}^{pv,C}$, $OMC_{PP}^{pv,H}$, $OMC_{ECP}^{pv,C}$), formulated in (18a-20a), where (OMC_{PP}^{V}, OMC_{ECP}^{V}) are the specific variable, and (OMC_{PP}^{AF}, OMC_{ECP}^{AF}) are the specific annual fixed O&M costs, respectively.

$$OMC_{PP}^{pv,C} = \sum_{r=1}^{DMP} \left(\frac{TGEC \times OMC_{PP}^{V} + PPC \times OMC_{PP}^{AF} \times Cd}{DMP}\right) \times (1+i)^{-r} \quad (18a)$$

$$OMC_{PP}^{pv,H} = \sum_{r=1}^{DMP} \left(\frac{TGEH \times OMC_{PP}^{V} + PPC \times OMC_{PP}^{AF} \times Hd}{DMP}\right) \times (1+i)^{-r} \quad (19a)$$

$$OMC_{ECP}^{pv,C} = \sum_{r=1}^{DMP} \frac{\left(\frac{TCED}{Ef_D^{cw}}\right) \times OMC_{ECP}^{V} + CPC \times OMC_{ECP}^{AF} \times Cd}{DMP} \times (1+i)^{-r} \quad (20a)$$

For Strategy 2, the present value of the O&M cost of the heat plant (for cooling and heating durations) and heat-driven cooling plants (for the cooling duration) are given in (21a-23a), respectively.

$$OMC_{HP}^{pv,C} = \sum_{r=1}^{DMP} \left(\frac{TGHC \times OMC_{HP}^{V} + HPC \times OMC_{HP}^{AF} \times Cd}{DMP}\right) \times (1+i)^{-r} \quad (21a)$$

$$OMC_{HP}^{pv,H} = \sum_{r=1}^{DMP} \left(\frac{TGHH \times OMC_{HP}^{V} + HPC \times OMC_{HP}^{AF} \times Hd}{DMP}\right) \times (1+i)^{-r} \quad (22a)$$

$$OMC_{HCP}^{pv,C} = \sum_{r=1}^{DMP} \frac{\left(\frac{TCED}{Ef_{D}^{cw}}\right) \times OMC_{HCP}^{V} + CPC \times OMC_{HCP}^{AF} \times Cd}{DMP} \times (1+i)^{-r} \quad (23a)$$

2.1.5 Formulation of social carbon cost

Social carbon cost is determined for evaluating the resulting economic damages due to the emission of one more ton of CO2 [42]. In the case of Strategy 1, the present value of the accumulated social carbon cost emitted from electricity generation (used for cooling and heating) is formulated in (2a4) and (25a), respectively, where (CO2R) is the amount of carbon emission per unit fuel consumption. (SCCS) is the specific social carbon cost ($/ton). The second Strategy employs a nuclear heat source with no carbon emissions.

$$SCC_{PP}^{pv,C} = \sum_{r=1}^{DMP} \frac{TGEC \times HRPP \times CO2R \times SCC^{S}}{DMP} \times (1+i)^{-r} \quad (24a)$$

$$SCC_{PP}^{pv,H} = \sum_{r=1}^{DMP} \frac{TGEH \times HRPP \times CO2R \times SCC^{S}}{DMP} \times (1+i)^{-r} \quad (25a)$$

2.1.6 Formulation of the heat and electricity transmission cost

In the case of the electric-driven Strategy, the generated electricity is transmitted through the electrical T&D grid and delivered to the electric-driven cooling plant for district cooling or local electric heaters for heating applications. The specific cost of electricity T&D (T_{El}^{S}) is used for estimating the electricity T&D cost [43], [44]. The present value of electricity T&D cost required for cooling and heating ($T_{El}^{pv,C}$, $T_{El}^{pv,H}$), is given in (26a, 27a) respectively.

$$T_{El}^{pv,C} = \sum_{r=1}^{DMP} \frac{TGEC \times T_{El}^{S}}{DMP} \times (1+i)^{-r} \quad (26a)$$

$$T_{El}^{pv,H} = \sum_{r=1}^{DMP} \frac{TGEH \times T_{El}^{S}}{DMP} \times (1+i)^{-r} \quad (27a)$$

In the case of the heat-driven Strategy, hot water generated by the heat plant is transported by BHT pipelines to drive the heat-driven district cooling plant or supply the heating demand during winter. For an accurate heat transportation cost calculation, a techno-economic optimization for designing the heat transmission system is required, considering many factors such as supply/return temperature and pressure, distance, hourly transferred heat, pressure drop and needed pumping, different pipeline configurations, and insulation types

[32], [34]. Furthermore, optimum siting of nuclear plants is a complicated multi-criteria problem. Fig. 21 represents population-related reactor siting regulations suggested by the U.S. Nuclear Regulatory Commission [45]. The same design of an SMR implemented in different locations may result in other distance criteria depending on dose criteria, policy factors, and public acceptance [45], [46]. Therefore, the concept of specific cost of bulk heat transmission (T_{BH}^{S}) introduced in [47] is used in our model. The present value of the cost of bulk heat transmission required for cooling and heating ($T_{BH}^{pv,C}$, $T_{BH}^{pv,H}$), is given in (28a) and (29a) respectively.

$$T_{BH}^{pv,C} = \sum_{r=1}^{DMP} \frac{TGHC \times T_{BH}^{S}}{DMP} \times (1+i)^{-r} \quad (28a)$$

$$T_{BH}^{pv,H} = \sum_{r=1}^{DMP} \frac{TGHH \times T_{BH}^{S}}{DMP} \times (1+i)^{-r} \quad (29a)$$

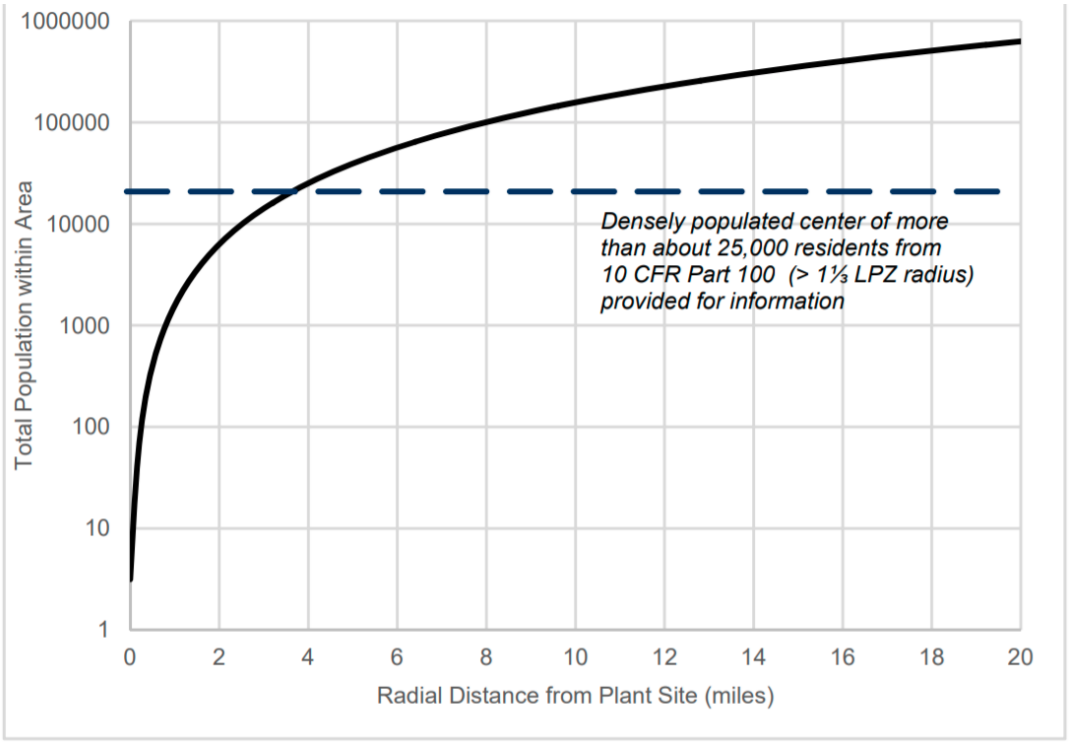

Figure 21: Population vs. radius distance of NPPs - RG guidance [45].

2.1.7 Formulation of the levelized costs of cooling and heating energy supply

The levelized costs are helpful to compare different approaches from a planning and policy-making point of view. For Strategy 1, the levelized cost to supply one (MWc.h) of cooling demand is given in (30a), and for Strategy 2 is provided in (31a). The levelized cost to supply one (MWt.h) of heating demand is given in (32a) for Strategy 1, and for Strategy 2, it is given in (33a). These levelized costs do not include the district distribution network

(infrastructure, piping, etc.) costs or individual heaters (used for heating by consumers in the case of Strategy 1) since we assume they already exist. Since the cooling demand is significantly larger than the heating demand in the hot climate regions, the construction cost of either the electrical power plant or heat plant is included only in the levelized cooling cost formulations. Concerning carbon emissions, the levelized social carbon cost emitted from the generated electricity (Strategy 1) for supplying the cooling and heating demand is formulated in (34a) and (35a), respectively, while no carbon is emitted from the nuclear approach.

$$LCC_{\mathrm{EDs}} = \frac{CC_{PP}^{pv} + FC_{PP}^{pv,C} + OMC_{PP}^{pv,C} + T_{El}^{pv,C} + CC_{ECP}^{pv} + OMC_{ECP}^{pv,C}}{\frac{TCED}{DMP} \times \sum_{n=1}^{DMP}(1+i)^{-n}} \quad (30a)$$

$$LCH_{\mathrm{EDs}} = \frac{FC_{PP}^{pv,H} + OMC_{PP}^{pv,H} + T_{El}^{pv,H}}{\frac{THED}{DMP} \times \sum_{n=1}^{DMP}(1+i)^{-n}} \quad (31a)$$

$$LCC_{\mathrm{HDs}} = \frac{CC_{HP}^{pv} + FC_{HP}^{pv,C} + OMC_{HP}^{pv,C} + T_{BH}^{pv,C} + CC_{HCP}^{pv} + OMC_{HCP}^{pv,C}}{\frac{TCED}{DMP} \times \sum_{n=1}^{DMP}(1+i)^{-n}} \quad (32a)$$

$$LCH_{\mathrm{HDs}} = \frac{FC_{HP}^{pv,H} + OMC_{HP}^{pv,H} + T_{BH}^{pv,H}}{\frac{THED}{DMP} \times \sum_{n=1}^{DMP}(1+i)^{-n}} \quad (33a)$$

$$LSCC_{PP}^{C} = \frac{SCC_{PP}^{pv,C}}{\frac{TCED}{DMP} \times \sum_{n=1}^{DMP}(1+i)^{-n}} \quad (34a)$$

$$LSCC_{PP}^{H} = \frac{SCC_{PP}^{pv,H}}{\frac{THED}{DMP} \times \sum_{n=1}^{DMP}(1+i)^{-n}} \quad (35a)$$

2.1.8 Case study

2.2 The effects of thermally driven district cooling on the power generation and transmission

Serving the cooling demand by heat-driven plants reduces the consumption and, consequently, the generation and transmission of electricity. In a power system, there are different power plants that use various fuels of different technologies, capacities, and technical constraints, with less or more generation costs. Optimal power flow (OPF) is a calculation method that minimizes the total electricity generation cost by determining the optimal outputs of the available power plants to meet the entire electrical needs of the power grid [48]. Expansion of the heat-driven district cooling systems of different capacities in different areas will benefit the power grid. Fig. 22 represents the developed algorithm for evaluating this matter. Formula (1b) is usually used for modeling a power plant generation cost (PPGC), which is a function of the power output in MW (P). The total cost of power

generation (TCPG), which needs to be minimized, is the sum of the generation costs of the online plants as formulated in (2b). (NPP) is the number of power plants, and a, b, and c are the cost coefficients. This algorithm is used to evaluate the operation of a typical power grid during the peak time, considering the electricity demand eliminated by an assumed thermally driven district cooling.

$$PPGC_p = c_p + b_p P_p + a_i {P_p}^2 \quad (1b)$$

$$TCPG = \sum_{p=1}^{NPP} PPGC_p \quad (2b)$$

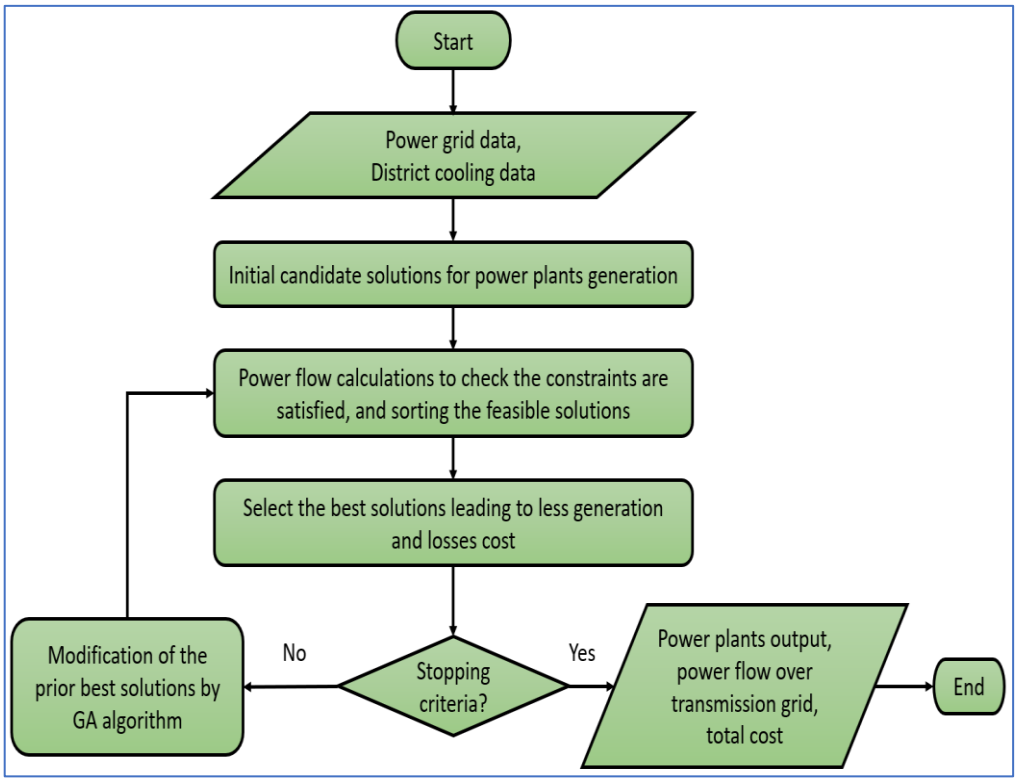

Figure 22: Algorithm of evaluating the effect of thermally driven district cooling on the power grid.

2.3 Optimization of the proposed system and its evaluation from the investor's perspective

The objective function of the optimization expressed in (1) is determined to minimize the present value of the system's total construction and hourly-based operation costs supplying typical cooling energy load, which is over the decision-making period (DMP) and based on discounted cash flow analysis. The system's design capacities and one-year hourly operation are the objective variables where the technical constraints must be satisfied. The construction cost of the heat supply station, heat transmission system, and cooling supply station (CC_{hss}, CC_{bht}, CC_{css}), are associated with their design capacities and technologies. The operation

cost of the mentioned systems (OC_{hss}, OC_{bht}, OC_{css}), (in addition to the nominal capacities and technologies), depends on the electricity and fuel prices and their operating schedule.

$$min. \quad OF = CC_{hss} + OC_{hss} + CC_{bht} + OC_{bht} + CC_{css} + OC_{css} \tag{1c}$$

2.3.1 Technical formulations

2.3.1.1 Technical equations of the cooling station

The cooling station is responsible for providing the forecasted hourly cooling demand (CD^i) using a combination of the candidate units: absorption chillers (AC), electric-driven compression chillers (CC), and cold storage (CS). The cooling capacities of the AC, CC, and CS expressed by (Cp_{ac}, Cp_{cc}, Cp_{cs}) respectively, are the design variables. The operation variables are their hourly cooling power expressed by (CG^i_{ac}, CG^i_{cc}, CG^i_{cs}), respectively. To ensure adequate cooling supply, the total cooling power during any given hour (i) must meet the cooling demand at that time, according to equation (2c). The cooling power generated by the chillers should not exceed their nominal capacity, as expressed in equations (3c, 4c). Additionally, the hourly increase or decrease in cooling power should remain within a practical range to ensure smooth operation and prevent sudden fluctuations, as indicated in equations (5c, 6c). The parameters (RR_{ac}, RR_{cc}) represent the ramp rates of the absorption and compression chillers, respectively, defined as a percentage of the nominal capacity.

$$CD^i = CG^i_{ac} + CG^i_{cc} + CG^i_{cs} \qquad i = 1, \dots, N \tag{2c}$$

$$CG^i_{ac} \le Cp_{ac} \qquad i = 1, \dots, N \tag{3c}$$

$$CG^i_{cc} \le Cp_{cc} \qquad i = 1, \dots, N \tag{4c}$$

$$CG^{i-1}_{ac} - Cp_{ac}\, RR_{ac} \le CG^i_{ac} \le CG^{i-1}_{ac} + Cp_{ac}\, RR_{ac} \qquad i = 2, \dots, N \tag{5c}$$

$$CG^{i-1}_{cc} - Cp_{cc}\, RR_{cc} \le CG^i_{cc} \le CG^{i-1}_{cc} + Cp_{cc}\, RR_{cc} \qquad i = 2, \dots, N \tag{6c}$$

The cold storage operation is subject to certain constraints given in equations (7c- 10c). The negative value of the variable (CG^i_{cs}) represents the cold storage charging power, and its positive value represents the discharging power. The charging and discharging power is limited to the maximum hourly rates (RR^{ch}_{cs}, RR^{dch}_{cs}), respectively, as expressed in (7c). The variable (SE^i_{cs}) represents the stored cooling energy at a specific hour (i), which can be calculated by equation (8c). Obviously, the discharged power during each hour must not exceed the stored energy according to (9c), and the charging power must not exceed the available free capacity of the cold storage according to (10c).

$$-RR^{ch}_{cs} \le CG^i_{cs} \le RR^{dch}_{cs} \qquad i = 1, \dots, N \tag{7c}$$

$$SE^i_{cs} = SE^{i-1}_{cs} - CG^{i-1}_{cs} \qquad i = 2, \dots, N \tag{8c}$$

$$CG_{ac}^{i} \le SE_{cs}^{i}, \quad Discharging, \quad CG_{cs}^{i} > 0 \quad i = 1, \dots, N \quad (9c)$$

$$-CG_{cs}^{i} \le Cp_{cs} - SE_{cs}^{i}, \quad Charging, \quad CG_{cs}^{i} < 0 \quad i = 1, \dots, N \quad (10c)$$

2.3.1.2 Technical equations of the heat transmission system

The heat transmission system consists of a heat exchanger on the heat station side, supply/return water pipelines, pressure-boosting pumping equipment, and a heat exchanger on the cooling station side. The thermal capacity of the heat exchanger on the heat station side (Cp_{hex}) is modeled in equation (11c). This capacity is designed in order to cover the thermal power required by the absorption chillers plus the losses over the transmission pipeline. In these equations (Cp_{ac}) represents the total capacity of the absorption chilling technology, and (COP_{ac}) denotes its average coefficient of performance. The heat transmission losses (Q^{HTL}, MWt) is estimated by equation (12c) [34], where (L) represents the one-way length of the pipeline (m), (s) is the insulation thickness (mm), (hi) is the insulation conductivity (W/m.K), and (ΔT_{bht}) represents the temperature difference between supply and return water.

$$Cp_{hex} = Q^{HTL} + (Cp_{ac}/COP_{ac}) \quad (11c)$$

$$Q^{HTL} = \frac{2 \times 10^{-6}\, \pi\, L\, \Delta T_{bht}\, hi}{\ln\left(1 + 2\frac{s}{D}\right)} \quad (12c)$$

The heat transfer area (A_{hex}, m^2) of the heat exchanger on the heating station side, which is of the plate type, is formulated in equation (13c). In this equation, ($LMTD$) is the logarithmic mean temperature difference, which can be calculated according to (14c). (ΔT_A) is the temperature difference between the inlet hot water and outlet cold water, and (ΔT_B) is the temperature difference between the outlet hot water and the inlet cold water. The heat transfer coefficient (U) in (W/m^2.K), is a parameter of the heat exchanger [49]. Similar formulations are employed for designing the heat exchanger on the cooling station side; however, in that case, the calculations do not include the heat transmission losses.

$$A_{hex} = \frac{Cp_{hex}}{U \cdot LMTD} \quad (13c)$$

$$LMTD = \frac{\Delta T_A - \Delta T_B}{\ln \Delta T_A - \ln \Delta T_B} \quad (14c)$$

The hourly transported heat (Q_{bht}^{i}, MWt) given in (15c), establishes a connection between the objective variables of the cooling and heating sides. Equations (16c – 19c) are used to calculate the practical range for heat transmission based on the pipe diameter. In these equations ($\dot{m}_{bht}^{i}$) stands for the mass flow rate (kg/s), (C_p) represents the specific heat capacity of water (Ws/kg.K), (ρ) is the density of water (kg/m^3), and (c) is the flow velocity

(m/s). The thermal power transmission limits (20c) associated with a given diameter are determined by assuming a feasible range for the flow velocity (19c) and using equation (18c). It is crucial to satisfy this constraint during the optimization process to ensure the system operates within the specified thermal power transmission limits.

$$Q_{bht}^{i} = Q^{HTL} + (CG_{ac}^{i}/COP_{ac}) \qquad i = 1, \dots, N \qquad (15c)$$

$$Q_{bht}^{i} = \frac{\dot{m}_{bht}^{i}\, C_p\, \Delta T_{bht}}{10^6} \qquad i = 1, \dots, N \qquad [35]\ (16c)$$

$$\dot{m}_{bht}^{i} = \rho\, c\, D^2/4 \qquad i = 1, \dots, N \qquad (17c)$$

$$Q_{bht}^{i} = \frac{D^2\, C_p\, \Delta T_{bht}\, \pi\, \rho\, c}{4 \times 10^6} \qquad i = 1, \dots, N \qquad (18c)$$

$$c^{Min} \le c^{i} \le c^{Max} \qquad i = 1, \dots, N \qquad (19c)$$

$$Q_{bht}^{Min} \le Q_{bht}^{i} \le Q_{bht}^{Max} \qquad i = 1, \dots, N \qquad (20c)$$

Pumping power is necessary to compensate for the pressure drop caused by friction losses along the pipeline. The complex nonlinear equations given in equations (21c – 26c) [50], [51] should be solved to find the hourly pumping power consumption required to balance the pressure drop. The pressure drop along the pipeline ($\Delta P, kPa$) is formulated in (23c), where (Re), the Reynolds number, calculated by equation (21c).

The flow velocity ranges from (0.5 m/s) to (4 m/s), while the pipe diameter ranges from (0.5 m) to (2.5 m), resulting in Reynolds numbers ranging from (850 340) to (34 013 605). When the Reynolds number exceeds (4000), the flow becomes turbulent. Therefore, to estimate the friction factor (f) in turbulent flows, the Colebrook-White equation (22c) is used [51]. In these equations, (Sg) represents the specific gravity of water with a density of (1 g/cm3), and (ν, ε) denote the kinematic viscosity of water and the roughness of the pipe, respectively. The required electrical pumping power (P, MWe) is formulated in (24c), with (η_{ps}) representing the pump's efficiency.

Due to the nonlinearity of these equations, directly including them in the optimization would result in time-consuming calculations that may not be feasible within a reasonable time. Furthermore, the friction factor cannot be calculated directly and should be solved by iterative trial and error procedures, e.g., the Newton–Raphson [51]. To address this issue, a subprogram illustrated in Fig. 23 is proposed to linearize the pumping power as a function of the transported thermal power as expressed in (25c). These linear equations will be used to estimate the pumping power. The coefficients (A_D, B_D) in equation (25c) can be determined using curve fitting tools for different pipe diameters. The capacity of the

pumping station (Cp_{ps}) is considered an objective variable by imposing the constraint (26c) during the optimization process.

$$Re = c\ D/\nu \quad (21c)$$

$$\frac{1}{\sqrt{f}} = -2log\left(\frac{\varepsilon/D}{3.7} + \frac{2.51}{Re\sqrt{f}}\right) \quad (22c)$$

$$\Delta P = 0.81\ L\ f\ \dot{m}_{bht}^2\ Sg/\rho^2 D^5 \quad (23c)$$

$$P = 10^{-3}\ \dot{m}_{bht}\ \Delta P/\rho\ \eta_{ps} \quad (24c)$$

$$P^i = A_D\ Q_{bht}^i + B_D \qquad i = 1, \dots, N \quad (25c)$$

$$Q_{bht}^i \le (Cp_{ps} - B_D)/\ A_D \qquad i = 1, \dots, N \quad (26c)$$

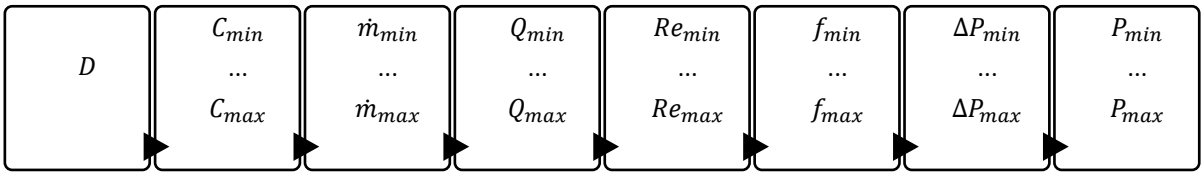

Figure 23: Linearization steps of the pumping power equation.

2.3.1.3 Technical equations of the heat supply station

The heat station supplies the required thermal power to drive the absorption chillers. The primary heat source utilized in this system is a nuclear heat-only reactor called Teplator, while the alternative option is gas boiler technology. Heat storage is also incorporated into the system, which can effectively contribute to peak shaving and enhance the load following. The total thermal power injected into the BHT pipeline is the combined supplied thermal power from these units, as formulated in (27c, 28c) (neglecting the heat exchanger losses). This supplied thermal power must cover the thermal power requirements of the absorption chillers, in addition to the pipeline losses, as given in equation (15c). In these equations (Q_{nhp}^i, Q_{gb}^i) represent the generated heat by the nuclear plants and gas boilers, respectively, and (Q_{hs}^i) represents the hourly charged or discharged power of the heat storage.

$$Q_{hss}^i = Q_{nhp}^i + Q_{hs}^i + Q_{gb}^i \qquad i = 1, \dots, N \quad (27c)$$

$$Q_{hss}^i = Q_{bht}^i \qquad i = 1, \dots, N \quad (28c)$$

The thermal output power of nuclear heat units and gas boilers is constrained to their nominal respective nominal capacity ($N_{nhp} \cdot Cp_{nhp}, Cp_{gb}$), as formulated in equations (29c, 31c). The variable (N_{nhp}) represents the number of nuclear plants, where each plant has a capacity of (Cp_{nhp}). The hourly change in thermal power (increase or decrease) should remain within the feasible operating limits of the heat source, as specified in equations (30c, 32c). The parameters (RR_{nhp}, RR_{gb}) indicate the ramp rates of the nuclear heat units and gas boilers, respectively, defined as a percentage of their nominal capacity.

$$Q_{nhp}^{i} \le N_{nhp} Cp_{nhp} \qquad i = 1, \dots, N \qquad (29c)$$

$$Q_{nhp}^{i-1} - Cp_{nhp} RR_{nhp}^{down} \le Q_{nhp}^{i} \le Q_{nhp}^{i-1} + Cp_{nhp} RR_{nhp}^{up} \qquad i = 2, \dots, N \qquad (30c)$$

$$Q_{gb}^{i} \le Cp_{gb} \qquad i = 1, \dots, N \qquad (31c)$$

$$Q_{gb}^{i-1} - Cp_{gb}\, RR_{gb} \le Q_{gb}^{i} \le Q_{gb}^{i-1} + Cp_{gb}\, RR_{gb} \qquad i = 2, \dots, N \qquad (32c)$$

The operation of the heat storage is subject to constraints formulated in (33c – 36c). The negative value of the variable (Q_{hs}^{i}) models the charging time, and the positive value determines the discharging mode. The charging and discharging power should not exceed the maximum hourly rates (RR_{hs}^{ch}, RR_{hs}^{dch}), respectively, according to (33c). The variable (SE_{hs}^{i}) represents the stored thermal energy at each hour (i), which should satisfy the energy balance as formulated in (34c, 35c). The charging power during any hour should not exceed the heat storage's free capacity at that time, according to (36c). These equations govern the operation of the heat storage.

$$-RR_{hs}^{ch} \le Q_{hs}^{i} \le RR_{hs}^{dch} \qquad i = 1, \dots, N \qquad (33c)$$

$$SE_{hs}^{i} = SE_{hs}^{i-1} - Q_{hs}^{i-1} \qquad i = 2, \dots, N \qquad (34c)$$

$$Q_{hs}^{i} \le SE_{hs}^{i}, \quad Discharging, \quad Q_{hs}^{i} > 0 \qquad i = 1, \dots, N \qquad (35c)$$

$$-Q_{hs}^{i} \le Cp_{hs} - SE_{hs}^{i}, \quad Charging, \quad Q_{hs}^{i} < 0 \qquad i = 1, \dots, N \qquad (36c)$$

2.3.2 Economic model

2.3.2.1 Construction and operation costs of the cooling station

The costs of the system can be divided into construction and operation costs. The initial capital cost of the cooling station (IC_{css}), which includes absorption chillers, compression chillers, and cold storage, is formulated in (37c). Given a large cooling demand on a city scale, it is assumed that the cooling station employs the largest commercially available size of chillers. Therefore, it is assumed that the curve of the economics of scale has reached a saturation point, meaning that further increases in chiller size would not result in considerable cost savings. Consequently, the initial capital cost of chillers is formulated per unit capacity of cooling power, where (α_{ac} , α_{cc}) represent the specific initial capital cost of the absorption and compression chilling units, respectively. The initial capital cost of the cold storage (IC_{cs}) is determined by a nonlinear equation that relates to the tank size (V_{cs}^{s}, m3) (38c). This equation is characterized by parameters (α_{cs} , β_{cs}). The tank size itself depends on the design's thermal capacity (Cp_{cs}^{s}), efficiency (η_{cs}), and supply/return water temperature difference (ΔT_{cs}), as expressed in (39c) [52][53]. Including this nonlinear model in the objective function increases the calculation time. A practical approach is adopted to facilitate this model, where a set of candidate capacities for the cold storage is assumed, and

their corresponding initial capital costs are calculated and tabulated. During the optimization process, integer zero-one variables (x_s) are used to select the optimum option from the candidates using equation (40c). In this equation, (s) represents the candidate number among the (M) options, and the initial capital cost of the selected one is calculated by (41c).

$$IC_{css} = \alpha_{ac}\ Cp_{ac} + \alpha_{cc}\ Cp_{cc} + IC_{cs} \quad (37c)$$

$$IC_{cs}^{s} = \alpha_{cs}\ \ (V_{cs}^{s})^{\beta_{cs}} \quad (38c)$$

$$V_{cs}^{s} = (3.6 \times 10^{9})\ Cp_{cs}^{s}/(\rho\ c_p\ \eta_{cs}\ \Delta T_{cs}) \quad (39c)$$

$$Cp_{cs} = \sum_{s=1}^{M} x_s\ Cp_{cs}^{s} \quad x_s = 0, 1, \quad \sum x_s = 1 \quad (40c)$$

$$IC_{cs} = \sum_{s=1}^{M} x_s\ IC_{cs}^{s} \quad x_s = 0, 1 \quad (41c)$$

The annual variable and fixed O&M costs of the cooling station are formulated in (42c, 43c), respectively, and their total present value (OMC_{css}) over the decision-making period is given in (44c). In these equations, the parameters (EC_{ac}, EC_{cc}, EP^{i}, SOM_{ac}^{v}, SOM_{cc}^{v}, SOM_{ac}^{f}, SOM_{cc}^{f}) represent the electricity consumption rates of AC and CC, electricity price, and specific variable and fixed O&M cost ($/MWh, $/MW/yr) of the units, respectively. The interest rate (IR) is used to calculate the present values. The variable O&M cost of the cold storage is considered within its annual fixed costs. The present value of the reconstruction cost (RC_{css}) is also included, which is applicable when the unit's lifetime is less than the DMP.

$$OM_{css}^{av} = \sum_{i=1}^{N}[(CG_{ac}^{i}\ SOM_{ac}^{v} + CG_{cc}^{i}\ SOM_{cc}^{v}) + (CG_{ac}^{i}\ EC_{ac} + CG_{cc}^{i}\ EC_{cc})\ EP^{i}] \quad (42c)$$

$$OM_{css}^{af} = Cp_{ac}\ SOM_{ac}^{f} + Cp_{cc}\ SOM_{cc}^{f} + Cp_{cs}\ SOM_{cs}^{f} \quad (43c)$$

$$OMC_{css} = \sum_{j=1}^{DMP}(\ OM_{css}^{av} + OM_{css}^{af})/(1 + IR)^{j} + RC_{css} \quad (44c)$$

2.3.2.2 Construction and operation costs of the BHT system

The initial capital cost of the heat transmission system is calculated by equation (45c), which includes the costs associated with the pipeline and its insulation (IC_{pipe}), pressure-boosting pumps (IC_{pump}), and heat exchangers at the heat station and cooling station sides (IC_{hex}^{hss}, IC_{hex}^{css}).

$$IC_{bht} = IC_{pipe} + IC_{pump} + IC_{hex}^{hss} + IC_{hex}^{css} \quad (45c)$$

The capital cost of the pipeline, which has a one-way length of (L, m), is determined using the formulations proposed by [54]. The outer diameter of the pipe (D_{out}) is calculated

according to equation (46c), and the weight of the pipe (Wt_{pipe}) is given in (47c). The parameters ($K1$, $K2$, $W1$, $W2$, $W3$) depend on the pipe's thickness and material. The required volume of the insulation (V_{ins}) is calculated using equation (48c) [34]. The initial capital cost of the pipe is then calculated by equation (49c), where (α_{pipe}) represents the cost of the pipe material (\$/kg), (β_{pipe}) is associated with installation costs, (γ_{pipe}) represents the right-of-way costs, and (δ_{pipe}) stands for the cost of the insulation (\$/m3).

$$D_{out} = K1\, D_{in} + K2 \tag{46c}$$

$$Wt_{pipe} = W1\, D_{in}^2 + W2\, D_{in} + W3 \tag{47c}$$

$$V_{ins} = \left(\frac{\pi}{4}\right)\, [(D_{in} + s)^2 - s^2]\; 10^{-6} \tag{48c}$$

$$IC_{pipe} = 2\, L\, (\alpha_{pipe}\, Wt_{pipe} + \beta_{pipe}\, D_{out}^{0.48} + \gamma_{pipe} + \delta_{pipe}\, V_{ins}) \tag{49c}$$

The capital cost of the pump (IC_{pump}) is modeled as a linear function of the nominal capacity in (50c). The present value of the BHT operation cost over the decision-making period is formulated in (51c), where (P^i) represents the hourly electricity consumption formulated in (25c), (EP^i), is the electricity price, and (IR) is the annual interest rate. The pressure drop is assumed to be the same for both the supply and return pipes. The present value of the cost of the pipe reconstruction (RC_{bht}) is also included, which may be required during the DMP.

$$IC_{pump} = 2\, \alpha_{pump}\, Cp_{pump} \tag{50c}$$

$$OMC_{bht} = 2 \sum_{j=1}^{DMP} \sum_{i=1}^{N} P^i\, EP^i\; (1 + IR)^{-j} + RC_{bht} \tag{51c}$$

The initial capital cost of the heat exchanger (IC_{hex}) is given in (52c), which has the cost parameters ($\alpha_{Hex}, \beta_{Hex}, \gamma_{Hex}$). This equation is used for both heat exchangers on the heating and cooling station sides. The design areas (A_{hex}) of these heat exchangers are calculated using equation (13c).

$$IC_{hex} = \alpha_{Hex}\, (\beta_{Hex} + \gamma_{Hex}\, A_{hex}) \tag{52c}$$

2.3.2.3 Construction and operation costs of the heat supply station

The number of nuclear plants (N_{nhp}), the capacities of the gas boilers (Cp_{gb}) and heat storage (Cp_{hs}) are considered objective variables to be optimized. The total capital cost of these units is given in (53c). A similar approach and formulation as those used for the capital cost estimation of cold storage in equations (38c- 41c) are applied here to calculate the heat storage capital cost (IC_{hs}). The initial capital cost of the nuclear plants (IC_{nhp}) is a discrete function of the number of nuclear plants, where (α_{nhp}) represents the one-plant capital cost.

The capital cost of the gas boiler is a continuous linear function of the boiler's capacity where (α_{gb}) is the specific capital cost per thermal MW.

$$IC_{hss} = \alpha_{nhp}\, N_{nhp} + \alpha_{gb}\, Cp_{gb} + IC_{hs} \quad (53c)$$

The heat station's annual variable and fixed O&M costs are calculated by equations (54c, 55c), respectively, and their total present value is given by equation (56c). In these equations (Q^i) represents the hourly thermal power, and the subscripts (hss, nhp, gb, hs) refer to the heat supply station, nuclear heat units, gas boiler, and heat storage, respectively. The superscripts ($a, v, f,$) denote annual, variable, and fixed costs, respectively. The abbreviations (SFC and SOM) stand for the specific fuel cost and specific O&M costs ($/MWh), while (EC and EP) represent the electricity consumption rate and electricity price, respectively. The present value of the reconstruction cost of the heat station (RC_{hss}) is included when the unit's lifetime is shorter than the DMP.

$$OM^{av}_{hss} = \sum_{i=1}^{N} Q^i_{nhp}\left[\left(SFC_{nhp} + SOM^v_{nhp}\right) + EC_{nhp}\, EP^i\right] + Q^i_{gb}\left[\left(SFC_{gb} + SOM^v_{gb}\right) + EC_{gb}\, EP^i\right] \quad (54c)$$

$$OM^{af}_{hss} = Cp_{nhp}\, SOM^f_{nhp} + Cp_{gb}\, SOM^f_{gb} + Cp_{hs}\, SOM^f_{hs} \quad (55c)$$

$$OMC_{hss} = \sum_{j=1}^{DMP} \left(OM^{av}_{hss} + OM^{af}_{hss}\right)/(1+IR)^j + RC_{hss} \quad (56c)$$

2.3.3 Solution algorithm

The optimization of the proposed district cooling system is a complex problem that involves various interdependent variables and constraints. The presence of both integer and continuous variables, combined with the nonlinearity of the equations, adds further complexity to the optimization process. Therefore, a unique algorithm is developed to solve this MINLP problem within a reasonable time effectively.

Upon reviewing the formulations, it becomes evident that certain variables play a crucial role in the complexity of the problem. These variables include the diameter of the pipeline (D) and its insulation (s), the temperature differences across the system (ΔT), the number of nuclear plants (N_{nhp}), and the capacity of the thermal energy storages (Cp_{hs}, Cp_{cs}). To facilitate the optimization process in a systematic approach, the design variables are categorized into two groups, along with the operation variables addressed in Table 3.

The optimization process is structured in several steps, illustrated in Fig. 24. Step 1 involves gathering the necessary input data, such as the demand data, electricity and fuel prices, techno-economic parameters of the system, and candidate options for the objective

variables. In Step 2, a set of M candidate solutions is generated, assigning values to the variables in Group A (such as D, s, etc.). These values are then applied to all the techno-economic equations of the system, directly resulting in the linearization and simplification of several equations in Step 3. In Step 4, the linearization of the pumping power and its cost calculation is performed. As a result, a mixed integer linear optimization problem remains, which can be efficiently solved in Step 5. Here, the variables in Group B and the operational variables in Group C are optimized. The objective function is calculated, and the local optimum solution among the M cases is saved in Step 6. The calculation cycle continues from Step 2, generating new M cases for the variables in Group A. This repetitive process continues until all possible candidate solutions have been evaluated, ultimately determining the optimum solution in Steps 7 and 8.

Table 3: Objective variables.

Design variables					
Group A		Group B			
Symbol	Definition	Symbol	Definition		
$\boldsymbol{T_{hs}^{s}}$	Heat station supply temperature.	N_{nhp}	Number of nuclear heat plants.		
$\boldsymbol{T_{hs}^{r}}$	Heat station return temperature.	Cp_{hs}	Capacity of heat storage.		
$\boldsymbol{T_{bht}^{s}}$	Supply temperature of BHT.	Cp_{cs}	Capacity of cold storage.		
$\boldsymbol{T_{bht}^{r}}$	Return temperature of BHT.	Cp_{gb}	Capacity of gas boiler unit.		
$\boldsymbol{D}$	Inner diameter of transmission pipeline.	Cp_{ac}	Capacity of absorption chillers.		
$\boldsymbol{s}$	Insulation thickness of the pipeline.	Cp_{cc}	Capacity of compression chillers		
		Cp_{hex}	Capacity of heat exchangers.		
Group C: Operation variables					
$\boldsymbol{Q_{nhp}^{i}}$	Hourly thermal power of nuclear plants.	Q_{gb}^{i}	Hourly thermal power of gas boilers.	Q_{hs}^{i}	Hourly thermal power of heat storage.
$\boldsymbol{C_{ac}^{i}}$	Hourly cooling power of absorption chillers.	C_{cc}^{i}	Hourly cooling power of compression chillers.	C_{cs}^{i}	Hourly cooling power of cold storage.

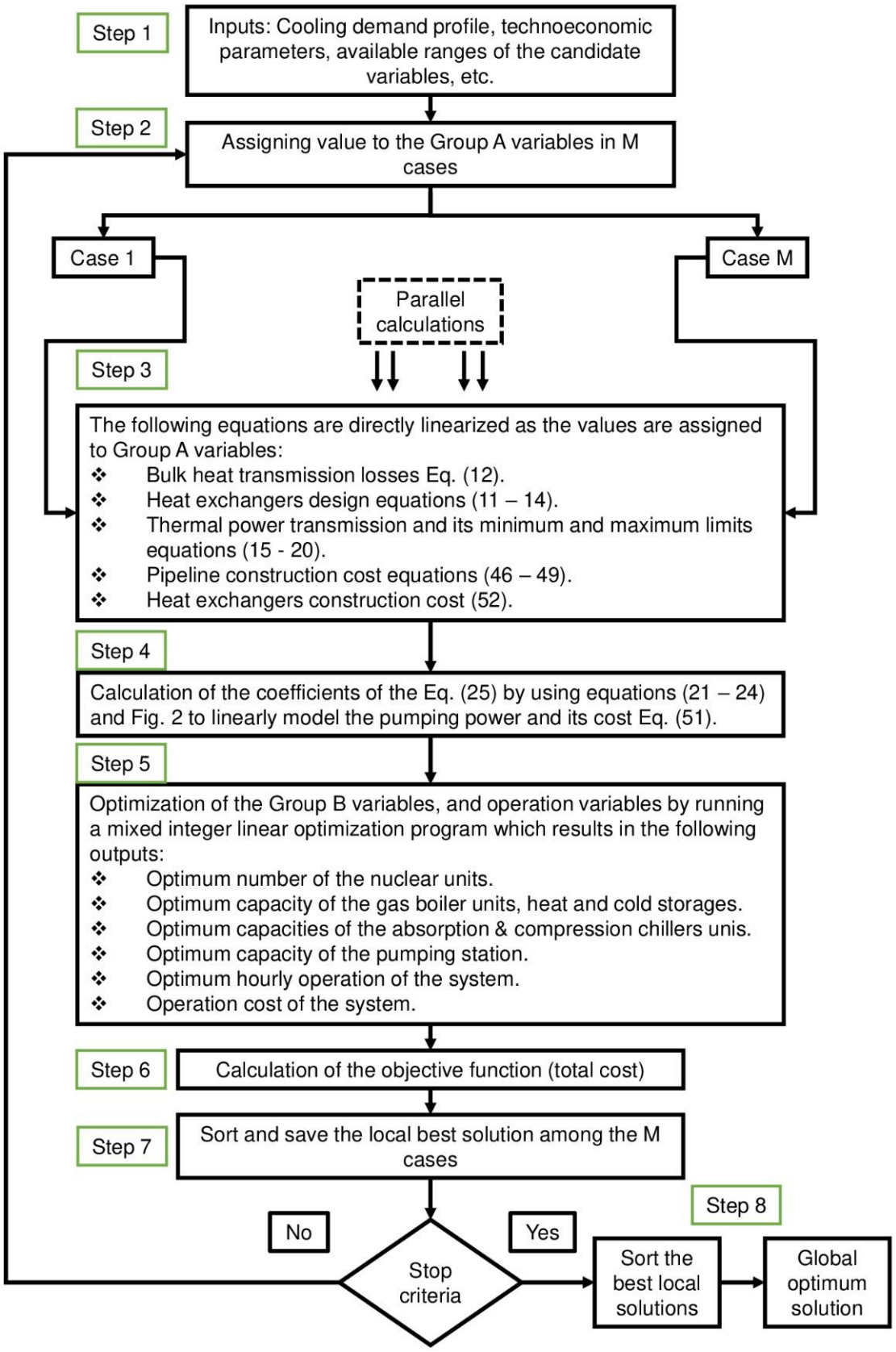

Figure 24: The proposed algorithm for the optimization process.

3 Case studies and results

3.1 Case study and results of evaluation of the proposed system from an energy policy perspective

3.1.1 Case study

Five Scenarios addressed in Table 4 are investigated for supplying a typical large-scale C&H demand (LCHDC-1) given in Table 5. LCHDC-1 represents a cooling demand capacity (CDC) of 750 MWc, which is almost twice the capacity of The Pearl Qatar DCP (450 MWc, which supplies 45,000 residents living in 15,000 apartments and 700 villas) [55] [56]. The DMP is 60 years, and the annual interest rate (i) is 4%. The efficiencies assumed in the calculations are addressed in Table 6. The heat distribution losses are between (4% - 20%) depending on the heat demand density [32]; here, we assumed 85% efficiency for chilled and hot water district distribution.

Table 4: Scenarios.

	Energy source	**Energy carrier**	**Cooling system**	**Heating system**
Scenario 1	Coal power plant	Electricity T&D grid	District electric-driven	Electric local heaters
Scenario 2	Internal combustion power plant	Electricity T&D grid	District electric-driven	Electric local heaters
Scenario 3	Nuclear power plant	Electricity T&D grid	District electric-driven	Electric local heaters
Scenario 4	Combined cycle power plant with 90% carbon capture	Electricity T&D grid	District electric-driven	Electric local heaters
Scenario 5	Nuclear heat-only plant (Teplator)	Heat transmission pipelines (70 km)	District heat-driven	District heating

Table 5: Typical linearized cooling and heating load duration curve.

LCHDC-1		**Cooling and heating periods over 60 years.**	
CDC (MWc)	750	Cd (hr.)	341,640
HDC (MWt)	150	Hd (hr.)	183,960
PCD (MWc)	600	PCP (hr.)	262,800
ACD (MWc)	450	ACP (hr.)	78,840
PHD (MWt)	120	PHP (hr.)	105,120
AHD (MWt)	80	AHP (hr.)	78,840

Table 6: Efficiencies of the district thermal energy distribution and local heating.

Scenarios 1- 4			Scenario 5		
Ef_D^{cw}	Chilled water distribution efficiency	85%	Ef_D^{cw}	Chilled water distribution efficiency	85%
Ef_{LH}	Local electric heaters efficiency	100%	Ef_D^{hw}	Hot water distribution efficiency	85%

3.1.1.1 Electric-driven Scenarios data

Scenarios 1-4 are the electric-driven alternatives. Table 7 lists the specific costs of the four different electrical power plant technologies (reported by [57]) considered in these Scenarios. Regarding fuel, natural gas prices were predicted to be between $1.973 and 6.5 $/MMbtu by 2050 [57][3]. Here, an average price of 3 $/MMbtu is assumed for the natural gas. The fuel price of the coal and SMR power plants are presented in ($/MMbtu) based on the reported prices in [58][57].

The specific cost of electricity T&D varies in different countries and territories. In our analyses, we assume the reported electricity delivering cost of the commercial sector in Southern Alberta (40 $/MWe.h) reported in [59]. The estimation of losses between a power plant and consumers is between 8% and 15% of the generated power [43]; therefore, we have 90% efficiency of electricity T&D for Scenarios (1-4). The specific social carbon cost is estimated to be between 35-55 ($/ton) [60]; in our calculations, 35 ($/ton) is assumed.

Typical specifications of compression cycle chilling for Scenarios (1- 4), considered in our calculations, are given in Table 8.

Table 7: Electrical power plants specifications and costs extracted from [61]**.**

	Scenario 1	**Scenario 2**	**Scenario 3**	**Scenario 4**
Fuel	Coal	Natural gas	Fresh nuclear fuel	Natural gas
Heat rate (HRPP) (MMbtu/MWe.h)	8.638	8.295	10.046	7.124
Fuel price (FP) ($/MMbtu)	1.98	3	0.7	3
Specific construction cost (CC_{PP}^{S}) ($/MWe)	3,676,000	1,810,000	6,191,000	2,481,000

Specific fixed O&M cost (OMC_{PP}^{AF}) ($/MWe.yr)	40,580	35,160	95,000	27,600
Specific variable O&M cost (OMC_{PP}^{V}) ($/MWe.h)	4.5	5.69	3.0	5.840
Carbon emission rate (CO2R) (ton/MMbtu)	0.09344	0.053	0	0.00544
Lifetime (lt_{PP}) (years)	40	30	60	40
Reconstruction cost percentage (RCP)	30%	30%	30%	30%
Specific cost of electricity transmission (T_{El}^{S}) ($/MWe.h)	40			
Electricity T&D efficiency $Ef_{T\&D}^{El}$	90%			

Table 8: The specifications and specific costs of the typical electric-driven cooling plant [62]**.**

	Compression cycle cooling plant
Coefficient of performance COP_{EDC}	4
Specific construction cost ($/MWc) CC_{EDC}^{S}	590,000
Specific fixed O&M cost, including the variable O&M cost ($/MWc.yr) OMC_{EDC}^{AF}	37,390
Lifetime (years) lt_{EDC}	20
Reconstruction cost percentage (RCP)	30%

3.1.1.2 Heat-driven Scenario data

The proposed heat-driven approach in this study is Scenario 5, where a nuclear SMR (Teplator) is the heat source. Table 9 illustrates the Teplator costs used in the calculations. The estimated construction cost of a Teplator with a capacity of up to 150 MWt is reported in [63]. Different distances (between Teplator and DCP) and different scales of transported heat result in another specific cost of heat transmission. Table 10 illustrates BHT's estimated specific construction cost for a 70 km long pipeline for various scales of annual supplied heat [47]. The last row is calculated using the curve fitting method, and 4.64 ($/MWt.h) is used for the BHT cost of Scenario 5 in supplying LCHDC-1. The heat losses over 150 km long BHT estimated by Safa [32] represent less than 2% of the total transported power, so we assume 98% efficiency for 70 km of BHT (Scenario 5). Implementation of the LiBr-H2O

chillers in the district cooling systems is more common thanks to the refrigerant (H2O) that is available, not expensive, not toxic, and due to its high latent heat of evaporation, a significant amount of cooling can be produced [64]. The typical absorption LiBr-H2O chilling specifications used for Scenario 5 are given in Table 11, extracted from [62].

Table 9: Teplator costs.

	CC_{HP}^{S} ($/MWt)	OMC_{HP}^{AF} ($/MWt.yr)	FP ($/MMbtu)	OMC_{HP}^{V} ($/MWt.yr)	CO2R (ton/MWt.h)	lt_{HP} (years)	RCP
Teplator	233,333	18,000	0	1	0	60	30%

Table 10: Specific cost and efficiency of bulk heat transmission (Scenario 5) [47]**.**

Annual transported heat (GWt.h/y)	Specific BHT Cost (for 70 km distance) T_{BH}^{S} ($/MWt.h)	BHT efficiency Ef_{T}^{BH}
28	84.22	98%
111	39.28	98%
444	14.74	98%
1778	7.08	98%
> 4000	4.64	98%

Table 11: The specifications and specific costs of the heat-driven cooling plant [62]**.**

	Single-stage absorption cooling plant
Coefficient of performance (COP_{HDC})	0.7
Specific construction cost ($/MWc) ($CC_{HDC}^{S}$)	801,000
Specific fixed O&M cost, including the variable O&M cost ($/MWc.yr) ($OMC_{HDC}^{AF}$)	13,380
Lifetime (years) (lt_{HDC})	20
Reconstruction cost percentage (RCP)	30%

3.1.2 Results

3.1.2.1 Electricity saving

For covering the assumed LCHDC-1, the calculated capacities of the cooling plant (CPC), electrical power plant (PPC, Scenarios 1-4), and heat plant (HPC, Scenario 5) are given in Table 12. The cooling plant with a capacity of 882 MWc is needed, which is of compression type for Scenarios 1- 4 and absorption type in the case of Scenario 5. Scenarios 1-4 require

an electrical power capacity of 243 MWe; in contrast, Scenario 5 needs a heat plant of 1286 MWt. Therefore, Scenario 5 could eliminate 243 MWe of electrical power generation, transmission, and distribution capacities needed in Scenarios 1- 4.

Table 12: Plants capacities required for supplying annual energy needs of LCHDC-1.

Scenarios 1- 4		**Scenario 5**	
Compression CPC (MWc)	882	Absorption CPC (MWc)	882
PPC (MWe)	243	HPC (MWt)	1286

The cooling and heating energy demand associated with LCHDC-1 is shown in Fig. 25 (A). In the case of Scenarios 1-4, the electricity generation required to supply this demand is illustrated in Fig. 25 (B). Simply dividing the electricity generation by the energy needs indicates that Scenario 5 could eliminate electricity generation of (0.32 MWe.h) per cooling unit and (1.1 MWe.h) per heating demand. In contrast, according to the results shown in Fig. 25 (A, C), Scenario 5 needs (1.71, 1.2) of (MWt.h) heat generation and transmission per unit of cooling and heating energy demand, respectively. These numbers confirm the capability of the heat-driven district cooling and heating to reduce the pressure on the power grids, peak power shaving, improve the power system load factor, and reduce the electrical infrastructure expansion costs.

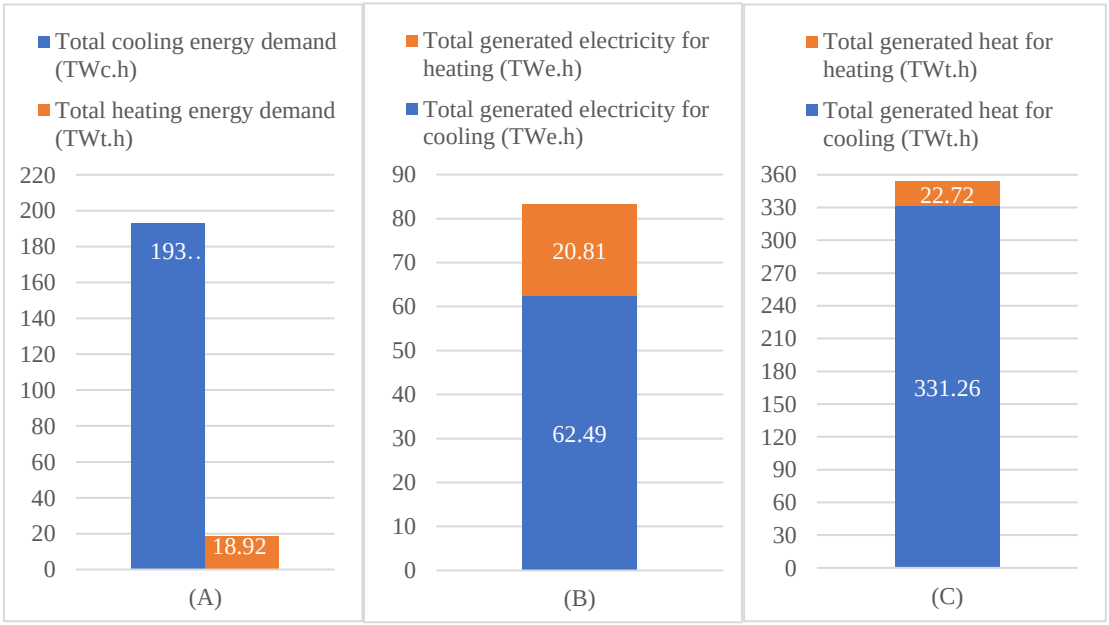

Figure 25: The energy needs of LCHDC-1 (A), electricity generation by Scenarios 1-4 (B), and heat generation by Scenario 5 (C).

3.1.2.2 Carbon emission saving

Supplying C&H demand by nuclear energy either in the form of electricity drives an electric-driven system (Scenario 3) or heat drives a heat-driven system (Scenario 5), which eliminates considerable carbon emissions and saves the associated social carbon cost, as given in Table 13. The eliminated amount of CO2 emissions in metric tons per (MWc.h) cooling demand is (0.26, 0.14, 0.01) and (0.89, 0.48, 0.04) per heating demand (MWt.h) compared with Scenarios 1, 2, and 4, respectively.

Table 13: Carbon emissions and social carbon cost.

	Scenario 1	Scenario 2	Scenario 3	Scenario 4	Scenario 5
Carbon emission per unit cooling demand (ton/MWc.h)	0.26	0.14	0	0.01	0
Carbon emission per unit heating demand (ton/MWt.h)	0.89	0.48	0	0.04	0
Levelized cost of carbon emission per unit cooling demand ($/MWc.h)	9.14	4.98	0	0.44	0
Levelized cost of carbon emission per unit heating demand ($/MWt.h)	31.07	16.93	0	1.49	0
Total PV of carbon cost from supplying cooling demand (M$)	666	363	0	32	0
Total PV of carbon cost from supplying heating demand (M$)	222	121	0	11	0

3.1.2.3 Economics of the Scenarios

The results illustrated in Fig. 26 and Fig. 27 confirm the potential economic feasibility of Scenario 5, where its total PV of costs is (38%, 35%, 45%, 35%) less than Scenarios 1- 4, respectively. Since Scenario 4 is the alternative option after Scenario 5, let's discuss these two Scenarios in more detail.

The factors that play essential roles are (electricity vs. heat) transmission costs, (natural gas vs. spent nuclear fuel) costs, and (electrical power plant vs. heat plant) construction costs. Thanks to the unique feature of reusing the SNF by Teplator, we have a neglectable fuel cost in Scenario 5; in contrast, the fuel consumption in Scenario 4 represents about 17% of its total cost. In the case of the heat-driven Scenario 5, as cooling and heating demand is higher, the needed annual transported heat is larger, resulting in a lower specific cost of BHT (Table 8).

According to Fig. 25 (C), the total generated heat covering the assumed demand model (LCHDC-1) over 60 years is about 354 TWt.h. Consequently, the annual transported heat is about 5,900 GWt.h; therefore, referring to Table 10, the specific BHT is only (4.16 $/MWt.h) for Scenario 5. In contrast, in Scenario 4, the specific electricity transmission cost is (40 $/MWe.h). Although the generated and transported heat in Scenario 5 (Fig. 25 (C)) is more than four times larger than the electricity in Scenario 4 (Fig. 25 (B)), we have a BHT cost of about 50% less than electricity transmission.

The heat plant in Scenario 5 has a lower construction cost than the power plant in Scenario 4 (the heat plant does not have costly electrical infrastructures like a turbine, electricity generator, power substations, etc., and generates heat under low temperature and pressure). According to the given formulations in Section 2. 1 and the costs and data given in Table 7 and Table 9, the calculated PV of construction costs of the heat plant in Scenario 5 is about 50% less than the construction costs of the power plant in Scenario 4.

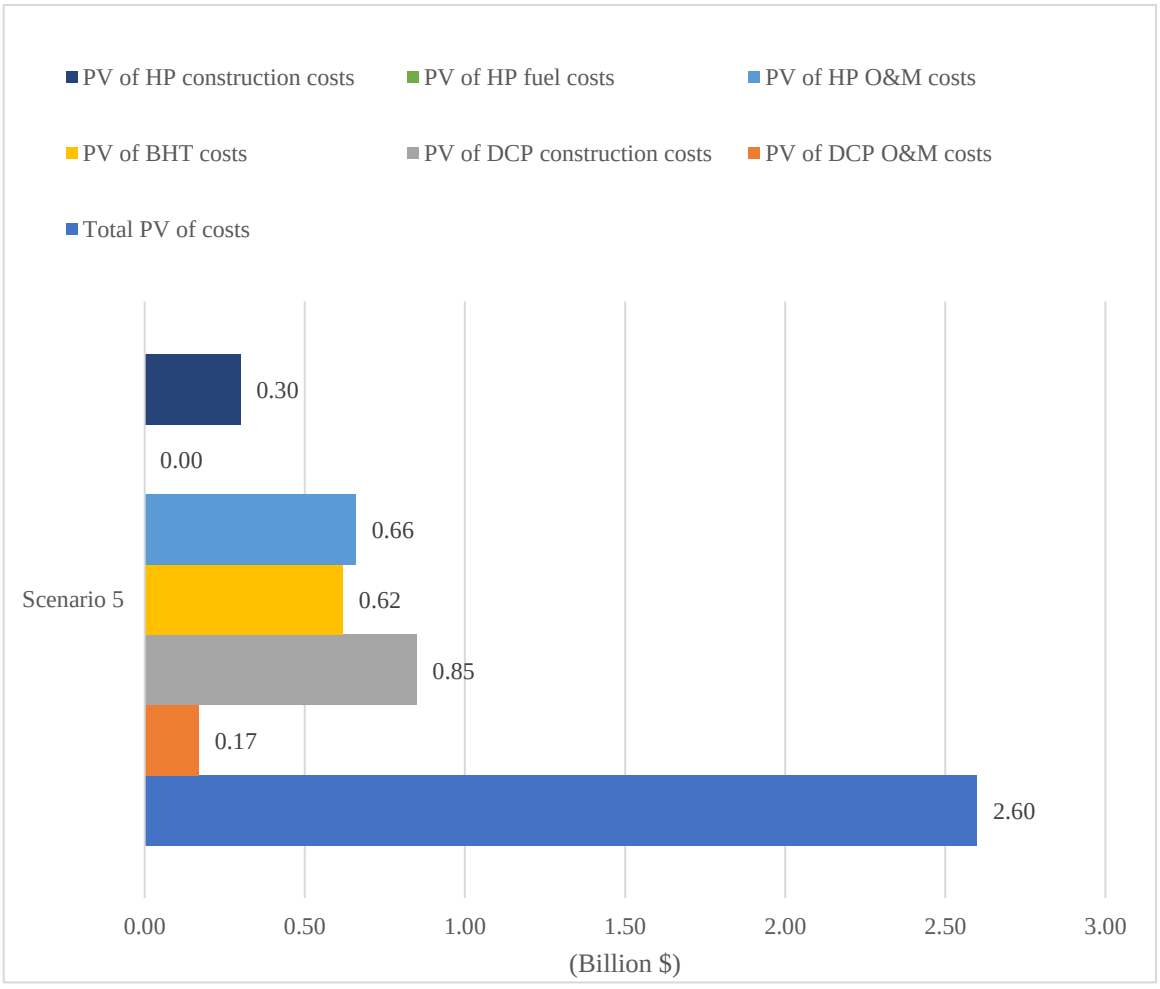

Figure 26: Present value of costs: the proposed heat-driven Scenario 5.

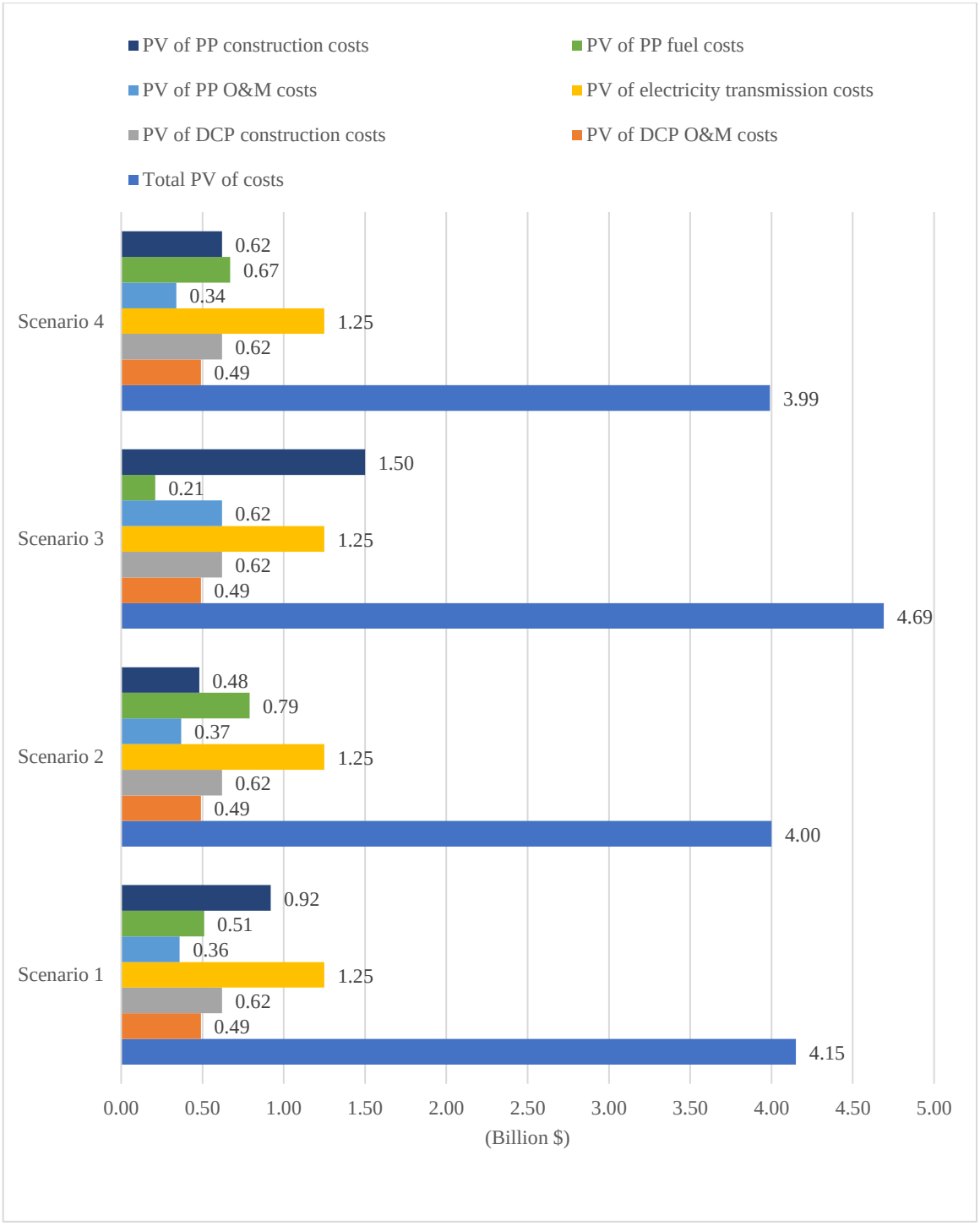

Figure 27: Present values of costs: the electric-driven Scenarios 1- 4.

The calculated levelized present values of costs for one unit of cooling and heating energy demand are illustrated in Fig. 28. Although the CO2 emission cost is not included, Scenario 5 offers to supply each (MWc.h) cooling demand with (34%, 30%, 43%, 31%) lower cost than the other electric-based Scenarios (1- 4), respectively. Obviously, district heating using the proposed low-cost nuclear heat generation in Scenario 5 is much cheaper than electric local heaters in other Scenarios.

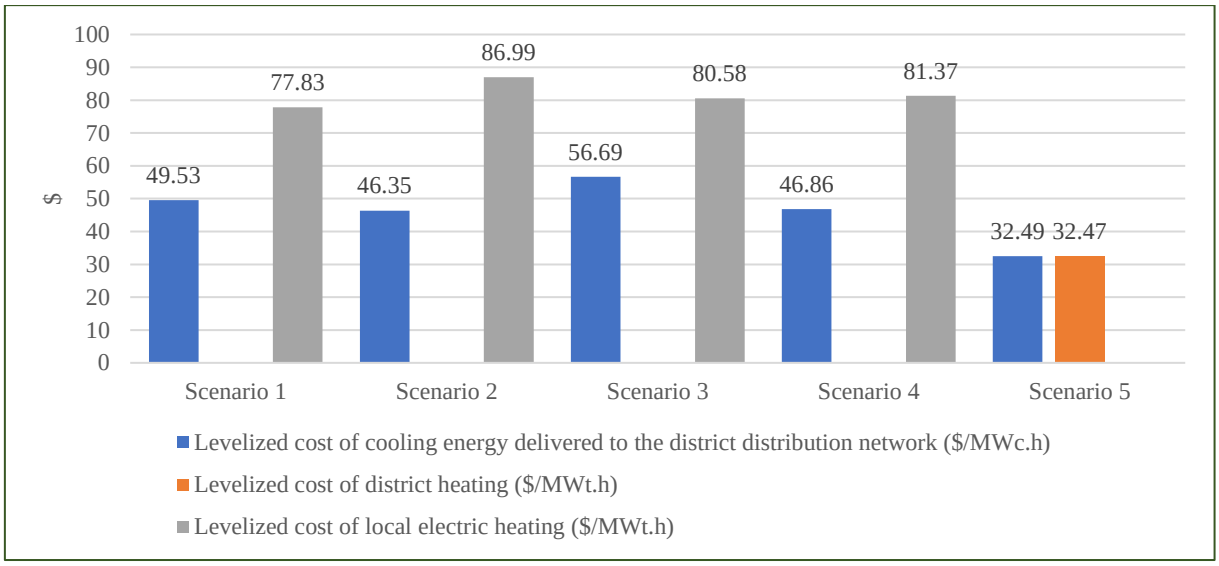

Figure 28: Levelized cost of delivered cooling and heating energy.

3.1.2.4 Sensitivity analyses of the proposed system from an energy policy viewpoint

The fuel prices or the construction and operational costs of the plants differ from project to project; a sensitivity analyzing model is developed, assuming various combinations of hypothetical cost fluctuations addressed in Table 14. For the demand model (LCHDC-1), Scenarios 4 and 5 are evaluated based on different costs of the three critical factors, i.e., construction, energy transmission, and fuel. Similar calculations could be performed for other Scenarios. The results are illustrated in Fig. 29. Although not considering the social carbon cost, several sensitivity cases confirm the potential economic viability of the proposed heat-driven cooling approach. For instance, even though the specific cost of the heat transmission and Teplator construction are doubled, and simultaneously, the specific cost of both electricity transmission and power plant construction drop by 70%, Scenario 5 is still competitive.

Table 14: Hypothetical changes in construction, fuel, and energy transmission costs.

Scenario 5			**Scenario 4**		
Teplator construction cost ($/MWt)	**Nuclear spent fuel cost ($/MWt.h)**	**Bulk heat transmission cost ($/MWt.h)**	**Combined Cycle PP construction cost ($/MWe)**	**Natural gas fuel price ($/MWe.h)**	**Electricity T&D cost ($/MWe.h)**
+50%	0.5	+50%	-30%	-30%	-30%
+100%	1	+100%	-50%	-50%	-50%
+200%	3	+200%	-70%	-70%	-70%

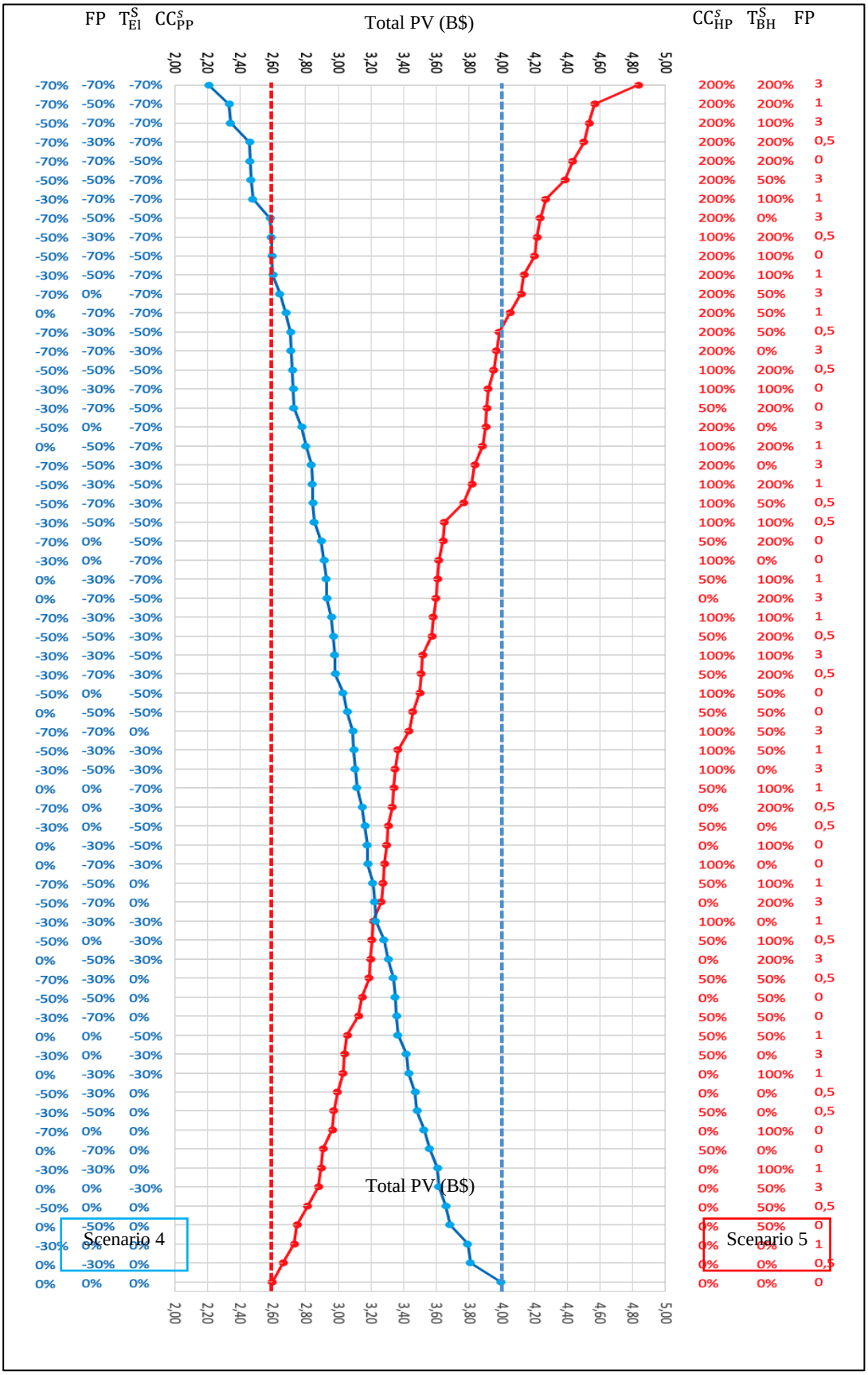

Figure 29: Evaluation of Scenarios 4 and 5 under different fuel, energy transmission, and capital costs.

While these results are promising for the considered large scale of C&H demand (LCHDC-1), it is important to also investigate the proposed Scenario 5 for the smaller demand scales. Table 15 represents two typical medium and small scales of LCHDC. The required power generation and cooling plant capacities and the energy generation needed to supply the assumed LCHDC-2 and LCHDC-3 are reported in Table 16. According to the results illustrated in Fig. 30 (A, B, C), the small scales of cooling/heating demands and higher specific cost of BHT decrease the potential economic benefits of Scenario 5 compared with Scenario 4.

Table 15: Typical cooling and heating demands.

	LCHDC-2 medium scale	**LCHDC-3 small scale**
CDC (MWc)	312.5	62.5
HDC (MWt)	62.5	25
PCD (MWc)	250	50
ACD (MWc)	187	37.5
PHD (MWt)	50	20
AHD (MWt)	33	15
TCED (MWc.h)	80,443,080	16,096,500
THED (MWt.h)	7,857,720	3,285,000

Table 16: Required capacities of electrical/heat plants and energy generation for supplying LCHDC-2, LCHDC-3.

Scenarios 1- 4	**LCHDC-2**	**LCHDC-3**	**Scenario 5**	**LCHDC-2**	**LCHDC-3**
CPC (MWc)	368	73.5	CPC (MWc)	368	73.5
PPC (MWe)	101	20	HPC (MWt)	536	107
TGEC (MWe.h)	26,025,702	5,207,691	TGHC (MWt.h)	137,957,606	27,605,042
TGEH (MWe.h)	8,643,492	3,613,500	TGHH (MWt.h)	9,433,037	3,943,577
AGECH (MWe.h)	577,820	147,000	AGHCH (MWt.h)	2,456,510	525,810
$\mathbf{T}_{El}^{S}$ ($/MWe.h)	40	40	T_{BH}^{S} ($/MWt.h)	7.08	14.74

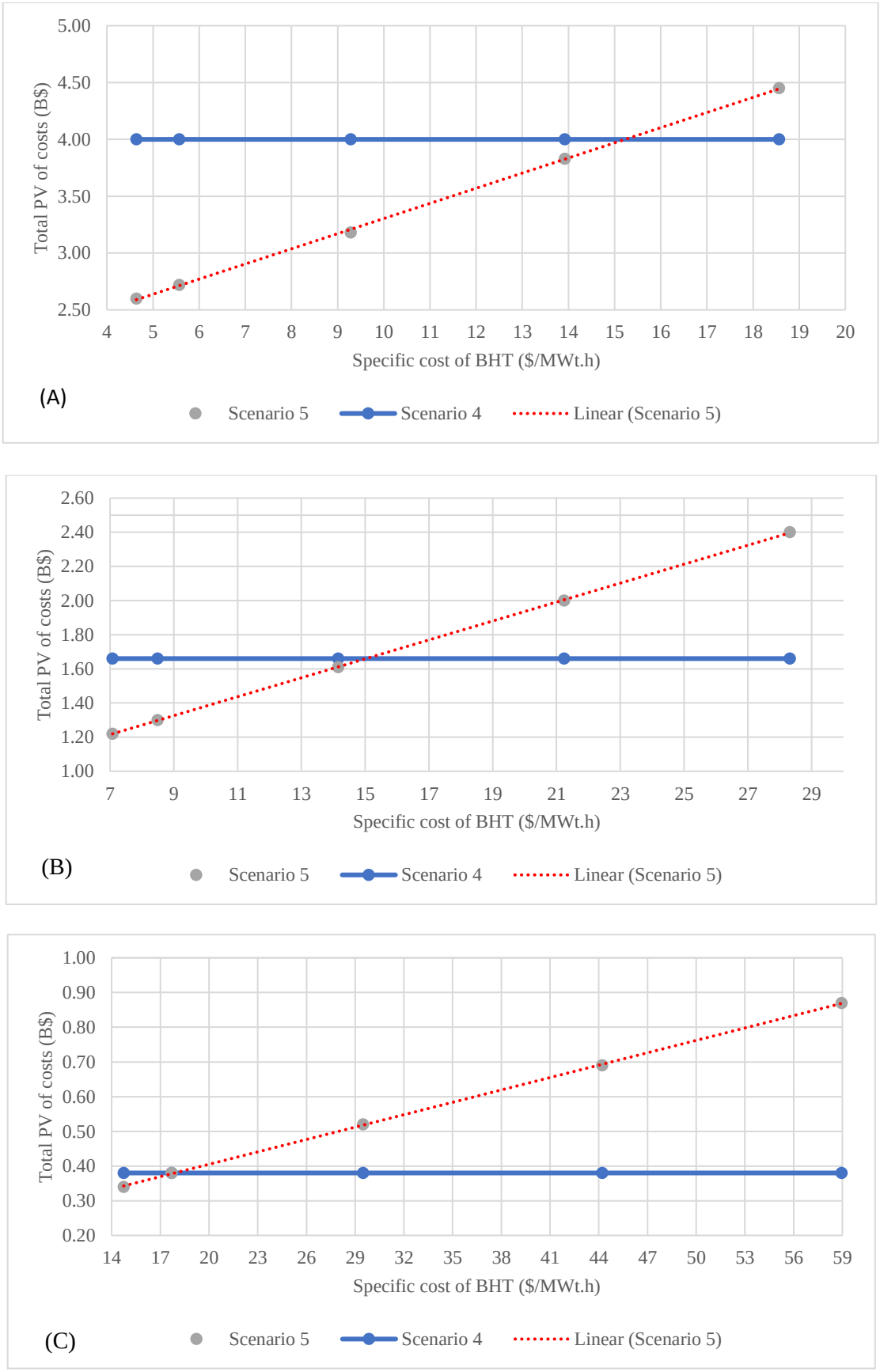

Figure 30: Sensitivity of Scenario 5 to specific BHT cost (A: LCHDC-1, B: LCHDC-1, C: LCHDC-3).

3.2 Case study and results of the evaluation of the effects of the proposed system on a power grid

3.2.1 Case study

To evaluate the other benefits of the proposed approach on the power grids, the notorious IEEE-39 bus power system is considered, as it is shown in Fig. 31. This system has ten power plants and 46 transmission lines. The cost function coefficients of the power plants are given in Table 17. The electrical power demands of the 39 regions are given in Table 18.

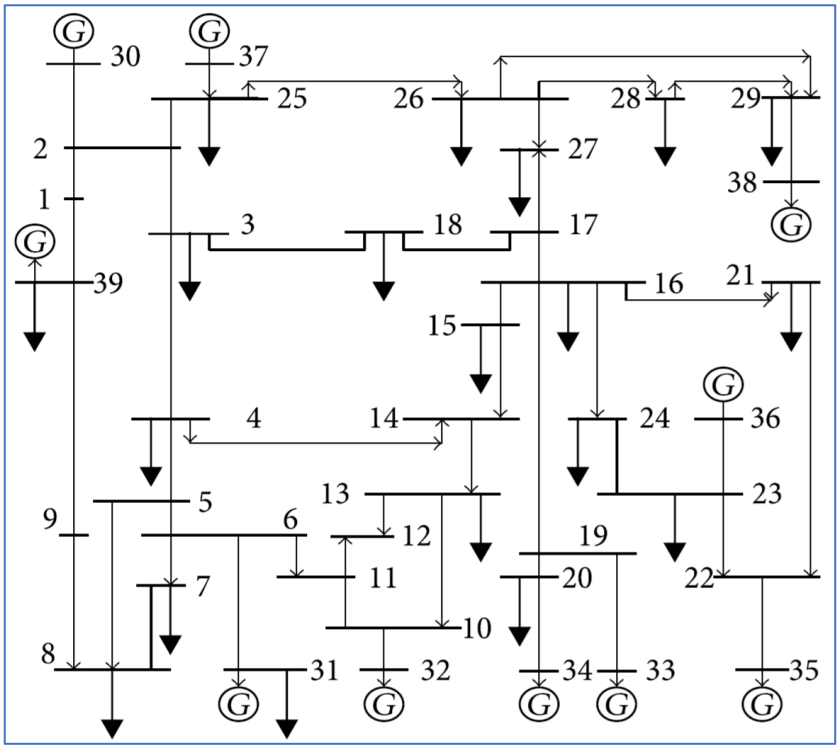

Figure 31. IEEE 39 bus New England power system [65].

Table 17: Cost function coefficients of the power plants [66].

Bus no.	**Coefficients**		
	a_i	b_i	c_i
30 (Gen 1)	0.074	1.083	100
31 (Gen 2)	0.089	1.033	70
32 (Gen 3)	0.074	1.083	100
33 (Gen 4)	0.089	1.033	70
34 (Gen 5)	0.053	1.17	40
35 (Gen 6)	0.074	1.083	100
36 (Gen 7)	0.089	1.033	70
37 (Gen 8)	0.074	1.083	100
38 (Gen 9)	0.089	1.033	70

39 (Gen 10)	0.053	1.17	40

Table 18: Electrical power demands of IEEE 39 bus.

Bus	**1**	**2**	**3**	**4**	**5**	**6**	**7**	**8**
P_D	97.6	0	322	500	0	0	233.8	522
Bus	**9**	**10**	**11**	**12**	**13**	**14**	**15**	**16**
P_D	6.5	0	0	8.53	0	0	320	329
Bus	**17**	**18**	**19**	**20**	**21**	**22**	**23**	**24**
P_D	0	158	0	680	274	0	247.5	308.6
Bus	**25**	**26**	**27**	**28**	**29**	**30**	**31**	**32**
P_D	224	139	281	206	283.5	0	9.2	0
Bus	**33**	**34**	**35**	**36**	**37**	**38**	**39**	**-**
P_D	0	0	0	0	0	0	1104	-

Several scenarios are considered to evaluate the benefits of developing heat-driven district cooling systems. Scenario A represents the situation where the cooling needs are supplied by air conditioners or central electric chillers, assuming that in hot climate states, the cooling sector shares about 50% of the electricity peak demand [5]. Therefore, in other scenarios, the heat-driven district cooling systems are assumed to replace the electric-based cooling to provide a part of the cooling demand equivalent to 50% of the electricity demand. Consequently, the electrical demand is reduced by 50%.

This idea is applied on bus 4 – Scenario B, buses (4 & 20) – Scenario C, and buses (4 & 20 & 16) – Scenario D, respectively. Moreover, to show how the heat-driven cooling approach is potent in the extreme reduction of the electricity cost and how it can postpone the expansion of the power transmission and generation systems, Scenario E is simulated where 50% of the electricity demand in all regions is assumed to be eliminated by thermally driven cooling technologies.

3.2.2 Results

The optimum load flow problem is calculated for all scenarios, and Table 19 summarizes and compares the results. The peak electrical generation capacity is reduced from 6,300 MW (scenario A) to 3,143 MW in scenario E, saving 3,157 MW of power generation capacity. As more electrical demand is eliminated, the electricity generation cost per MWh reduces

since low power demand allows the power plants to operate within their optimal generation-cost range.

Table 19: Optimal power flow results.

Power plant	A (MW)	B (MW)	C (MW)	D (MW)	E (MW)
Gen 1	626	604	571	554	311
Gen 2	529	507	478	464	260
Gen 3	627	604	570	554	312
Gen 4	530	492	457	444	258
Gen 5	826	815	757	733	430
Gen 6	628	600	563	546	309
Gen 7	515	495	467	454	258
Gen 8	564	564	561	546	309
Gen 9	534	503	473	460	258
Gen 10	921	862	814	791	438
Total generation (MW)	6300	6046	5711	5546	3143
Saving of generation capacity	0	254	589	754	3157
Electricity cost ($/MW.hr)	47.35	45.44	43	41.78	24.29

The results reported in Table 20 confirm heat-driven cooling systems' capability to save power transmission capacity. As larger capacities of heat-driven cooling systems are operated, a more considerable cost of future power system expansion is saved. Scenario E has reduced the power flow over the transmission network to nearly half compared with Scenario A.

Table 20: Transmission network power flow.

From bus	To bus	Power flow scenario A (MW)	Power flow Scenario E (MW)	Power reduction

2	1	270.908	146.969	-45.75%
1	39	168	90	-46.43%
2	3	455	242	-46.81%
25	2	44	17	-61.36%
30	2	634	311	-50.95%
3	4	127	71	-44.09%
3	18	5	6	20.00%
5	4	101	45	-55.45%
14	4	262	132	-49.62%
6	5	452	228	-49.56%
5	8	348	179	-48.56%
6	7	442	226	-48.87%
11	6	366	189	-48.36%
31	6	524	255	-51.34%
7	8	214	112	-47.66%
8	9	48	31	-35.42%
9	39	27	16	-40.74%
10	11	363	189	-47.93%
10	13	265	134	-49.43%
32	10	636	312	-50.94%
12	11	2	1	-50.00%
13	12	7	4	-42.86%
13	14	258	129	-50.00%
15	14	9	10	11.11%
16	15	318	167	-47.48%
16	17	325	170	-47.69%
19	16	676	360	-46.75%
21	16	295	148	-49.83%
24	16	11	4	-63.64%

17	18	153	74	-51.63%
17	27	165	90	-45.45%
20	19	168	95	-43.45%
33	19	508	261	-48.62%
34	20	842	432	-48.69%
22	21	565	284	-49.73%
22	23	57	29	-49.12%
35	22	627	309	-50.72%
23	24	326	163	-50.00%
36	23	517	258	-50.10%
25	26	243	134	-44.86%
37	25	564	311	-44.86%
26	27	110	51	-53.64%
26	28	9	5	-44.44%
29	26	43	22	-48.84%
29	28	205	108	-47.32%
38	29	533	273	-48.78%

3.3 Case study and results of optimization and evaluation from investor's perspective

3.3.1 Case study

To examine the optimization method, this study utilizes the one-year hourly cooling demand profile of Qatar, which was previously modeled and reported by Alghool et al. [67]. This demand profile, with a peak of 4100 MWc, is scaled down by 50% to a peak of 2050 MWc for the case study conducted here. The objective is to optimize the proposed system to meet this scaled-down demand. Teplator, the primary candidate heat source, can supply hot water within a temperature range of (98 – 200 ˚C) [63]. This case study considers a single-effect lithium bromide solution-based absorption technology that operates with hot water at 95 ˚C. This technology is among the most common and practical types available [68][69]. Therefore, specific temperature values are predetermined and indicated in Fig. 32 and Table 21 to ensure compatibility with these technologies. Although the temperatures are predetermined for this typical case study, the same algorithm can be applied when exploring

alternative heat generation options (e.g., higher temperature sources) and different absorption chilling technologies (e.g., double effect). The designed algorithm incorporates a parallel calculation feature, enabling efficient solution finding within a reasonable time.

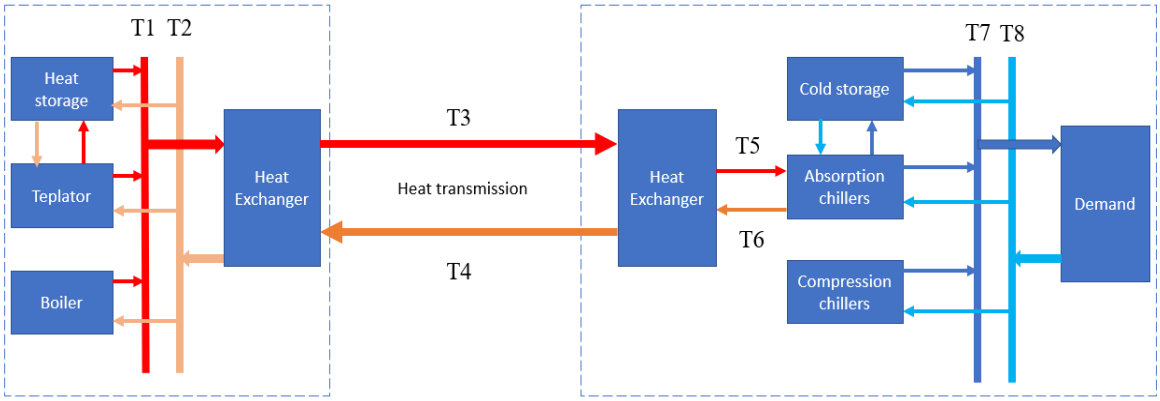

Figure 32: The system's temperatures.

Table 21: The assumed temperatures in the system.

Heat station supply/return temperatures (˚C)	**T1/T2**	**170 / 90**	**Temperatures of supply/return hot water driving absorption chillers (˚C)**	**T5/T6**	**95/ 55**
Transmission supply/return temperatures (˚C)	T3/T4	120/ 70	Temperatures of supply/return chilled water (˚C)	T7/T8	5/ 13

The physical and technical parameters used in the calculations are given in Table 22. For the heat transmission system, it is assumed that the heat station is located 20 km away from the cooling station. Consequently, the total length of the supply/return hot water pipe is 40 km. A recommended flow velocity range of (0.5 m/s – 4 m/s) is considered to ensure proper system operation and avoid potential damages such as mechanical stress and erosion [32]. Plate-type heat exchangers are considered to be installed on both sides of the pipeline: one receives heat from the heat station, and the other delivers it to the absorption cooling units. These heat exchangers are assumed to have similar specifications. The overall heat transfer coefficient for water-to-water heat exchangers is reported to be in the range (850 -1700 W/(m K)) [70]. This case study assumes a typical value of (1500 W/(m K)) as the overall heat transfer coefficient.

The power ramp rates of the heat and cold supply units are crucial for effective load following in the system. The hourly change in nuclear power is restricted within a range of (+10%, - 5%) of the nominal unit's capacity to ensure smooth operation. This study neglects

thermal storage losses due to their minimal impact, as weekly losses are estimated to be only 1% for a 5000 m3 tank, and the roundtrip efficiency is about 98% [53].

Table 22: Physical and technical parameters of the system.

System	Parameter	Symbol	Value	Ref.
Heat transfer fluid: Water	Density (kg/m3)	ρ	958	[35]
	Specific heat capacity (J/kg. K)	C_p	4220	[35]
	Kinematic viscosity (m^2/s)	ν	0.294×10^{-6}	-
Heat transmission	Distance between heat station and chilling station (m)	L	20 000	-
	Weight and outer diameter calculation parameters of the schedule 80 steel pipe Eqs. (46, 47)	$K1$ $K2\ (m)$ $W1\ (kg/m^3)$ $W2\ kg/m^2)$ $W3\ (kg/m)$	1.101 0.006349 1330 75.18 0.9268	[50]
	Maximum flow velocity (m/s)	c^{Max}	4	[32]
	Minimum flow velocity (m/s)	c^{Min}	0.5	-
	Pump efficiency	η_P	75%	[35]
	Lifetime of pipeline	LT_{TP}	50	[35]
Heat exchangers	Overall heat transfer coefficient W/(m K)	U	1500	[70]
	Efficiency	η_{hex}	80%	[35]
	Lifetime of heat exchanger	LT_{hex}	25	
Teplator	Increasing power ramp rate (MW/hr)	RR_{nhp}^{up}	± 10%	-
	Decreasing power ramp rate (MW/hr)	RR_{nhp}^{down}	± 5%	-
	Electricity consumption (MWeh/MWth)	EC_{nhp}	1%	-
	Lifetime of Teplator (year)	LT_{nhp}	50	
Gas boiler	Power ramp rate (MW/hr)	RR_{gb}	± 100%	-
	Electricity consumption (MWeh/MWth)	EC_{gb}	0.14%	[71]
	Efficiency	η_{gb}	103%	[71]
	Lifetime of gas boiler (year)	LT_{gb}	25	[71]
Heat storage	Charging/discharging power (MWt/hr)	RR_{hs}	2% of the capacity	-
	Electricity consumption (MWeh/MWth)	EC_{hs}	1%	[53]

	Charging/discharging efficiency	η_{hs}	100%	[53]
	Lifetime of heat storage	LT_{hs}	50	-
Cold storage	Charging/discharging power (MWc/hr)	RR_{cs}	2% of the capacity	-
	Electricity consumption (MWeh/MWch)	EC_{cs}	1%	-
	Charging/discharging efficiency	η_{cs}	100%	-
	Lifetime of cold storage (year)	LT_{cs}	50	-
Absorption chiller	Power ramp rate (MWc/hr)	RR_{ac}	± 20%	-
	Electricity consumption (MWeh/MWch)	EC_{ac}	5%	-
	Average COP	COP_{ac}	0.85	[72]
	Lifetime of absorption chillers (year)	LT_{ac}	25	-
Compression chiller	Power ramp rate (MWc/hr)	RR_{cc}	± 20%	-
	Electricity consumption (MWeh/MWch)	EC_{cc}	27%	-
	Average COP	COP_{cc}	4	-
	Lifetime of compression chillers (year)	LT_{cc}	25	-

Table 23 provides the candidate solutions for the design variables considered in this study. It includes the candidate numbers of nuclear plants, with each unit having a capacity of 150 MWt, as well as the candidate capacities of the gas boiler, absorption chillers, and compression chiller. The candidate capacities are assumed within a wide range up to the peak demand. Furthermore, various candidate diameters are assumed for the heat transmission pipeline, allowing for flexibility in system design. In terms of insulation, a single option is considered for the type and thickness to simplify the calculations. Limiting the insulation options puts the focus on other critical variables.

Table 23: Candidate options for design variables.

	Variable	**Symbol**	**Value**
Heat station variables	Number of nuclear plants	N_{nhp}	0 – 14
	Capacity of heat storage (MWth)	Cp_{hs}	[0, 2000, 4000, 8000, 12 000, 20 000]
	Capacity of gas boiler (MWt)	Cp_{gb}	0 – peak thermal demand
Heat transmission variables	Pipe diameter (m)	D_{in}	[0, 0.5, 0.7, 1, 1.2, 1.5, 1.7, 1.9, 2, 2.1, 2.2, 2.5]
	Pipe (iron) absolute roughness (mm)	ε	0.2

	Insulation type: thermal conductivity (W/m.K)	*hi*	0.03
	Insulation thickness (mm)	*s*	200
Chilling station variables	Capacity of absorption chilling (MWc)	Cp_{ac}	0 – Peak cooling demand
	Capacity of compression chilling (MWc)	Cp_{cc}	0 – Peak cooling demand
	Capacity of cold storage (MWch)	Cp_{cs}	[0, 2000, 4000, 8000, 12 000, 20 000]

The values of the design variables are accepted as optimal when they result in the minimum total cost while satisfying the technical constraints. The objective function, which encompasses the total capital and operation cost, is calculated using the economic parameters addressed in Table 24. For the calculations, electricity and gas prices are assumed to be (144 $/MWeh, and 41 $/MWth) respectively. These values correspond to the average non-household consumer prices in the European Union [73] [74].

Table 24: Construction and operation cost factors.

	System	**Construction cost**	**Annual fixed O&M cost**	**Variable O&M cost**
Cooling station	Absorption chiller (37) [28]	$\alpha_{ac} = 801\,000$ (€/MWc)	13 380 (€/MWc/yr)	-
	Compression chiller (37) [28]	$\alpha_{cc} = 590\,000$ (€/MWc)	37 390 (€/MWc/yr)	-
	Cold storage (38)	$\alpha_{cs} = 7450$ (€/m^3) $\beta_{cs} = 0.53$	8.6 (€/MWch/yr)	0
Heat transmission system	Pipeline Eq. (49) [34] [54]	$\alpha_{pipe} = 0.82$ (€/kg) $\beta_{pipe} = 185$ (€/$kg^{0.48}$) $\gamma_{pipe} = 6.8$ (€/m) $\delta_{pipe} = 110$ (€/m^3) (Polyurethane foam insulation)	0.04% of the capital cost	0
	Pump Eq. (50) [50]	$\alpha_{pump} = 1000$ $/$MWe$ (€)	Included in the pipeline FO&M cost	Table 6 Eq 50
	Heat exchanger Eq. (52)	$\alpha_{hex} = 1$ $\beta_{hex} = 11\,000$ (€) $\gamma_{hex} = 150$ (€/m^2)	Included in the pipeline FO&M cost	0
Heat station	Teplator (53) [63] [75]	$\alpha_{nhp} = 30\,000\,000$ (€)	18 000 (€/MWt/yr)	1 (€/MWth)
	Gas boiler (53) [71]	$\alpha_{gb} = 50\,000$ (€/MWt)	1900 (€/MWt/yr)	0.9 (€/MWth)

Heat storage (38) [53]	$\alpha_{hs} = 7450\ (€/m^3)$ $\beta_{hs} = 0.53$	8.6 (€/MWth/yr)	0

3.3.2 Results

A base scenario introduced is an entirely electric-driven district cooling system utilizing compression chillers and cold storage to be compared to the proposed system. This system is optimized to efficiently supply a one-year hourly cooling demand with a peak of 2050 MWc. The optimized system's capacities and corresponding capital and O&M costs are addressed in Table 25. The O&M cost of the compression chillers, mainly associated with electricity consumption, constitutes 85% of the total cost. Among the options for cold storage (referenced in Table 4), the most suitable choice is the largest one, with a capacity of 20,000 MWh. The total capacity of the chillers is 1668 MWc, less than the peak demand (2050 MW). Therefore, the cold storage effectively covered 382 MWc of the peak demand.

Table 25: The achieved design capacities and costs associated with the base scenario.

		Optimum design capacity	Annual O&M cost (M$)	Present value of O&M cost over DMP (M$)	Capital cost (M$)
Compression chilling	Cp_{cc}	1668 MWc	322.92	6937.1	1168.7
Cold storage	Cp_{cs}	20 000 MWch / 400 MW	0.172	3.695	17.233
Total capital and operation cost of the system:			323.1	6940.8	1185.9
				8126.7 M$	

After evaluating the electric-driven scenario discussed in the previous subsection, we present the optimization results for the thermally driven DCS. Before initiating the optimization cycle, several constraints and parameters are calculated. Table 26 presents the calculated coefficients for the linear equations that model the one-way water transmission pumping power and the heat transmission constraints and heat station shutdown periods associated with each pipe diameter. The minimum and maximum limits of thermal power transmission for each diameter are associated with the feasible flow velocity range of (0.5 m/s – 4 m/s). When the required thermal power to operate the absorption chillers falls below the minimum transmission limit due to low cooling demand, the heat station will be temporarily out of service. Therefore, the heat station shutdown periods are considered in the optimization process. The data given in Table 26 indicate that larger pipes have larger minimum and maximum heat transmission limits. As a result, when larger pipes are

employed in the system, they have the capacity to cover a higher cooling demand during peak times. However, they lead to an extension in the duration during which the low cooling demand cannot be met. There is another tradeoff between pumping power and the capital cost of the pipe. Using a larger pipe to transport the same amount of thermal power results in reduced pumping power requirements; in contrast, it comes with an increased initial capital cost for the pipe.

Table 26: Linearized pumping power coefficients, thermal power transportation limits, and shutdown periods of heat station associated with the pipe diameters.

D (m)	$P^i = A_D\, Q^i_{bht} + B_D \quad (26)$ Based on a 20 km distance.		Minimum thermal power (MW)	Maximum thermal power (MW)	Heat station and transmission hourly shutdown periods over a year due to low demand and transmission limit.			
	A_D	B_D			From	To	From	To
0.5	0.0298	-1.6116	20	159	1	744	-	-
0.7	0.0198	-2.0988	39	311	1	1433	8187	8784
1	0.0129	-2.7845	79	635	1	1440	8041	8784
1.2	0.0103	-3.2208	114	914	1	1440	8041	8784
1.5	0.0079	-3.8523	179	1429	1	2166	8041	8784
1.7	0.0068	-4.261	229	1835	1	2184	8041	8784
1.9	0.006	-4.6616	287	2293	1	2214	8041	8784
2	0.0056	-4.8592	318	2540	1	2262	8041	8784
2.1	0.0053	-5.0552	350	2800	1	2598	8041	8784
2.2	0.005	-5.2496	384	3074	1	2766	8041	8784
2.5	0.0043	-5.8243	496	3969	1	2898	7326	8784

Table 27 presents the achieved optimum design capacities for the system proposed in this study. In the optimized configuration, absorption chillers cover approximately (70%) of the peak cooling demand, while electric-driven compression chillers contribute only (12%). Additionally, cold storage plays an important role in covering (18%) of the peak cooling demand. The heat station incorporates eleven nuclear plants (Teplator) with a combined thermal capacity of 1650 MW to supply the thermal power required for driving the absorption chillers. Among the assumed options for thermal storages, the larger ones are selected as heat and cold storage, emphasizing their cost-effective role in this system. The optimized system employs supply/return heat transmission pipes with an optimal inner diameter of (1.9 m). Each supply and return pipe requires a total pumping power of (5.4 MW). The thermal capacity of heat exchanger-1 (on the heating side) is 1675 MW, which transfers heat from the heating station to the transmission pipeline cycle. Heat exchanger-2,

with a capacity of 1650 MW, transfers thermal power from the transmission cycle to the absorption chillers.

Although the proposed system has a capital cost that is 77% higher than the base scenario (Table 25), its considerably lower operation cost makes it a more cost-effective solution. The present value of the total cost of the optimized system is nearly 34% less than the cost of the base electric-driven system. It is important to note that these cost calculations are based on a 4% interest rate, and different optimum solutions may arise when considering higher interest rates.

Table 27: The optimized design capacities and achieved costs for the proposed system.

		Symbol	**Optimum design variable**	**Annual operation cost (M$)**	**Present value of operation cost over DMP (M$)**	**Capital cost (M$)**
Heat station	Nuclear plants	N_{nhu}	11 (11×150 =1650 MW)	47.5	1020.3	330
	Heat storage	Cp_{hs}	20 000 MWth/400MW	0.17	3.69	6.52
	Gas boiler	Cp_{gb}	0	0.00	0	0
Heat transmission	Heat exchanger 1	Cp_{hex} A_{hex}	1675 MW 33 597 m^2	6.92	148.68	6
	Heat exchanger 2	Cp_{hex} A_{hex}	1650 MW 57 057 m^2			10.18
	Pipe	D_{in}	1.9 m			173.03
	Insulation	s	200 mm			6.35
	Pumps	Cp_{pump}	2×5.4 MWe	6.42	138	19.32
Cooling station	Absorption chilling	Cp_{ac}	1424 MWc	63.77	1369.6	1354.7
	Compression chilling	Cp_{cc}	244 MWc	28.02	608	170.91
	Cold storage	Cp_{cs}	20 000 MWch /400 MWc	0.17	3.69	17.23
The total cost of the optimum design and operation of the system				152.97	3292	2094.2
					5386.2 M$	

According to the energy balance calculations outlined in Table 28, absorption chillers fulfill approximately 92% of the annual cooling energy demand, while compression chillers

provide only 7%. Consequently, the optimized system significantly reduced the annual electricity consumption by 69% compared to the base electric-driven scenario, which reflects a significant carbon elimination.

Table 28: System's energy balance.

Annual energy balance	**Proposed system**				**Electric-driven system**
Heat generation (TWh)	Teplator: 7.294			Heat storage (fully charged in advance): 0.02	0
Electricity consumption (GWh)	Teplator	Pumping	Absorption chillers	Compression chillers	Compression chillers
	72.94	44.614	310.41	133.2	1809.4
	Total: 561.16				
Cooling generation (TWh)	Absorption chillers	Compression chillers		Cold storage (fully charged in advance)	Compression chillers + precharged cold storage
	6.2081	0.4933		0.02	(6.7015 + 0.02)
Total cooling demand (TWh)	6.7215				

Fig. 33 illustrates the cost of the optimized system associated with various pipe diameters assumed in Table 23. While it was technically feasible to transport 1675 MW of heat using a 1.7 m diameter pipe (as indicated in Table 26), according to the fitted curve, the 1.8 m diameter pipe emerged as a slightly superior solution. This is due to the lower pumping cost associated with the 1.8 m diameter pipe, which offset its higher capital cost.

Fig. 34 provides a visual representation of the optimum hourly operation of the cooling station. It demonstrates that cold storage and compression chillers play a crucial role when the cooling demand is low, particularly when the thermal power required to drive the absorption chillers falls below the minimum heat transmission limit. During these periods, cold storage and compression chillers are necessary to ensure a sufficient cooling supply. Moreover, they effectively contribute to peak shaving and enhancing load following. By incorporating this supplementary equipment, the DCS becomes more adaptable and capable

of responding to fluctuations in cooling demand, ultimately leading to a more reliable operation.

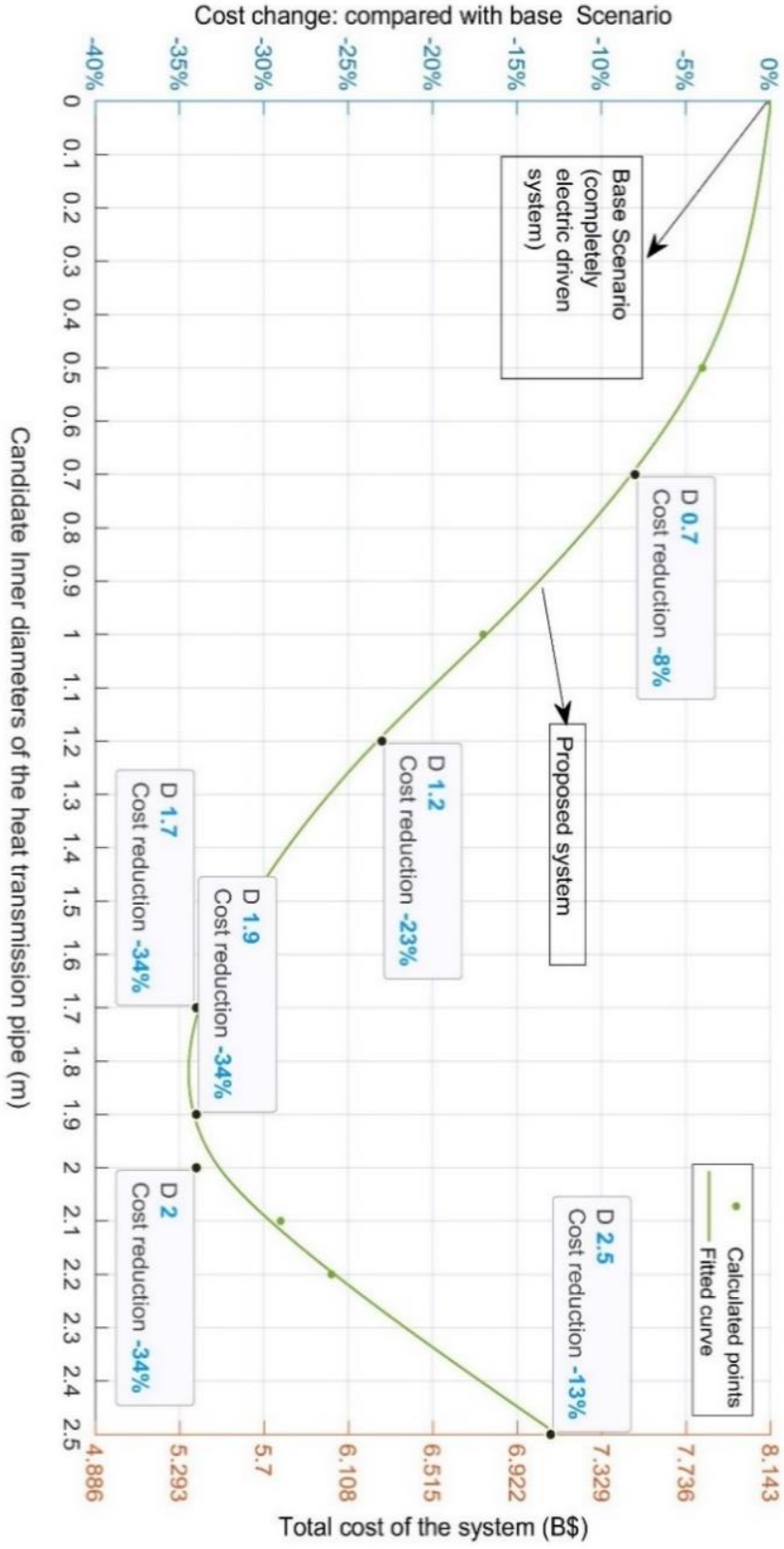

Figure 33: The total cost of the optimized system corresponding to heat transmission pipe diameters (for a 20 km distance case).

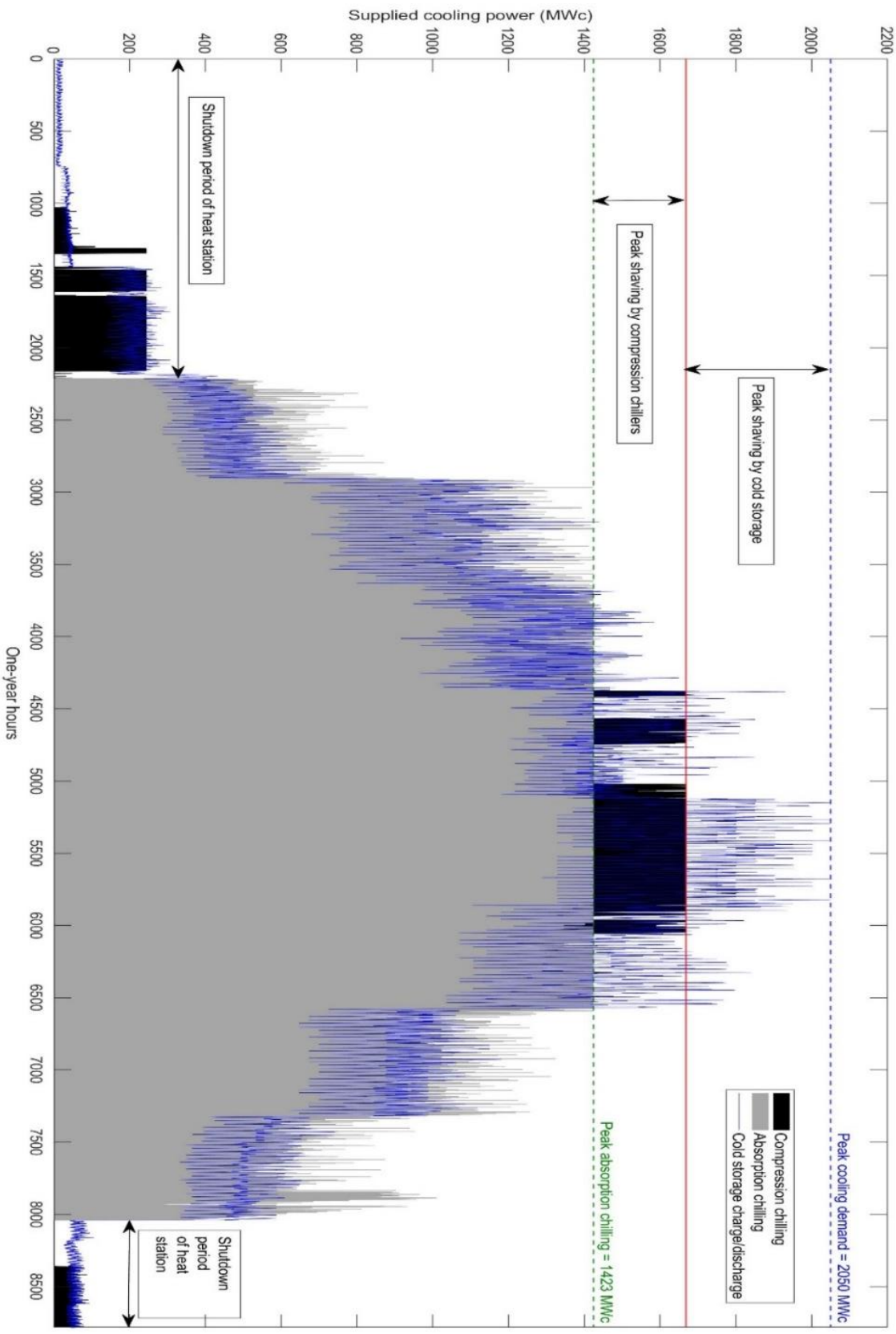

Figure 34: Optimized operation scheduling of the cooling station.

3.3.2.1 Sensitivity analysis

The reported results in Table 25 show that the economics of the electric-driven scenario is highly influenced by its operation costs, mainly due to the high electricity price and significant electricity consumption rate. The sensitivity analysis on electricity price, as illustrated in Fig. 35, confirms that the proposed thermally driven system becomes more competitive than the electric-driven system as the electricity price increases and vice versa. However, even with a considerable reduction in electricity price (e.g., 60%), the proposed thermally driven system remains the optimum solution in several cases. This sensitivity analysis also shows that the optimum diameter of the heat transmission pipe is not significantly influenced by electricity price. The pipe diameter remains within the range of (1.7 m – 2 m) for several cases, as shown in Fig. 35.

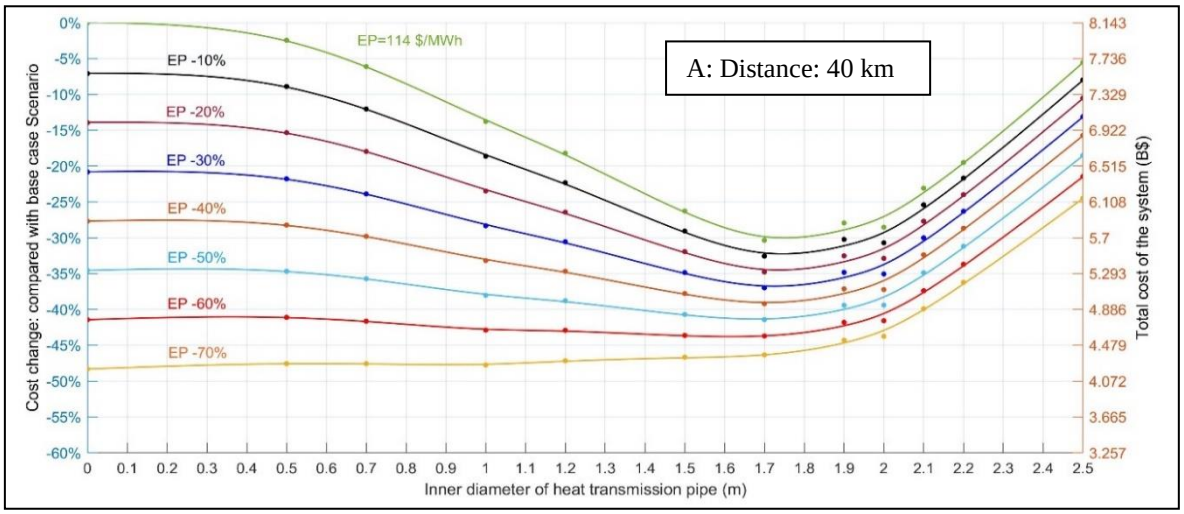

Figure 35: Optimization sensitivity to electricity price.

Another sensitivity analysis illustrated in Fig. 36 evaluates the proposed system considering different distances between the heat generation and cooling stations, assuming a fixed transmission pipe diameter of 1.7 m. When the electricity price is relatively high (e.g., 144 $/MWh), the proposed thermally driven system seems economically viable even for distances of up to 130 km. On the other hand, the electric-driven scenario is more cost-effective when the electricity price is relatively low (e.g., 43 $/MWh). This is particularly true in situations where the thermally driven system requires a heat transmission distance exceeding 25 km.

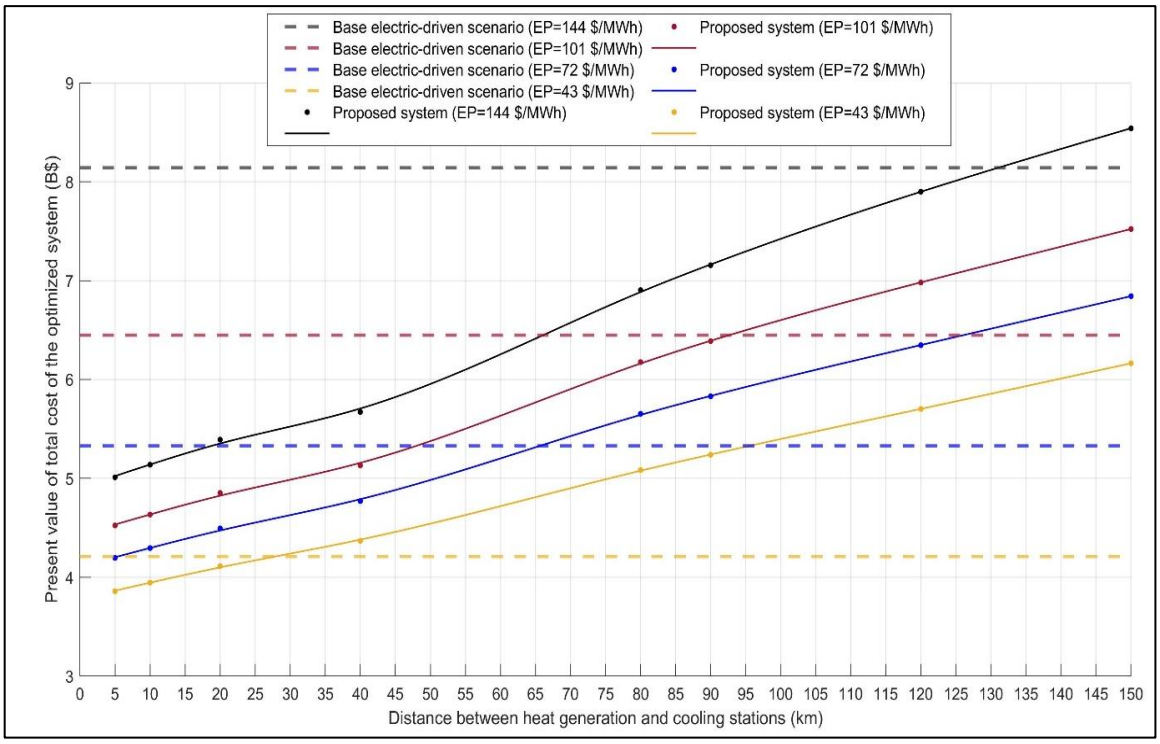

Figure 36: The proposed system's cost sensitivity to distance and electricity price compared to the base scenario.

3.3.2.2 Reliability of the method and results

The proposed methodology and algorithm in this study have been implemented using MATLAB. The reliability of the Algorithm and the accuracy of the results are well-founded. The Algorithm employs a comprehensive searching method that evaluates all predefined candidate options for the Group A variables, such as the pipeline's diameter (as evident in Fig. 33, which clearly illustrates the optimum diameter value among the candidate range). Moreover, in each iteration associated with the selected options for variables belonging to Group A, the robust mixed-integer linear programming function, "intlinprogin" in MATLAB, is employed. This function aids in finding the optimum variables of Group B and the operation variables, contributing to the effectiveness and efficiency of the optimization process. An in-depth analysis of the results confirms that the defined constraints are fully satisfied and the design capacities fall within the predetermined ranges. For instance, the energy balance is successfully achieved, as demonstrated in Table 28, and the load-following capability is aptly portrayed in Fig. 34. Furthermore, the resulting optimum design capacities, presented in Table 27, align with the available options determined in Table 23. Additionally, the sensitivity analysis depicted in Fig. 35 and Fig. 36 aligns with logical expectations. For instance, increasing the distance and electricity price indeed impact the economics of the proposed thermally driven system, and the sensitivity analysis accurately

captures these dynamics. In summary, the use of MATLAB and the thorough evaluation of the results demonstrate the proposed methodology's robustness and accuracy, contributing to our findings' credibility and validity.

4 Conclusions

Using nuclear energy (such as TEPLATOR technology that produces heat) integrated with heat-driven district cooling systems can provide an economical solution when serving the increasing cooling/heating demand, eliminates the unwanted energy conversion steps, minimizes the power system expansion and operation costs, and fulfills the pollution reduction targets. This approach has many vital advantages for hot climate regions with fast cooling demand growth. A demand that constitutes a significant part of electricity consumption and, at the same time, leads to the highest pollution emission rates worldwide. The proposed strategy and the formulated method from an energy policy perspective are applicable in many countries and provide a practical framework for studying and comparing the competitive scenarios aiming to serve the cooling/heating demand from economical and environmental viewpoints.

This study also proposes a detailed integrated district cooling system primarily powered by nuclear heat and develops an optimization method for its design and operation from investors’s viewpoint. The system consists of three main parts: a heat station, a heat transmission system, and a cooling station. The heat supply options include a heat-only SMR called Teplator, gas boilers, and heat storage. The diameter of the pipe used for heat transmission is a crucial variable in the system design. Cooling equipment options are absorption chillers, compression chillers, and cold storage. The objective is to minimize the total cost, and the decision-making variables involve the design capacities, technology selection, and hourly operation of the main components. The system is optimized to supply a typical large-scale cooling demand with a peak demand of (2050 MWc). The results validate the feasibility of utilizing nuclear heat for district cooling applications. The optimized design determines employing 11 nuclear plants, each with a capacity of 150 MWt, eliminating the need for gas boilers. Through the optimization process, the largest capacities for heat storage and cold storage (20,000 MWth) were chosen, reflecting the techno-economic advantages of employing thermal energy storage to enhance the load-following capability and increase the capacity factor of the system.

This innovative approach effectively addresses two critical challenges in the air conditioning sector: high electricity consumption and the associated carbon emissions. Covering 92% of the cooling demand energy by absorption chillers driven by nuclear heat leads to considerable electricity and carbon emission savings of 69% compared to an electric-driven scenario. However, auxiliary compression chillers are still necessary for peak shaving, enhancing the load following and covering the low cooling demands periods when absorption chillers are inactive due to the heat transmission limits. The economic competitiveness of the proposed system is confirmed, with a cost reduction of 34% for the 20 km heat transmission case compared to the electric-driven scenario. The sensitivity analyses demonstrate the influence of electricity price and heat transmission distance on the system's economics. As the distance decreases and electricity price increases, the proposed system becomes increasingly advantageous, and vice versa.

There is potential to modify and apply the proposed method to assess different types of energy sources for district cooling applications in future studies. Additionally, the method can be extended to evaluate systems with higher heat source temperatures that can drive double-effect absorption chillers. While this study focused on modeling the capacities of the supply units and heat transmission pumping as a whole, further optimization can be pursued to achieve more detailed sizing, placement of pumping stations, and configuration of the chillers. These additional steps can complement the overall optimization process and provide more comprehensive results for the system design and operation.

It should be noted that the achieved results are not general since the considered costs can vary from country to country. In real energy systems, the real levelized costs should be used in the proposed method. However, the sensitivity analysis proves that the proposed strategy can be an economical solution for various cost fluctuations.

References

[1] F. Birol, "The future of cooling: opportunities for energy-efficient air conditioning," *International Energy Agency*, 2018.

[2] H. R. Europe, "Heating and Cooling Facts and Figures," *URL: https://www. isi. fraunhofer. de/content/dam/isi/dokumente/cce/2017/29882 _ Brochure _ Heating-and-Cooling_web. pdf*, 2017.

[3] Center Bipartisan Policy, "Annual energy outlook 2020," *Energy Information Administration, Washington, DC*, vol. 12, pp. 1672–1679, 2020.

[4] K. K. W. Wan, D. H. W. Li, W. Pan, and J. C. Lam, "Impact of climate change on building energy use in different climate zones and mitigation and adaptation implications," *Appl Energy*, vol. 97, pp. 274–282, 2012.

[5] V. Eveloy and D. S. Ayou, "Sustainable District Cooling Systems: Status, Challenges, and Future Opportunities, with Emphasis on Cooling-Dominated Regions," *Energies (Basel)*, vol. 12, p. 235, Nov. 2019, doi: 10.3390/en12020235.

[6] N. Howarth, N. Odnoletkova, A. Alshehri Thamir and Almadani, A. Lanza, and T. Patzek, "Staying Cool in A Warming Climate: Temperature, Electricity and Air Conditioning in Saudi Arabia," *Climate*, vol. 8, no. 1, p. 4, 2020.

[7] C. Alalouch, S. Al-Saadi, H. AlWaer, and K. Al-Khaled, "Energy saving potential for residential buildings in hot climates: The case of Oman," *Sustain Cities Soc*, vol. 46, p. 101442, Apr. 2019, doi: 10.1016/J.SCS.2019.101442.

[8] T. Salameh, M. E. H. Assad, M. Tawalbeh, C. Ghenai, A. Merabet, and H. F. Öztop, "Analysis of cooling load on commercial building in UAE climate using building integrated photovoltaic façade system," *Solar Energy*, vol. 199, pp. 617–629, Mar. 2020, doi: 10.1016/J.SOLENER.2020.02.062.

[9] G. Sarraf, W. Fayad, T. E. Sayed, and S.-P. Monette, "Unlocking the potential of district cooling the need for GCC governments to take action," *Booz & Co.(now Strategy&)*, 2012.

[10] I. S. Bayram, M. Koç, O. Alrawi, and H. Al-Naimi, "Direct load control of air conditioners in Qatar: An empirical study," in *2017 IEEE 6th International Conference on Renewable Energy Research and Applications (ICRERA)*, 2017, pp. 1007–1012. doi: 10.1109/ICRERA.2017.8191209.

[11] D. Alghool, T. Elmekkawy, M. Haouari, and A. Elomari, "Data of the design of solar assisted district cooling systems," *Data Brief*, p. 105541, 2020.

[12] O. Alrawi, I. S. Bayram, S. G. Al-Ghamdi, and M. Koc, "High-resolution household load profiling and evaluation of rooftop pv systems in selected houses in qatar," *Energies (Basel)*, vol. 12, no. 20, p. 3876, 2019.

[13] I. S. Bayram, M. Koç, O. Alrawi, and H. Al-Naimi, "Direct load control of air conditioners in Qatar: An empirical study," in *2017 IEEE 6th International Conference on Renewable Energy Research and Applications (ICRERA)*, 2017, pp. 1007–1012. doi: 10.1109/ICRERA.2017.8191209.

[14] "Key energy statistics, 2019." Accessed: Feb. 10, 2022. [Online]. Available: https://www.iea.org/countries/

[15] V. Eveloy and D. S. Ayou, "Sustainable district cooling systems: Status, challenges, and future opportunities, with emphasis on cooling-dominated regions," *Energies (Basel)*, vol. 12, no. 2, p. 235, 2019.

[16] W. Gang, S. Wang, F. Xiao, and D. C. Gao, "District cooling systems: Technology integration, system optimization, challenges and opportunities for applications," *Renewable and Sustainable Energy Reviews*, vol. 53, pp. 253–

264, Jan. 2016, doi: 10.1016/J.RSER.2015.08.051.
[17] T. el Sayed, W. Fayad, S. P. Monette, and G. Sarraf, “Unlocking the Potential of District Cooling: The Need for GCC Governments to Take Action,” *Booz & Co.(now strategy&), New York*, 2012.
[18] D. F. Dominković *et al.*, “Potential of district cooling in hot and humid climates,” *Appl Energy*, vol. 208, pp. 49–61, 2017.
[19] P. Lamers, “summerheat publishable final report en.” Nov. 2016.
[20] T. Avanessian and M. Ameri, “Energy, exergy, and economic analysis of single and double effect LiBr–H2O absorption chillers,” *Energy Build*, vol. 73, pp. 26–36, 2014, doi: https://doi.org/10.1016/j.enbuild.2014.01.013.
[21] J. Vujić, R. M. Bergmann, R. Škoda, and M. Miletić, “Small modular reactors: Simpler, safer, cheaper?,” *Energy*, vol. 45, no. 1, pp. 288–295, Sep. 2012, doi: 10.1016/j.energy.2012.01.078.
[22] F. Reitsma, M. H. Subki, J. C. Luque-Gutierrez, and S. Bouchet, *Advances in Small Modular Reactor Technology Developments*, 2020th ed. 2020.
[23] R. Skoda *et al.*, “TEPLATOR: Nuclear District Heating Solution,” 2020.
[24] D. Mašata, J. Jiřičková, and R. Škoda, “„TEPLATOR: Basic economic study for the construction and operation,” *Nuclear Energy for New Europe*, 2020.
[25] IEA, “The future of cooling,” *Opportunities for Energy-Efficient Air Conditioning*. OECD/IEA, 2018.
[26] I. Andric and S. G. Al-Ghamdi, “Climate change implications for environmental performance of residential building energy use: The case of Qatar,” *Energy Reports*, vol. 6, pp. 587–592, Feb. 2020, doi: 10.1016/J.EGYR.2019.09.030.
[27] N. O. Bell, J. I. Bilbao, M. Kay, and A. B. Sproul, “Future climate scenarios and their impact on heating, ventilation and air-conditioning system design and performance for commercial buildings for 2050,” *Renewable and Sustainable Energy Reviews*, vol. 162, p. 112363, Jul. 2022, doi: 10.1016/J.RSER.2022.112363.
[28] H. A. Saleh Abushamah and R. Skoda, “Nuclear energy for district cooling systems – Novel approach and its eco-environmental assessment method,” *Energy*, vol. 250, p. 123824, Jul. 2022, doi: 10.1016/J.ENERGY.2022.123824.
[29] A. Inayat and M. Raza, “District cooling system via renewable energy sources: A review,” *Renewable and Sustainable Energy Reviews*, vol. 107, pp. 360–373, Jun. 2019, doi: 10.1016/J.RSER.2019.03.023.
[30] F. Sun, W. Xu, H. Chen, B. Hao, and X. zhao, “Configuration optimization of solar-driven low temperature district heating and cooling system integrated with distributed water-lithium bromide absorption heat pumps,” *Solar Energy*, vol. 253, pp. 401–413, Mar. 2023, doi: 10.1016/J.SOLENER.2023.02.039.
[31] M. Jannatabadi, H. R. Rahbari, and A. Arabkoohsar, “District cooling systems in Iranian energy matrix, a techno-economic analysis of a reliable solution for a serious challenge,” *Energy*, vol. 214, p. 118914, Jan. 2021, doi: 10.1016/J.ENERGY.2020.118914.
[32] H. Safa, “Heat recovery from nuclear power plants,” *International Journal of Electrical Power & Energy Systems*, vol. 42, no. 1, pp. 553–559, Nov. 2012, doi: 10.1016/J.IJEPES.2012.04.052.
[33] M. Leurent, P. da Costa, M. Rämä, U. Persson, and F. Jasserand, “Cost-benefit analysis of district heating systems using heat from nuclear plants in seven European countries,” *Energy*, vol. 149, pp. 454–472, Apr. 2018, doi: 10.1016/J.ENERGY.2018.01.149.

[34] K. C. Kavvadias and S. Quoilin, "Exploiting waste heat potential by long distance heat transmission: Design considerations and techno-economic assessment," *Appl Energy*, vol. 216, pp. 452–465, Apr. 2018, doi: 10.1016/J.APENERGY.2018.02.080.

[35] P. Hirsch, K. Duzinkiewicz, M. Grochowski, and R. Piotrowski, "Two-phase optimizing approach to design assessments of long distance heat transportation for CHP systems," *Appl Energy*, vol. 182, pp. 164–176, Nov. 2016, doi: 10.1016/J.APENERGY.2016.08.107.

[36] P. C. Basu, "Site evaluation for nuclear power plants – The practices," *Nuclear Engineering and Design*, vol. 352, p. 110140, Oct. 2019, doi: 10.1016/J.NUCENGDES.2019.06.002.

[37] R. Loisel, V. Alexeeva, A. Zucker, and D. Shropshire, "Load-following with nuclear power: Market effects and welfare implications," *Progress in Nuclear Energy*, vol. 109, pp. 280–292, Nov. 2018, doi: 10.1016/J.PNUCENE.2018.08.011.

[38] W. Zhang, X. Jin, and W. Hong, "The application and development of district cooling system in China: A review," *Journal of Building Engineering*, vol. 50, p. 104166, Jun. 2022, doi: 10.1016/J.JOBE.2022.104166.

[39] R. Nikbakhti, X. Wang, A. K. Hussein, and A. Iranmanesh, "Absorption cooling systems – Review of various techniques for energy performance enhancement," *Alexandria Engineering Journal*, vol. 59, no. 2, pp. 707–738, Apr. 2020, doi: 10.1016/J.AEJ.2020.01.036.

[40] I. E. Commission and others, "Efficient electrical energy transmission and distribution," *Switzerland, IEC*, 2007.

[41] W. Hüls Güido, W. Lanser, S. Petersen, and F. Ziegler, "Performance of absorption chillers in field tests," *Appl Therm Eng*, vol. 134, pp. 353–359, 2018, doi: https://doi.org/10.1016/j.applthermaleng.2018.02.013.

[42] Z. Zhen, L. Tian, and Q. Ye, "A simple estimate for the social cost of carbon," *Energy Procedia*, vol. 152, pp. 768–773, 2018, doi: https://doi.org/10.1016/j.egypro.2018.09.243.

[43] International Electrotechnical Commission, "Efficient electrical energy transmission and distribution," *Report, Switzerland*, 2007.

[44] R. L. Fares and C. W. King, "Trends in transmission, distribution, and administration costs for U.S. investor-owned electric utilities," *Energy Policy*, vol. 105, pp. 354–362, Jun. 2017, doi: 10.1016/J.ENPOL.2017.02.036.

[45] US Nuclear Regulatory Commission, "Population-Related Siting Considerations for Advanced Reactors," *NRC Staff Prepared White Paper*, 2020.

[46] IAEA. and IAEA, *Managing siting activities for nuclear power plants*. International Atomic Energy Agency, 2022.

[47] D. D. Andrews *et al.*, *Background report on EU-27 district heating and cooling potentials, barriers, best practice and measures of promotion*. Publications Office of the European Union, 2012.

[48] H. A. S. Abushamah, M. R. Haghifam, and T. G. Bolandi, "A novel approach for distributed generation expansion planning considering its added value compared with centralized generation expansion," *Sustainable Energy, Grids and Networks*, vol. 25, p. 100417, Mar. 2021, doi: 10.1016/J.SEGAN.2020.100417.

[49] L. Zhang, Y. Wang, and X. Feng, "A framework for design and operation optimization for utilizing low-grade industrial waste heat in district heating and

cooling," *Energies (Basel)*, vol. 14, no. 8, p. 2190, 2021.

[50] C. Chang, X. Chen, Y. Wang, and X. Feng, "An efficient optimization algorithm for waste Heat Integration using a heat recovery loop between two plants," *Appl Therm Eng*, vol. 105, pp. 799–806, Jul. 2016, doi: 10.1016/J.APPLTHERMALENG.2016.04.079.

[51] E. S. Menon, *Working Guide to Pump and Pumping Stations: Calculations and Simulations*. Gulf Professional Publishing, 2009.

[52] F. Ochs, A. Dahash, A. Tosatto, and M. Bianchi Janetti, "Techno-economic planning and construction of cost-effective large-scale hot water thermal energy storage for Renewable District heating systems," *Renew Energy*, vol. 150, pp. 1165–1177, May 2020, doi: 10.1016/J.RENENE.2019.11.017.

[53] "Technology Data for Energy Storage," 2018. Accessed: Oct. 11, 2022. [Online]. Available: https://ens.dk/en/our-services/projections-and-models/technology-data/technology-data-energy-storage

[54] M. Z. Stijepovic and P. Linke, "Optimal waste heat recovery and reuse in industrial zones," *Energy*, vol. 36, no. 7, pp. 4019–4031, Jul. 2011, doi: 10.1016/J.ENERGY.2011.04.048.

[55] "The Pearl Qatar." Accessed: Sep. 13, 2021. [Online]. Available: https://www.qatarcool.com/Districts/of/Mg%3D%3D

[56] D. F. Dominković *et al.*, "Potential of district cooling in hot and humid climates," *Appl Energy*, vol. 208, pp. 49–61, Dec. 2017, doi: 10.1016/J.APENERGY.2017.09.052.

[57] F. Zhou, L. Page, R. K. Perrons, Z. Zheng, and S. Washington, "Long-term forecasts for energy commodities price: What the experts think," *Energy Econ*, vol. 84, p. 104484, Oct. 2019, doi: 10.1016/J.ENECO.2019.104484.

[58] G. P. Herrera, M. Constantino, B. M. Tabak, H. Pistori, J. J. Su, and A. Naranpanawa, "Long-term forecast of energy commodities price using machine learning," *Energy*, vol. 179, pp. 214–221, Jul. 2019, doi: 10.1016/J.ENERGY.2019.04.077.

[59] "Delivered Cost of Electricity Report – May 2020. (n.d.). Retrieved September 22." Accessed: Sep. 28, 2021. [Online]. Available: https://www.aeso.ca/market/market-and-system-reporting/delivered-cost-of-electricity/

[60] Z. Zhen, L. Tian, and Q. Ye, "A simple estimate for the social cost of carbon," *Energy Procedia*, vol. 152, pp. 768–773, Oct. 2018, doi: 10.1016/J.EGYPRO.2018.09.243.

[61] C. Cost, "Performance Characteristic Estimates for Utility Scale Electric Power Generating Technologies," *US Energy Information Administration, Sargent and Lundy*, 2020.

[62] V. Hübner, K. Kallmann, S. Piller, N. Thamling, D. Hesse, and A. Wetzel, "Meeting cooling demands in summer by applying heat from cogeneration," *Berl\'\in: Berliner Energieagentur GmbH*, 2008.

[63] R. Skoda *et al.*, "TEPLATOR: nuclear district heating solution," in Proceedings of International Conference Nuclear Energy for New Europe. 2020.

[64] T. Avanessian and M. Ameri, "Energy, exergy, and economic analysis of single and double effect LiBr–H2O absorption chillers," *Energy Build*, vol. 73, pp. 26–36, Apr. 2014, doi: 10.1016/J.ENBUILD.2014.01.013.

[65] Y. Zhang, T. Li, G. Na, and G. Li, "Optimized Extreme Learning Machine for Power System Transient Stability Prediction Using Synchrophasors," *Math Probl Eng*, vol. 2015, pp. 1–8, Nov. 2015, doi: 10.1155/2015/529724.

[66] G. S. Jang, D. Hur, J. K. Park, and S. H. Lee, “A modified power flow analysis to remove a slack bus with a sense of economic load dispatch,” *Electric Power Systems Research*, vol. 73, no. 2, pp. 137–142, Feb. 2005, doi: 10.1016/J.EPSR.2004.07.001.

[67] D. Alghool, T. Elmekkawy, M. Haouari, and A. Elomri, “Data of the design of solar assisted district cooling systems,” *Data Brief*, vol. 30, p. 105541, Jun. 2020, doi: 10.1016/J.DIB.2020.105541.

[68] C. Lahoud, M. el Brouche, C. Lahoud, and M. Hmadi, “A Review of single-effect solar absorption chillers and its perspective on Lebanese case,” *Energy Reports*, vol. 7, pp. 12–22, 2021, doi: https://doi.org/10.1016/j.egyr.2021.09.052.

[69] “Absorption chillers and heat pumps.” Accessed: Nov. 07, 2022. [Online]. Available: http://worldenergy.co.kr/en/catalogue-2/

[70] S. Lazarević, V. Čongradac, A. Andjelkovic, M. Kljajić, and Ž. Kanović, “District heating substation elements modeling for the development of the real-time model,” *Thermal Science*, vol. 23, p. 31, Oct. 2019, doi: 10.2298/TSCI181226031L.

[71] Danish Energy Agency, “Technology Data for Generation of Electricity and District Heating,” 2020.

[72] “World Energy Absorption Chiller Absorption Chiller & Heater Absorption Heat Pump.” Accessed: Oct. 11, 2022. [Online]. Available: https://www.worldenergyeurope.eu/products.html

[73] “Electricity prices for non-household consumers in EU.” Accessed: Oct. 20, 2022. [Online]. Available: https://ec.europa.eu/eurostat/statistics-explained/index.php?title=Electricity_price_statistics#Electricity_prices_for_non-household_consumers

[74] “Natural gas prices for non-household consumers in EU.” Accessed: Oct. 20, 2022. [Online]. Available: https://ec.europa.eu/eurostat/statistics-explained/index.php?title=Natural_gas_price_statistics#Natural_gas_prices_for_non-household_consumers

[75] H. A. S. Abushamah, D. Masata, M. Mueller, and R. Skoda, “Economics of reusing spent nuclear fuel by Teplator for district heating applications,” *Int J Energy Res*, vol. 46, no. 5, pp. 5771–5788, 2022, doi: https://doi.org/10.1002/er.7521.

List of Student's Publications on the Dissertation Subject

[1] ABUSHAMAH, H.A.S., MAŠATA, D., JIŘIČKOVÁ, J., ŠKODA, R. Optimization of Sizing and Operation of a Nuclear District Heating System Using Teplator, Gas Boiler and Heat Storage. In *Proceedings of the International Conference Nuclear Energy for New Europe (NENE 2022)*. Ljubljana: Nuclear Society of Slovenia, 2022. s. „910.1"-„910.8". ISBN: 978-961-6207-53-9 ,Nový RIV obor: **Nuclear related engineering**

[2] ABUSHAMAH, H. A. S., HAGHIFAM, M., BOLANDI, T. G. A novel approach for distributed generation expansion planning considering its added value compared with centralized generation expansion. *Sustainable Energy, Grids and Networks*, 2021, roč. 25, č. March 2021, s. 1-18. ISSN: 2352-4677 ,Nový RIV obor: **Electrical and electronic engineering**

[3] ABUSHAMAH, H.A.S., JIŘIČKOVÁ, J., ŠKODA, R. Nuclear Based Approach for Multi Energy Applications. In *Elektrotechnika a informatika 2021. Elektrotechnika, elektronika, elektroenergetika*. Plzeň: Západočeská univerzita v Plzni, 2021. s. 5-8. ISBN: 978-80-261-1019-4 Původní RIV obor: **JA - Elektronika a optoelektronika, elektrotechnika** ,Nový RIV obor: **Electrical and electronic engineering**

[4] ABUSHAMAH, H.A.S., JIŘIČKOVÁ, J., ŠKODA, R., MAŠATA, D. Evaluating the TEPLATOR concept as a nuclear heating solution compared with other alternatives in the Czech Republic. In *Proceedings of the International Conference Nuclear Energy for New Europe (NENE 2021)*. Ljubljana: Nuclear Society of Slovenia, 2021. s. 210.1-210.8. ISBN: 978-961-6207-51-5 ,Nový RIV obor: **Nuclear related engineering**

[5] ŠKODA, R., ABUSHAMAH, H.A.S. Nuclear solution for district cooling and its benefits on the power system. In *Proceedings of ICAPP 2021*. Abu Dhabi: Khalifa University, 2021. s. 1-9. ISBN: neuvedeno ,Nový RIV obor: **Nuclear physics**

[6] ABUSHAMAH, H. A. S., MAŠATA, D., MÜLLER, M., ŠKODA, R. Economics of reusing spent nuclear fuel by Teplator for district heating applications. *INTERNATIONAL JOURNAL OF ENERGY RESEARCH*, 2022, roč. 46, č. 5, s. 5771-5788. ISSN: 0363-907X ,Nový RIV obor: **Nuclear related engineering**

[7] ABUSHAMAH, H. A. S., BURIAN, O., ŠKODA, R. Design and Operation Optimization of a Nuclear Heat-Driven District Cooling System. *INTERNATIONAL JOURNAL OF ENERGY RESEARCH*, 2023, roč. Volume 23, ISSN: 0363-907X ,Nový RIV obor: **Nuclear related engineering**

[8] ABUSHAMAH, H. A. S., ŠKODA, R. Nuclear energy for district cooling systems - Novel approach and its eco-environmental assessment method. *ENERGY*, 2022, roč. 250, č. July 2022, s. 1-19. ISSN: 0360-5442 ,Nový RIV obor: **Nuclear related engineering**

[9] MAŠATA, D., ABUSHAMAH, H.A.S., JIŘIČKOVÁ, J., ŠKODA, R. Nuclear Power for the Decarbonization of the District Heating Sector in the Czech Republic. In *Proceedings of the International Conference Nuclear Energy for New Europe (NENE 2022)*. Ljubljana: Nuclear Society of Slovenia, 2022. s. „1201.1"-„1201.8". ISBN: 978-961-6207-53-9 ,Nový RIV obor: **Nuclear related engineering**